

**HYDROGEN PRODUCTION FROM METHANOL STEAM REFORMING IN A
MICROWAVE REACTOR**

A THESIS SUBMITTED TO
THE GRADUATE SCHOOL OF NATURAL AND APPLIED SCIENCES
OF
MIDDLE EAST TECHNICAL UNIVERSITY

BY

SOHRAB NIKAZAR

IN PARTIAL FULFILLMENT OF THE REQUIREMENTS
FOR
THE DEGREE OF MASTER OF SCIENCE
IN
CHEMICAL ENGINEERING

MARCH 2019

Approval of the thesis:

**HYDROGEN PRODUCTION FROM METHANOL STEAM REFORMING
IN A MICROWAVE REACTOR**

submitted by **SOHRAB NIKAZAR** in partial fulfillment of the requirements for the degree of **Master of Science in Chemical Engineering Department, Middle East Technical University** by,

Prof. Dr. Halil Kalıpçilar
Dean, Graduate School of **Natural and Applied Sciences** _____

Prof. Dr. Pınar Çalık
Head of Department, **Chemical Engineering** _____

Prof. Dr. Naime Aslı Sezgi
Supervisor, **Chemical Engineering, METU** _____

Prof. Dr. Timur Doğu
Co-Supervisor, **Chemical Engineering, METU** _____

Examining Committee Members:

Prof. Dr. Suna Balçı
Chemical Engineering, Gazi University _____

Prof. Dr. Naime Aslı Sezgi
Chemical Engineering, METU _____

Prof. Dr. Deniz Üner
Chemical Engineering, METU _____

Assist. Prof. Dr. Harun Koku
Chemical Engineering, METU _____

Assist. Prof. Dr. Bahar İpek Torun
Chemical Engineering, METU _____

Date: 01.03.2019

I hereby declare that all information in this document has been obtained and presented in accordance with academic rules and ethical conduct. I also declare that, as required by these rules and conduct, I have fully cited and referenced all material and results that are not original to this work.

Name, Surname: Sohrab Nikazar

Signature:

ABSTRACT

HYDROGEN PRODUCTION FROM METHANOL STEAM REFORMING IN A MICROWAVE REACTOR

Nikazar, Sohrab
Master of Science, Chemical Engineering
Supervisor: Prof. Dr. Naime Aslı Sezgi
Co-Supervisor: Prof. Dr. Timur Doğu

March 2019, 144 pages

Today's world is facing crucial environmental issues, such as climate change and greenhouse gas emission, mainly attributed to the overusing fossil fuels. An environmentally friendly and sustainable replacement is proton exchange membrane fuel cell system which is a promising technology fed by hydrogen. However, fuel cell's anode catalyst is sensitive to amount of CO in the feed stream. Steam reforming of methanol is an appropriate method for hydrogen production. Nevertheless, endothermic nature of this reaction brings its economic feasibility into question.

In this study, hydrogen was produced from methanol steam reforming (MSR) reaction. For this purpose, metal-loaded mesoporous carbon catalysts were synthesized and characterized. The catalyst activity was tested in the MSR reaction heated by a conventional heating method. Effect of catalyst calcination temperature, Cu/Zn ratio, total metal loading amount, and reaction temperature was investigated on the reaction product distribution, methanol conversion, and hydrogen yield. Furthermore, microwave was used as an alternative heat source which is more efficient than conventional heating method.

CMK-3 with the surface area of 1120 m²/g, pore volume of 3.7 cm³/g, and pore size of 3.7 nm was synthesized as the support material. Both support material and metal-loaded catalyst exhibited Type IV isotherm with H₂ hysteresis.

It was observed that the catalyst activity increases with increasing Cu/Zn ratio and total metal loading amount, while increasing the catalyst calcination temperature declines the catalyst activity. CO-free hydrogen was produced from the 18.75Cu6.25Zn/CMK-3/300 catalyst at 250°C in the conventionally-heated reactor system with methanol conversion of 93.0% and hydrogen yield of 94%. A higher methanol conversion was obtained in the microwave-focused heated reactor system compared to the conventionally-heated reactor system in addition to a higher energy efficiency. 97.5% methanol conversion and 95.6% hydrogen yield were achieved in this system at 300 °C.

Keywords: Methanol Steam Reforming, Hydrogen Production, Mesoporous Carbon Materials, Microwave-Focused Heating, CMK-3.

ÖZ

MİKRODALGA REAKTÖRDE BUHARLI METANOL REFORMLAMADAN HİDROJEN ÜRETİMİ

Nikazar, Sohrab
Yüksek Lisans, Kimya Mühendisliği
Tez Danışmanı: Prof. Dr. Naime Aslı Sezgi
Ortak Tez Danışmanı: Prof. Dr. Timur Doğu

Mart 2019, 144 sayfa

Çoğunlukla fosil yakıtların aşırı kullanılmasına bağlı olarak iklim değişikliği ve sera gazı emisyonu gibi önemli çevresel sorunlarla günümüz dünyası karşı karşıya kalmaktadır. Hidrojenle beslenen gelecek vaat eden teknoloji olan proton değişim membrian yakıt hücresi, çevre dostu ve sürdürülebilir değişimi olan bir sistemdir. Fakat, yakıt hücresinin anot katalizörü, besleme akışındaki CO miktarına duyarlıdır. Metanolün buharla reformlanması, hidrojen üretimi için uygun bir yöntemdir. Bununla birlikte bu reaksiyonun endotermik oluşu ekonomik fizibiliteli sorusuna neden olmaktadır.

Bu çalışmada, buharlı metanol reformlanması reaksiyonundan (MSR) hidrojen üretilmiştir. Bu amaçla, metal yüklü mezogözenekli karbon katalizörler sentezlenmiş ve karakterize edilmiştir. Katalizör aktivitesi, geleneksel ısıtma yöntemiyle ısıtılarak MSR reaksiyonunda test edilmiştir. Katalizör kalsinasyon sıcaklığının, Cu/Zn oranının, toplam metal yükleme miktarının ve reaksiyon sıcaklığının ürün dağılımına, metanol dönüşümüne ve hidrojen verimine etkileri araştırılmıştır. Ayrıca, geleneksel ısıtma yönteminden daha verimli olan alternatif bir ısı kaynağı olarak mikrodalga kullanılmıştır.

$1120 \text{ m}^2/\text{g}$ yüzey alanına, $3,7 \text{ cm}^3/\text{g}$ gözenek hacmine ve $3,7 \text{ nm}$ gözenek çapına sahip CMK-3 destek malzemesi olarak sentezlenmiştir. Destek malzemesi ve metal yüklü katalizör H₂ histeresis ile Tip IV izoterm göstermiştir.

Katalizör aktivitesinin artan Cu/Zn oranı ve toplam metal yükleme miktarı ile arttığı, artan katalizör kalsinasyon sıcaklığıyla ise azaldığı görülmüştür. Geleneksel olarak ısıtılmış reaktör sisteminde %93 metanol dönüşümü ve %94 hidrojen verimi ile 250°C 'de 18.75Cu6.25Zn/CMK-3/300 katalizöründen CO içermeyen hidrojen üretilmiştir. Mikrodalga odaklı ısıtılmış reaktör sisteminde, daha yüksek enerji verimliliğine ek olarak, geleneksel olarak ısıtılmış reaktör sistemine göre daha yüksek bir metanol dönüşümü elde edilmiştir. %97,5 metanol dönüşümüne ve %95,6 hidrojen verimi 300°C 'de bu sistemde sağlanmıştır.

Anahtar Kelimeler: Metanolün Buharlı Reformlanması, Hidrojen Üretimi, Mezogözenekli Karbon Malzemeler, Mikrodalga Odaklı Isıtma, CMK-3

To My Lovely Family

ACKNOWLEDGMENTS

In the completion of thesis, I am indebted to Prof. Dr. Naime Aslı Sezgi for her continuous support, compassion, and encouragement. Her knowledge and guidance helped me in all the time of research and writing of this thesis. I also would like to express my thanks to my co-supervisor Prof. Dr. Timur Doğu for his guidance.

I have been lucky to be a member of Kinetic Lab research group. I would like to thank Merve Sarıyer for all her efforts and contribution to my research. Abdulrehman Habib has been a great friend and labmate to me. I am also thankful for Arzu Arslan Bozdağ, İlker Şener, Pınar Değirmencioğlu, Saeed Ahmad Khan, and Seda Sivri for their support and kindness.

I wish to thank to my great friend, Talha Güneş, for his friendship.

I would like to also present my thanks to Mihrican Açıkgöz and Doğan Akkuş for being so helpful in performing my characterization tests, and also faculty members and the staff of Chemical Engineering department.

I would like to thank Shirin for her endless love, patience, unlimited support, and continuous encouragement throughout my years of study.

This journey would not have been possible without the support and guidance of my family. To my family, thank you for encouraging and inspiring me to follow my dreams.

Last but not the least, I would like to express my deep love and gratitude to my father, Prof. Dr. Manouchehr Nikazar. You have been my idol, teacher, and best friend. I believe you are still taking care of me, as always. You will always be in my heart, because in there you are alive. Miss you!

TABLE OF CONTENTS

ABSTRACT	v
ÖZ	vii
ACKNOWLEDGMENTS	x
TABLE OF CONTENTS	xi
LIST OF TABLES	xv
LIST OF FIGURES	xvii
CHAPTERS	
1. INTRODUCTION	1
2. HYDROGEN: TOWARDS A SUSTAINABLE ENERGY FUTURE	5
2.1. HISTORY AND PROPERTIES OF HYDROGEN	7
2.2. APPLICATIONS.....	8
2.3. PRODUCTION TECHNIQUES	10
2.3.1. HYDROCARBON REFORMING	11
2.3.2. PYROLYSIS.....	12
2.3.3. PLASMA REFORMING.....	12
2.3.4. AQUEOUS PHASE REFORMING	13
2.4. FUEL CELLS	13
2.5. ON-BOARD FUEL CELLS.....	16
3. METHANOL STEAM REFORMING	19
3.1. CHOOSING METHANOL AS FEEDSTOCK.....	19
3.2. METHANOL STEAM REFORMING (MSR) REACTION PROCESS	21
3.3. THERMODYNAMICS OF MSR	24

4. CATALYSTS	27
4.1. CATALYST CLASSIFICATIONS	30
4.2. HETEROGENEOUS CATALYSTS	31
4.2.1. HETEROGENEOUS CATALYSTS PREPARATION	32
4.2.2. SUPPORTED CATALYSTS	34
4.2.2.1. ORDERED MESOPOROUS MATERIALS.....	35
4.2.2.2. ORDERED MESOPOROUS CARBON MATERIALS	38
4.3. MSR CATALYSTS	43
5. MICROWAVE-ASSISTED MSR	47
5.1. HISTORY OF MICROWAVE	47
5.2. MICROWAVE HEATING.....	48
5.3. MICROWAVE APPLICATORS.....	52
5.4. MICROWAVE APPLICATIONS	54
5.4.1. MICROWAVE-ASSISTED CHEMICAL SYNTHESIS	54
5.4.2. MICROWAVE AND HETEROGENEOUS CATALYSIS	55
5.4.2.1. MICROWAVE-ASSISTED HYDROGEN PRODUCTION	57
5.5. OBJECTIVES OF THE STUDY	59
6. EXPERIMENTAL	61
6.1. MATERIAL PREPARATION	61
6.1.1. SBA-15 SYNTHESIS	61
6.1.2. CMK-3 SYNTHESIS	62
6.1.3. METAL LOADING INTO CMK-3	64
6.2. MATERIAL CHARACTERIZATION.....	66
6.2.1. NITROGEN ADSORPTION/DESORPTION	66

6.2.2. X-RAY DIFFRACTION (XRD)	67
6.2.3. THERMOGRAVIMETRIC ANALYSIS (TGA)	67
6.2.4. RAMAN SPECTROSCOPY	67
6.2.5. SCANNING ELECTRON MICROSCOPY (SEM)	67
6.3. ACTIVITY TESTS FOR MSR PROCESS	68
6.3.1. HYDROGEN PRODUCTION SYSTEM	68
6.3.1.1. CONVENTIONALLY-HEATED REACTOR SYSTEM	68
6.3.1.2. FOCUSED-MICROWAVE HEATED REACTOR SYSTEM.....	70
6.3.2. EXPERIMENTAL PROCEDURE.....	71
7. RESULTS AND DISCUSSION	73
7.1. CHARACTERIZATION RESULTS OF CATALYST	73
7.1.1. CHARACTERIZATION RESULTS OF THE SUPPORT	73
7.1.1.1. XRD RESULTS	74
7.1.1.2. RAMAN SPECTROSCOPY RESULTS	76
7.1.1.3. N ₂ ADSORPTION/DESORPTION RESULTS.....	76
7.1.1.4. TGA RESULTS	79
7.1.1.5. SEM RESULTS	80
7.1.2. CHARACTERIZATION RESULTS OF THE METAL-LOADED SUPPORT.....	84
7.1.2.1. XRD RESULTS	84
7.1.2.2. N ₂ ADSORPTION/DESORPTION RESULTS.....	88
7.1.2.3. TGA RESULTS	91
7.1.2.4. SEM RESULTS	91
7.2. CATALYTIC ACTIVITY RESULTS	98

7.2.1. CONVENTIONALLY-HEATED REACTOR SYSTEM	98
7.2.1.1. CATALYST CALCINATION TEMPERATURE EFFECT ON METHANOL CONVERSION AND HYDROGEN YIELD	99
7.2.1.2. EFFECT OF COPPER/ZINC RATIO ON METHANOL CONVERSION AND HYDROGEN YIELD	105
7.2.1.3. EFFECT OF TOTAL METAL LOADING ON METHANOL CONVERSION AND HYDROGEN YIELD	107
7.2.1.4. EFFECT OF REACTION TEMPERATURE ON METHANOL CONVERSION AND HYDROGEN YIELD	109
7.2.2. FOCUSED-MICROWAVE HEATED REACTOR SYSTEM	113
8. CONCLUSIONS	117
REFERENCES	121
APPENDICES	
A. CATALYST LOADING CALCULATIONS.....	131
B. XRD DATA AND CRYSTALLITE SIZE CALCULATION.....	133
C. EDX RESULTS OF THE CARBON MATERIALS.....	139
D. GC CALCULATION FACTORS	141
E. CALCULATION OF THE MOLE FRACTION OF EACH MSR PRODUCT, METHANOL CONVERSION, AND HYDROGEN YIELD	143

LIST OF TABLES

TABLES

Table 2.1. Specific energy of fuels.....	6
Table 2.2. Properties of elemental hydrogen.	8
Table 2.3. Non-reforming hydrogen production technologies.....	10
Table 2.4. Comparison of hydrocarbon reforming technologies	12
Table 2.5. Fuel cell types summary.	15
Table 3.1. Properties of methanol.	20
Table 3.2. The general operating conditions of the MSR reaction.	22
Table 4.1. History of the catalysis of industrial processes.....	29
Table 4.2. Unit operations in heterogeneous catalyst preparation	33
Table 4.3. Possible pathways of the ordered mesoporous materials synthesis.	37
Table 4.4. The ordered mesostructured carbon materials (CMK-n).	41
Table 4.5. MSR catalysts literature survey.	44
Table 5.1. The microwave development and evolution history.	48
Table 5.2. Energetic comparison of different bonds and microwave radiation at 2.45 GHz.	49
Table 5.3. Loss factors ($\tan \delta$) of different materials at 2.45 GHz and 20 °C.....	50
Table 5.4. Loss factors ($\tan \delta$) of the carbon materials at 2.45 GHz and 20 °C.....	51
Table 5.5. Comparison of the conventional and microwave heating methods.	52
Table 5.6. A survey on reported microwave-assisted chemical processes.	55
Table 6.1. Investigated parameters in the synthesis of CMK-3.....	64
Table 6.2. The studied parameters and catalysts used for the MSR reaction in the conventionally-heated reactor.	65
Table 6.3. The required amount of metal precursors for 0.3 g CMK-3.	65
Table 6.4. GC parameters and their setting values.....	69
Table 6.5. Temperature program for liquid and gas analyses	69

Table 7.1. Physical properties of the synthesized CMK-3 materials and the silica template.....	79
Table 7.2. Copper crystallite sizes in the synthesized catalysts with different calcination temperatures	86
Table 7.3. Physical properties of the synthesized catalysts.	90
Table 7.4. EDX results summary of the synthesized catalysts	98
Table 7.5. Average hydrogen production results from the catalysts with different Cu/Zn ratios.	107
Table 7.6. Average hydrogen production results from the catalysts with different total metal loading amount.	109
Table 7.7. Average hydrogen production results for both the conventionally-heated and the focused-microwave heated reactor systems at different temperatures (P=1 atm, H ₂ O/CH ₃ OH=1, Catalyst: 18.75Cu6.25Zn/CMK-3/300).....	115
Table 7.8. The focused-microwave reactor system energy consumption.....	116
Table B.1. PDF card for C.....	133
Table B.2. PDF card for CuO	134
Table B.3. PDF card for ZuO	136
Table B.4. PDF card for Na ₂ CO ₃	137

LIST OF FIGURES

FIGURES

Figure 1.1. Global surface temperature change.	1
Figure 1.2. CO ₂ concentration in the atmosphere and emissions from fuel combustion.	2
Figure 1.3. Major proved oil and gas reserves locations.....	3
Figure 2.1. Present unsustainable energy system.....	5
Figure 2.2. Hydrogen energy system introduction effect on the (a) environment and (b) global economy.	7
Figure 2.3. Schematic overview of hydrogen utilization in chemical production.	9
Figure 2.4. Schematic representation of a fuel cell	14
Figure 2.5. The fuel cell evolution and development timeline.	16
Figure 3.1. Methanol molecular structure.	20
Figure 3.2. Required start-up energy of various feedstocks.....	21
Figure 3.3. Equilibrium product distribution of MSR (1 atm, MeOH/H ₂ O molar ratio of 1).	25
Figure 4.1. The timeline of catalysis knowledge development.....	28
Figure 4.2. Classification of the catalysts	30
Figure 4.3. A heterogeneous catalysis at various levels.....	31
Figure 4.4. Two main mechanisms of heterogeneous catalysis: (a) Langmuir-Hinshelwood , (b) Eley-Rideal.....	32
Figure 4.5. Examples of nanoporous materials showing pore size domains.	35
Figure 4.6. Synthesis of different types of porous carbon materials by nanocasting method.....	38
Figure 4.7. Schematic representation of nanocasting concept	39
Figure 4.8. A schematic diagram of the ordered mesoporous carbon materials synthesis strategy.	40

Figure 4.9. (a) N ₂ adsorption-desorption isotherm at 77 K and pore size distribution of CMK-3 and SBA-15, (b) TEM images of highly ordered mesoporous channels of CMK-3.....	43
Figure 5.1. The electromagnetic spectrum.	49
Figure 5.2. Research papers published related to microwave-assisted processes of the carbon materials.....	51
Figure 5.3. The wave pattern created by mono-mode applicators.....	53
Figure 5.4. The mono-mode applicators heating mechanism.....	53
Figure 5.5. The multi-mode applicators heating mechanism.	54
Figure 6.1. Scheme of SBA-15 synthesis.	62
Figure 6.2. Scheme of CMK-3 synthesis.....	63
Figure 6.3. Conventionally-heated reactor system.	70
Figure 6.4. Microwave-focused reactor system.	71
Figure 7.1. (a)Low-angle and (b)enlarged low-angle XRD patterns of the synthesized SBA-15.	75
Figure 7.2. XRD patterns of the synthesized CMK-3 materials; (a) low angle and (b)wide-angle.	75
Figure 7.3. Raman spectra of the synthesized CMK-3 materials with different silica removing agents.....	76
Figure 7.4. N ₂ adsorption/desorption isotherms of the synthesized materials.....	78
Figure 7.5. Pore size distributions of SBA-15 and CMK-3 materials.	78
Figure 7.6. TGA results of the CMK-3 materials, performed under air.....	80
Figure 7.7. SEM images of SBA-15 at a)20000X and b)50000X magnifications. ...	81
Figure 7.8. SEM images of a)CMK-3/1-NaOH, b)CMK-3/1-HF, c)CMK-3/2-NaOH, d)CMK-3/2-HF, at 100000X magnification.	82
Figure 7.9. EDX analysis results of (a) CMK-3/1-NaOH and (b) CMK-3/1-HF.....	83
Figure 7.10. XRD patterns of all synthesized catalysts.	85
Figure 7.11. XRD patterns of the catalysts with different calcination temperatures.	86
Figure 7.12. XRD patterns of the catalysts with different Cu/Zn ratio.	87

Figure 7.13. XRD patterns of the catalysts with different total metal loading amount	88
Figure 7.14. N ₂ adsorption/desorption isotherms of the catalysts.....	89
Figure 7.15. Pore size distribution of the catalysts.	90
Figure 7.16. TGA results of the synthesized catalysts.....	91
Figure 7.17. (a) SEM image and (b) back scattered electron image of fresh 12Cu6Zn/CMK-3/300 at the magnification of 10000X.....	92
Figure 7.18. (a) SEM image and (b) back scattered electron image of fresh 12Cu6Zn/CMK-3/450 at the magnification of 10000X.....	93
Figure 7.19. EDX spectrum of fresh (a) 12Cu6Zn/CMK-3/300 and (b) 12Cu6Zn/CMK-3/450.....	93
Figure 7.20. SEM images at the magnifications of (a) 20000X and (b) 50000X, and (c) back scattered electron image of fresh 9Cu9Zn/CMK-3/300 at 20000X magnification.....	94
Figure 7.21. SEM images at the magnifications of (a) 20000X, (b) 50000X, (c) 100000X, and (d) back scattered electron image of fresh 13.5Cu4.5Zn/CMK-3/300 at 20000X magnification.....	95
Figure 7.22. SEM images at the magnifications of (a) 20000X, (b) 50000X, (c) 100000X, and (d) back scattered electron image of fresh 18.75Cu6.25Zn/CMK-3/300 at 20000X magnification.....	96
Figure 7.23. EDX spectrums of fresh (a) 9Cu9Zn/CMK-3/300, (b) 13.5Cu4.5Zn/CMK-3/300, and (c) 18.75Cu6.25Zn/CMK-3/300.....	97
Figure 7.24. Product distribution of two reproducible MSR experiments with the 12Cu6Zn/CMK-3/300 catalyst (P=1 atm,T=250°C,H ₂ O/CH ₃ OH=1).	100
Figure 7.25. Methanol conversion of two reproducible MSR experiments with the 12Cu6Zn/CMK-3/300 catalyst (P=1 atm,T=250°C,H ₂ O/CH ₃ OH=1).	100
Figure 7.26. Hydrogen yield of two reproducible MSR experiments with the 12Cu6Zn/CMK-3/300 catalyst (P=1 atm,T=250°C,H ₂ O/CH ₃ OH=1).	101
Figure 7.27. Product distribution of two reproducible MSR experiments with the 12Cu6Zn/CMK-3/450 catalyst (P=1 atm, T=250°C, H ₂ O/CH ₃ OH=1).	102

Figure 7.28. Methanol conversion of two reproducible MSR experiments with the 12Cu6Zn/CMK-3/450 catalyst (P=1 atm, T=250°C, H ₂ O/CH ₃ OH=1).....	102
Figure 7.29. Hydrogen yield of two reproducible MSR experiments with the 12Cu6Zn/CMK-3/450 catalyst (P=1 atm, T=250°C, H ₂ O/CH ₃ OH=1).....	103
Figure 7.30. Methanol conversions of the 12Cu6Zn/CMK-3 catalysts synthesized at different calcination temperatures (P=1 atm, T=250°C, H ₂ O/CH ₃ OH=1).....	104
Figure 7.31. Hydrogen yields of the 12Cu6Zn/CMK-3 catalysts synthesized at different calcination temperatures (P=1 atm, T=250°C, H ₂ O/CH ₃ OH=1).....	104
Figure 7.32. Effect of Cu/Zn ratio on the methanol conversion (P=1 atm, T=250°C, H ₂ O/CH ₃ OH=1).....	106
Figure 7.33. Effect of Cu/Zn ratio on the hydrogen yield (P=1 atm, T=250°C, H ₂ O/CH ₃ OH=1).....	106
Figure 7.34. Effect of total metal loading amount on methanol conversion (P=1 atm, T=250°C, H ₂ O/CH ₃ OH=1).....	108
Figure 7.35. Effect of total metal loading amount on hydrogen yield (P=1 atm, T=250°C, H ₂ O/CH ₃ OH=1).....	108
Figure 7.36. Effect of reaction temperature on the average product distribution (P=1 atm, H ₂ O/CH ₃ OH=1, Catalyst: 18.75Cu6.25Zn/CMK-3/300).....	110
Figure 7.37. Effect of reaction temperature on the average methanol conversion (P=1 atm, H ₂ O/CH ₃ OH=1, Catalyst: 18.75Cu6.25Zn/CMK-3/300).....	111
Figure 7.38. Effect of reaction temperature on the average hydrogen yield (P=1 atm, H ₂ O/CH ₃ OH=1, Catalyst: 18.75Cu6.25Zn/CMK-3/300).....	112
Figure 7.39. Average product distribution at different temperatures obtained from the focused-microwave heated reactor system (P=1 atm, H ₂ O/CH ₃ OH=1, Catalyst: 18.75Cu6.25Zn/CMK-3/300)	113
Figure 7.40. Average methanol conversion at different temperatures obtained from the focused-microwave heated reactor system (P=1 atm, H ₂ O/CH ₃ OH=1, Catalyst: 18.75Cu6.25Zn/CMK-3/300)	114

Figure 7.41. Average hydrogen yield at different temperatures obtained from the focused-microwave heated reactor system (P=1 atm, H ₂ O/CH ₃ OH=1, Catalyst: 18.75Cu6.25Zn/CMK-3/300).....	114
Figure C.1. EDX results of a)CMK-3/2-NaOH, b)CMK-3/2-HF.....	139

CHAPTER 1

INTRODUCTION

Earth is the only known planet in the galaxy that has the appropriate conditions of living. Unfortunately, it is suffering from many problems that need solution and immediate action. Climate change is one of the major dangers threatening our planet. Figure 1.1 demonstrates the change in global surface temperature with respect to the average temperature of the 20th century.

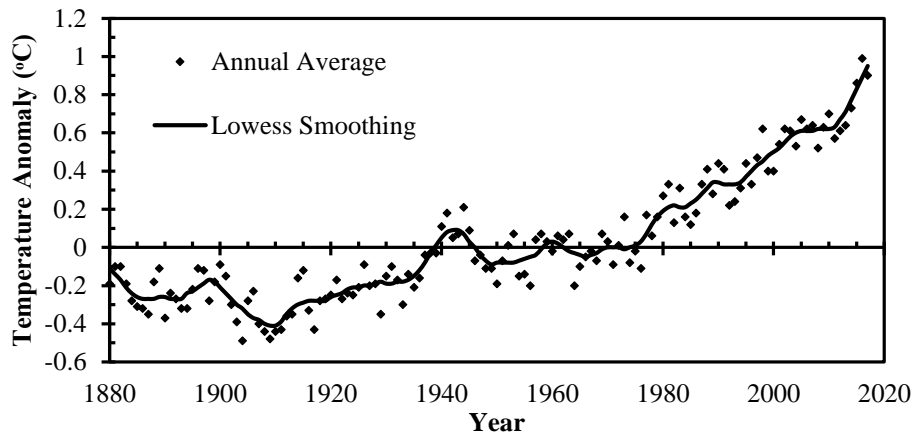


Figure 1.1. Global surface temperature change, data adapted from [1].

It is clear that surface temperature of earth is increasing dramatically with years. In particular, a new record of high annual average temperature was set in 2016 (14.85 °C) [1]. By 2018, all the years of the 20th century are sorted among the 18 warmest years (along with 1998) [2]. During the last 100 years, the earth's climate has become warmer around 1°C. Even such a small change in the earth temperature causes big changes, such as ices melting, rising the oceans and changing plants' life cycles [3].

Many scientists attribute the climate change mainly to emissions of some gases, such as CO₂, water vapor, methane, chlorofluorocarbons (CFCs), etc., called greenhouse gases. These substances accelerate the greenhouse effect of earth which causes the atmosphere temperature rise. Combustion of fossil fuels, which is still the main energy source of vehicles, emits a great deal of CO₂ due to the irreversible conversion of carbon into carbon dioxide. CO₂ emission, the main cause of the greenhouse effect and thus the climate change, has been increasing (Figure 1.2).

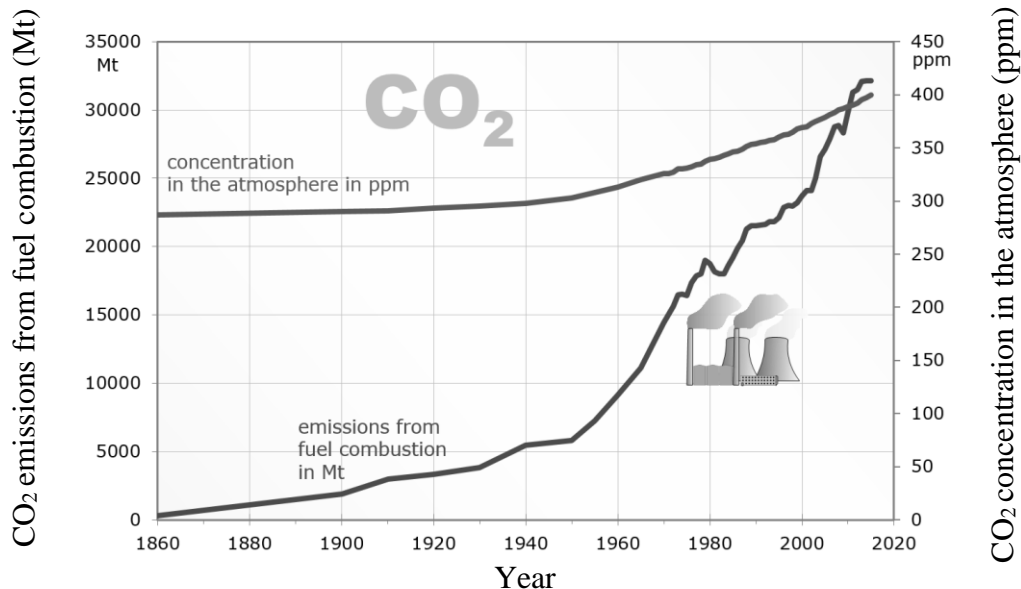


Figure 1.2. CO₂ concentration in the atmosphere and emissions from fuel combustion, reprinted from [4].

As well as the greenhouse gas emissions, combustion of the fossil fuels produces harmful pollutants for both public health and environment, such as volatile organic compounds (VOCs), NO_x, SO_x and CO [5].

On the other hand, fossil fuels, which are the nature gift given to humankind undoubtedly, are being consumed quickly. As a result, these non-renewable sources of energy are remarkably diminished. Furthermore, the fossil fuel sources are not only limited, but also geographically concentrated. As can be seen from Figure 1.3, the

fossil fuel reserves are not distributed in the world equally. According to OPEC estimations by 2017, over 81% of proved oil reserves are located in OPEC members countries [6]. In a similar fashion, estimations reveal that only Middle East contains around 43% of the world proved natural gas sources.

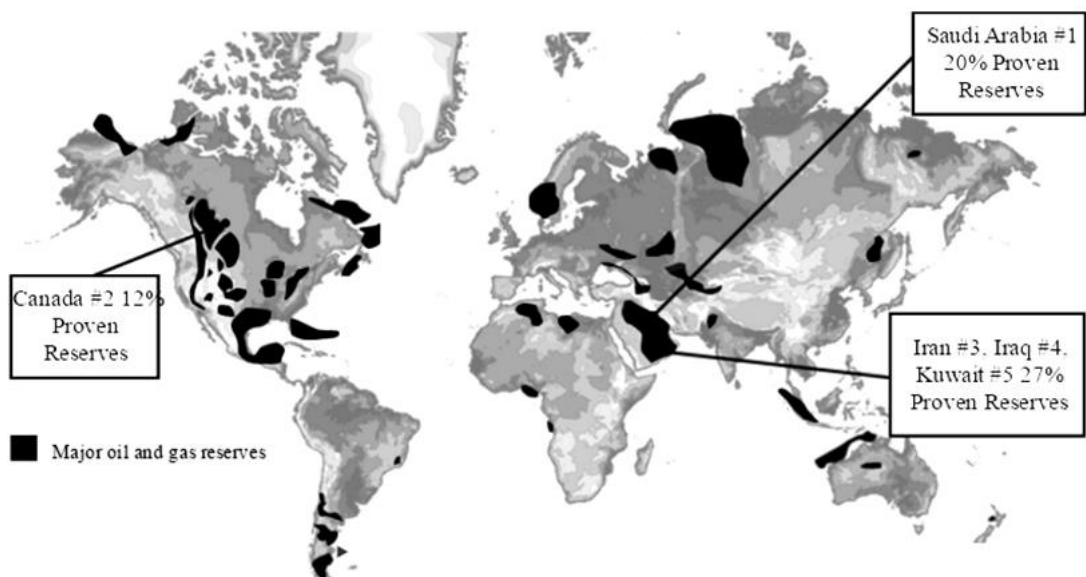


Figure 1.3. Major proved oil and gas reserves locations, reprinted from [7].

Consequently, it seems vital and urgent to find sustainable, unlimited, and environmentally friendly sources of energy to meet increasing need of energy.

One of the most promising energy carriers is hydrogen which makes the fuel cell operation feasible. Fuel cells are attractive systems operating with hydrogen and providing simple, cheap, high efficient and low or zero emission energy. Their broad application area consists of: automobiles, bicycles, backup power, space, and many more [8]. Hydrogen can be produced from a wide range of feedstocks and techniques. Recently, researchers have concentrated on developing onboard fuel cell systems to design cars driven by the fuel cell generated electric power. Steam reforming of methanol is an appropriate technique for this purpose due to the mild operation

conditions. Although, conversion of the carbon atom present in methanol molecule to either CO or CO₂ is inevitable, CO₂ emission of this reaction is less than that of common internal combustion engines [9]. Moreover, proper design of the catalyst used in methanol steam reforming reaction helps to suppress CO formation which deactivates fuel cell electrodes catalyst sites [10].

The recent approach to catalysis is nanocatalysis which is growing rapidly. It involves loading nanoparticles of active components onto nanostructured supports with high surface area. The most important properties of a catalytic process are the catalyst activity and selectivity, which can be both enhanced by the structure of support material. Nanostructured carbon materials are being studied widely due to their unique properties and capability to be used as catalyst support as well as many other applications.

An efficient and relatively new heating method for heating the processes is microwave heating. Focused-microwave process provides a uniform temperature distribution with a low energy input compared to the conventional heating methods, which are mainly electrical. The microwave heating source is electromagnetic waves which provide specific heating based on the characteristics of materials, unlike the conventional heating methods.

The present study focuses on the production of CO-free hydrogen with high yield from steam reforming of methanol. By nature, this process is endothermic and requires heat to proceed. For this purpose, the microwave heating was also employed, besides the common electrical heating; not only to provide a uniform temperature distribution, but also to decrease the process energy input.

CHAPTER 2

HYDROGEN: TOWARDS A SUSTAINABLE ENERGY FUTURE

Hydrogen itself is not a primary source of energy; it could be considered as an energy carrier like electricity in the future, which can be generated from various sources. In other words, hydrogen contains energy which can be converted to clean and efficient energy without releasing any harmful or pollutant emissions. Nowadays, utilization of fossil fuels is the main way to supply the world energy need. As Figure 2.1 illustrates, the current energy system is useful as long as the environment absorbs the pollutants. Therefore, the fossil fuels cannot be regarded sustainable.

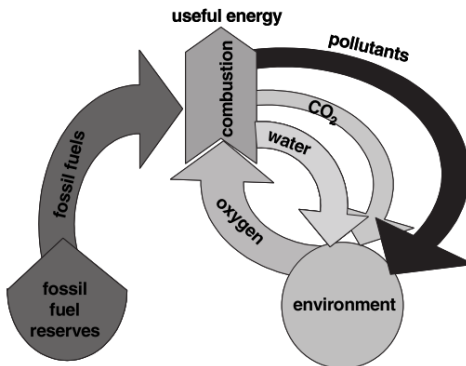


Figure 2.1. Present unsustainable energy system, reprinted from [11].

Hydrogen is the most probable energy carrier of the future due to its capability of clean burning and being producible from a wide range of renewable sources. Besides, hydrogen has the highest specific energy among the other fuels (Table 2.1) [12]. These properties make hydrogen a permanent sustainable energy carrier. Hydrogen is

considered sustainable, as long as it is produced from renewable and non-fossil based feedstocks.

Table 2.1. *Specific energy of fuels [12].*

Fuel	Specific energy (kW/kg)
<i>Liquid hydrogen</i>	33.3
<i>Hydrogen (at 200 bar)</i>	33.3
<i>Liquid natural gas</i>	13.9
<i>Natural gas (at 200 bar)</i>	13.9
<i>Petrol</i>	12.8
<i>Diesel</i>	12.6
<i>Coal</i>	8.2
<i>Methanol</i>	5.5
<i>Wood</i>	4.2
<i>Electricity (Li-ion battery)</i>	0.55

In spite of the fact that hydrogen utilization technologies are not mature enough so far, no major obstacle impeding widespread usage of hydrogen. Although it seems that utilization of the hydrogen energy system is important and effective, it is still difficult due to lack of established infrastructure. Figure 2.2 demonstrates how the hydrogen energy system influences the environment and global economy. It is clear that the earlier this transition begins, the more investments can be done in a new energy system establishment project.

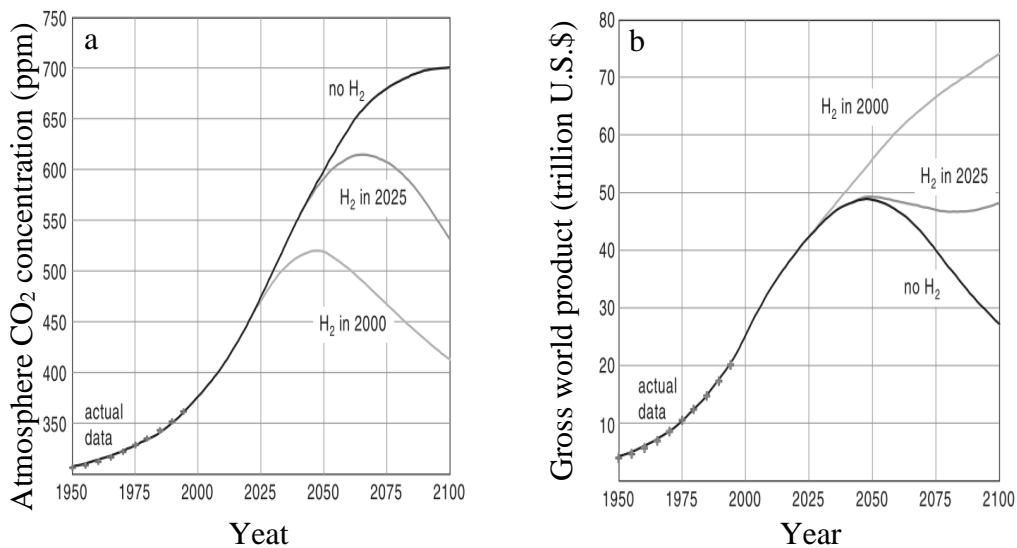


Figure 2.2. Hydrogen energy system introduction effect on the (a) environment and (b) global economy [11].

2.1. HISTORY AND PROPERTIES OF HYDROGEN

Hydrogen is composed of two Greek words; “hydro” and “genes” which together mean “water forming” [13]. The alchemist Paracelsus noticed flammable bubble formation by adding iron filings to sulfuric acid in the early 1500s. Robert Boyle also observed the same thing in 1671, but he did not discover hydrogen. Finally, Henry Cavendish collected the bubbles and concluded that they were different from other known gases in 1766. Later, he could show that burning of hydrogen results in water production which put an end to the common belief that water was an element [14]. It was named by Antoine Lavoisier in 1783 [15].

The most stable form of hydrogen atom has 1 proton, 1 neutron and 1 electron, called protium. There are two other isotopes, deuterium (D, with 2 neutrons) and tritium (T, with 3 neutrons) discovered in 1932 and 1934, respectively [13].

Hydrogen is the simplest and also most plentiful element in the universe. Sun, Jupiter and most of the stars are composed of hydrogen [14]. On earth, it is found in the form of water (around 1.08×10^5 mg/l) [13]. Its concentration in the atmosphere is less than 1 ppm by volume, since hydrogen atoms leave the atmosphere into space after entering

the atmosphere [14]. At the earth condition, hydrogen is present in the form of diatomic gaseous molecule (H_2). It is a colorless, odorless, tasteless, nontoxic, nonmetallic, and highly flammable gas. Some properties of hydrogen are tabulated in Table 2.2.

Table 2.2. Properties of elemental hydrogen [14,16].

Property	Value	Property	Value
<i>Atomic number</i>	1	<i>Thermal conductivity*</i> (W/m.K)	0.182
<i>Relative atomic mass</i>	1.008	C_p^* (J/g.K)	14.29
<i>State at 20°C</i>	gas	C_v^* (J/g.K)	10.16
<i>Electron configuration</i>	$1s^1$	<i>Diffusion coef. in air*</i> (cm ² /s)	0.61
<i>Molecular weight (g/mol)</i>	2.02	<i>Enthalpy*</i> (kJ/kg)	3858.1
<i>Melting point (°C)</i>	-259.16	<i>Entropy*</i> (kJ/kg)	53.14
<i>Boiling point (°C)</i>	-252.879	<i>Internal energy*</i> (kJ/kg)	2648.3
<i>Density*</i> (kg/m ³)	0.08375	<i>Flame temp. § (°C)</i>	2045
<i>Specific volume*</i> (m ³ /kg)	11.94	<i>Flammable range § (°C)</i>	4.0-75
<i>Viscosity*</i> (g/cm.s)	8.81×10^{-6}	<i>Ignition energy § (J)</i>	2×10^{-5}
<i>CAS number</i>	133-74-0	<i>Auto ignition temp. § (°C)</i>	500-585

* measured at normal temperature and pressure; 20 °C and 1 atm

§measured in the air

2.2. APPLICATIONS

Hydrogen is widely used to produce chemicals in industry. The mixture of H_2 and CO , called syngas, makes industrial synthesis of many chemicals possible, e.g. alcohols,

aldehydes, alkenes [17]. The main use of hydrogen is ammonia production. Around two thirds of the world hydrogen production is just used to convert ammonia by the Haber-Bosch process. Catalytic hydrogenation of organic compounds is one of the other major applications of hydrogen. There are lots of examples in this area; hydrogenating unsaturated vegetables and animal oils, reducing aldehydes and esters to alcohols, nitro compounds to amines etc [18]. Figure 2.3 represents a more comprehensive view of hydrogen usage for chemical production.

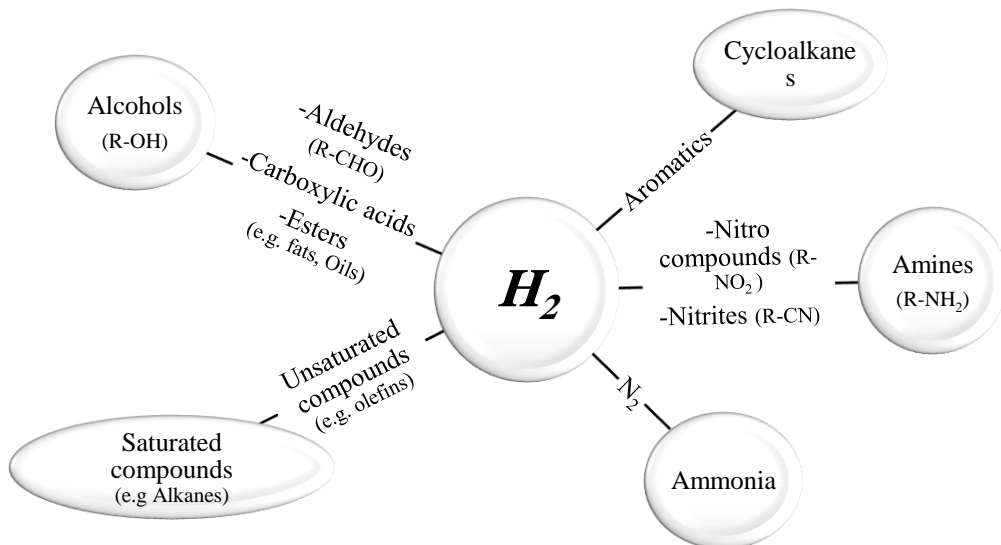


Figure 2.3. Schematic overview of hydrogen utilization in chemical production [17].

In addition, hydrogen is a very useful and important processing agent in petroleum refining operations, mainly in hydrotreating units. Various types of hydrotreating processes are operated in a refinery, such as hydrodesulphurization, hydroisomerisation, dearomatization, and hydrocracking [19]. Apart from the abovementioned applications, using hydrogen molecule as an energy carrier is also of

high importance. The major areas of hydrogen energy application are: power generation, transportation, navigation, and space programs [20].

2.3. PRODUCTION TECHNIQUES

Hydrogen can be produced using different techniques that some of them are commercial, while some are still developing. These techniques can be divided into two main categories; fuel processing and non-reforming methods. The main idea of fuel processing methods is to obtain the hydrogen stream, as the product, from a hydrogen-containing material. The following techniques are considered as fuel processing methods: Hydrocarbon reforming, pyrolysis, plasma reforming, and aqueous phase reforming. The non-reforming methods are summarized in Table 2.3.

Table 2.3. *Non-reforming hydrogen production technologies [5]*.

H₂ from biomass	<ul style="list-style-type: none">• <i>Biomass gasification</i>• <i>Biological hydrogen</i><ul style="list-style-type: none">– <i>Direct photolysis</i>– <i>Dark fermentation</i>– <i>Photo-fermentative processes</i>– <i>Microbial electrolysis cells</i>
H₂ from water	<ul style="list-style-type: none">• <i>Electrolysis</i><ul style="list-style-type: none">– <i>Alkaline electrolyzer</i>– <i>Proton exchange membrane electrolyzer</i>– <i>Solid oxide electrolysis cells</i>• <i>Thermochemical water splitting</i>• <i>Photoelectrolysis</i>

2.3.1. HYDROCARBON REFORMING

In case of using a hydrocarbon as the fuel, three techniques are available: steam reforming, partial oxidation, and autothermal reforming.

Steam reforming, which is one of the most developed and commercialized technologies of hydrogen production, involves reaction (2.1). In partial oxidation method (POX), partial combustion of the fuel produces hydrogen (reaction 2.2). Autothermal reforming (reaction 2.3) is a combination of both partial oxidation and steam reforming processes in order to supply required heat and increase hydrogen production. Reaction (2.4), which is called water-gas shift (WGS) reaction, the coke formation reaction (reaction 2.5), and the methanation reaction (reaction 2.6) are observed at high operating temperatures and in the presence of CO. The operating conditions of the process and the catalyst used strongly influence the coke formation. Steam reforming of methane is the most industrially-utilized technique to produce hydrogen so far. More than 50% of total global hydrogen consumption is supplied by this technique which has the conversion up to 85% [5, 20, 21]. A brief comparison between these three methods is shown in Table 2.4.

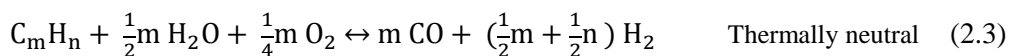
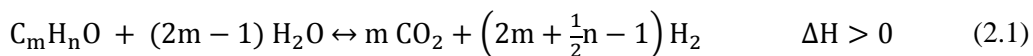


Table 2.4. Comparison of hydrocarbon reforming technologies [5].

Technology	Advantage	Disadvantage
Steam Reforming	<i>The highest industrial experience</i> <i>No need of oxygen</i> <i>The lowest operating temperature</i> <i>The highest H₂/CO ratio</i>	<i>The highest emissions</i>
Partial Oxidation (POX)	<i>No need of catalyst</i> <i>Low methane formation</i>	<i>Low H₂/CO ratio</i> <i>Very high process temperature</i> <i>Soot formation</i> <i>Process complexity</i>
Autothermal Reforming	<i>Low methane formation</i> <i>Lower temperature compared to POX</i>	<i>Limited industrial experience</i> <i>Requires air or oxygen</i>

2.3.2. PYROLYSIS

Pyrolysis is based on decomposition of a hydrocarbon to hydrogen and carbon in absence of water or oxygen. There is a bright future ahead of this method due to its remarkable advantages, such as less CO and CO₂ emissions, fuel flexibility, and simplicity. However, being prone to coke formation is one of the few challenges with this technology [5].

2.3.3. PLASMA REFORMING

An ionized gas generated by electrical discharges or heat is plasma. Plasma reforming method, which has the overall reaction network identical to the conventional reforming process, is still a developing and immature technology. In this method, the plasma provides the required energy and free radicals. Minimal cost, fuel flexibility, high efficiency, and low operating temperature are the reasons making plasma reforming an attractive technology [5, 21].

2.3.4. AQUEOUS PHASE REFORMING

Another developing method of hydrogen production is aqueous phase reforming. In this method, there is no need to vaporize the fuel and water. So it can be performed on the materials which are not vaporizable, such as glucose. Generally, the fuel used in this method is selected from carbohydrates or oxygenated hydrocarbons. Furthermore, the operating temperature is low [5].

2.4. FUEL CELLS

As discussed earlier, there is almost no doubt that a transition from environmentally not friendly and non-renewable energy sources to clean and sustainable ones is highly necessary. Hydrogen is a promising energy carrier that can be utilized in a high-efficiency power generation system with low CO₂ emissions. One of the most favored systems is fuel cell system which is able to generate power for both transportation and stationary power distributing applications. Fuel cell systems convert the chemical energy of hydrogen, the fuel, directly to electricity. A fuel cell, shown in Figure 2.4, generates direct current (DC) electricity through a simple and low-temperature electrochemical reaction (2.7). No moving part in the fuel cell system, as well as the single step process, adds simplicity to this technology. Although, both fuel cell systems and batteries generate DC electricity through electrochemical reactions, an important difference is the fuel cell can generate *continuous* power as long as it is fed by the required reactants, whereas the batteries store the power.



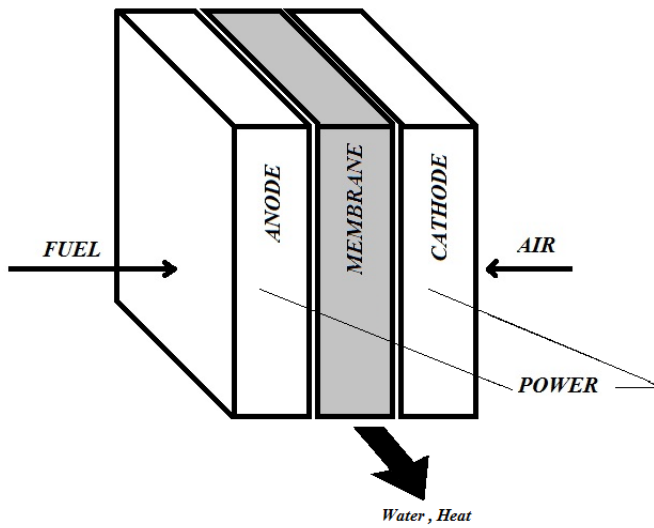


Figure 2.4. Schematic representation of a fuel cell [8].

To run the fuel cell, hydrogen can be supplied either in a form of a gaseous mixture (e.g. H₂ with CO₂, NO etc.) or as hydrocarbons (such as natural gas, methane or methanol). However, burning hydrocarbons results in unfavorable CO₂ emission. The required oxygen can be easily supplied from the ambient air. The only product of the fuel cell operation is water. It can be claimed that the fuel cell operation is virtually free of pollutant emissions, even oxides of nitrogen do not exist due to much lower operating temperature than that of internal combustion engines.

There are several types of fuel cells, but with the same design fundamentals. They are composed of two electrodes (anode and cathode) separated by an electrolyte or membrane. The fuel and air (or oxygen) are fed into the anode and the cathode, respectively. The catalysts loaded on the electrodes catalyze the electrochemical reaction. The needed ions for the reaction are transported via the medium between electrodes. There is also an external circuit to conduct the excess ions and hence the electrical power is provided. Fuel cell classification is based on the nature of their electrolyte which further determines their application area and operating conditions

[8, 12, 20, 22]. Table 2.5 summarizes the different fuel cell types and presents applications and power ranges of each type.

Table 2.5. *Fuel cell types summary [12].*

Fuel cell type	Operating T (°C)	Applications	Power range (kW)
<i>Proton exchange membrane (PEM)</i>	60-110	<i>Mobile, portable</i>	0.01-250
<i>Alkaline</i>	70-130	<i>Space, military, mobile</i>	0.1-50
<i>Direct methanol</i>	60-120	<i>Mobile, portable</i>	0.001-100
<i>Phosphoric acid</i>	175-210	<i>Medium to large-scale power generation</i>	50-1000
<i>Molten carbonate</i>	550-650	<i>Large-scale power generation</i>	200-100000
<i>Solid oxide</i>	500-1000	<i>Medium to large-scale power generation, vehicle auxiliary power, off-grid power</i>	0.5-2000

The first fuel cell was developed by Sir W. Grove in 1842. He produced electrical energy by means of combining hydrogen and oxygen. Despite the theoretical efforts of W. F. Ostwald to understand the basics of the fuel cell operation, it had remained as a scientific curiosity for more than a century till Francis T. Bacon, an English engineer, started working on the fuel cell in 1939. In 1952, he managed to construct a 5 kW fuel cell stack. The first practical applications of the fuel cell go back to U.S space programs. Gemini and Apollo programs utilized fuel cell systems successfully in order to supply power required for life support, guidance, and communications in the 1960s. Since the 1990s, the fuel cell companies have been developing and demonstrating fuel cell potential in many application areas, such as vehicles, bicycles,

golf carts, utility vehicles, backup power, portable power, boats, and underwater vehicles [8]. Figure 2.5 depicts the fuel cell evolution timeline.

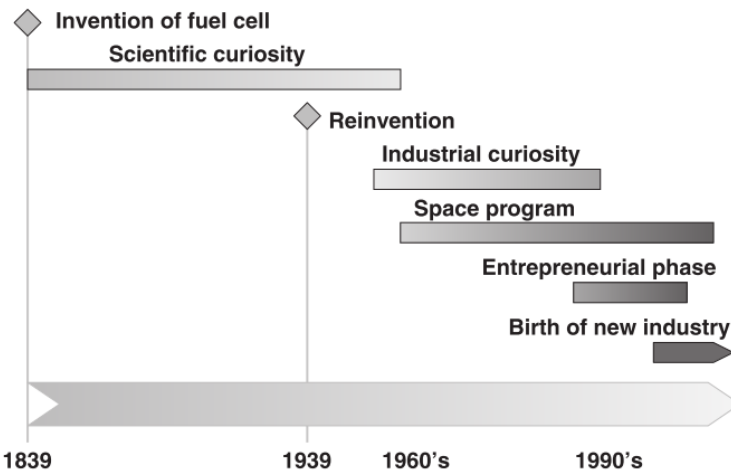


Figure 2.5. The fuel cell evolution and development timeline, reprinted from [8].

2.5. ON-BOARD FUEL CELLS

Nowadays, transportation mostly relies on the vehicles driven by petroleum products. Immense researches and vast investments have been done on petroleum products-driven vehicles for many decades. Besides the high emissions, the efficiency of these cars is still not high (around 25%). These major drawbacks of combustion engines do not exist in the fuel cell engine. A hydrogen fuel cell engine has an efficiency up to 65% and in case of utilizing the generated heat, the efficiency of 85% may be achieved [12]. Hydrogen supply can be in form of either on-board storage or on-board production. On-board storage (so-called direct hydrogen) is produced and stored elsewhere, while on-board production of hydrogen is done inside the system. In spite of no harmful emissions from the fuel cell and hence the vehicle, a few challenges prevent applying direct H₂ on-board storage tank in order to feed the fuel cell vehicles; such as H₂ storage and handling complexity, lack of refueling infrastructure, and high

weight of on-board H₂ tank (~5-6 times higher than gasoline and/or diesel tanks). Accordingly, on-board hydrogen production is considered as an alternative in order to overcome these challenges. It involves on-board reforming of a liquid hydrocarbon. Convenient fuel storage and handling and also better fuel distribution infrastructure are its advantages [23, 24]. However, CO and CO₂ emissions are inevitable as by-products of the hydrocarbon reforming and should be minimized. CO₂ increases the greenhouse effect and CO concentration higher than 100 ppm can easily poison the fuel cell electrodes by occupying the active sites [25].

Current market is very competitive with high demands and expectations that the on-board fuel cell vehicles must compete especially with internal combustion engines. Although these cars can travel between 400-600 km and generate 100 kW, there is still a long way to go to achieve the consumers' satisfaction. The current market demands can be summarized in the following parameters; safety, initial cost, reliability, ambient operating temperature, refueling time and reliability [12, 20, 23].

CHAPTER 3

METHANOL STEAM REFORMING

As is discussed in Chapter 2 (section 2.3), steam reforming of a liquid hydrocarbon is the most favorable technique to produce the highest yield of hydrogen. There are several hydrocarbons to produce hydrogen, such as methanol, ethanol, dimethylether (DME), gasoline, diesel etc. According to the considered application (on-board H₂ production for fuel cell vehicles), the aim is CO-free hydrogen production with minimized CO₂.

3.1. CHOOSING METHANOL AS FEEDSTOCK

Methanol or methyl alcohol is the simplest member of alcohols family with the formula of CH₃OH and the molecular structure given in Figure 3.1. It is a colorless, flammable liquid and miscible with water in all proportions. It is volatile and poisonous for human consumption, unlike ethanol. It is mainly used to produce chemicals and create fuels, antifreeze, and solvents. Some of methanol properties and its safety data sheet based on National Fire Protection Association (U.S.A) are demonstrated in Table 3.1.

Methanol is also called as wood alcohol or wood spirit. These archaic names originated from the methanol discovery story. The famous Irish chemist, Robert Boyle, discovered methanol as the wood distillation by-product in 1661. Methanol has been produced from destructive wood distillation for many years; however the modern way is the catalyzed direct combination of syngas, gaseous mixture of hydrogen and CO. The required syngas can be obtained from several sources such as natural gas, coal, oil, and biomass. Utilization of biomass-derived syngas is highly increasing; thus it is a renewable energy source.

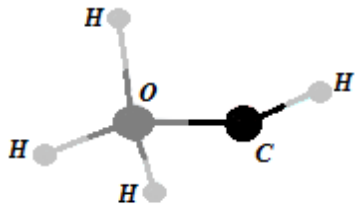


Figure 3.1. Methanol molecular structure [26].

Table 3.1. Properties of methanol [26, 27].

Property	Value	Property	Value
Molecular weight (g/mol)	32.042	Heat of combustion* (kJ/mol)	726.1
Melting point* (°C)	-97.8	Heat of vaporization* (kJ/mol)	37.34
Boiling point* (°C)	64.7	Vapor pressure* (kPa)	12.3
Density § (kg/m³)	0.81	Flash point* (°C)	15.6
Viscosity* (pa.s)	5.44×10^{-4}	Auto ignition temp. (in air) (°C)	464
CAS number	67-56-1		

* measured at normal temperature and pressure; 20 °C and 1 atm

§measured at 0 °C

There are several advantages associated with using methanol as the on-board hydrogen production feedstock. Methanol steam reforming (MSR) can be operated in atmospheric pressure. Due to absence of the strong carbon-carbon bonds in methanol structure, less energy is required to break the molecule; hence the reforming temperature is low (200-300 °C). This reforming temperature range is much lower

compared to that of the other common hydrocarbons such as ethanol (400 °C) and methane (500 °C) [28]. Consequently, the risk of coke formation and catalyst fouling is lower. The generated carbon monoxide is low; whereas, the high hydrogen to carbon ratio of methanol leads to high H₂ production. Additionally, minor efforts and cost will be expected to change the current refueling systems from gasoline and diesel to methanol. Furthermore, the study of L. R. Borup's group compared the needed start-up energy of the various fuels utilized in the on-board H₂ production system. The start-up energy is the required energy to increase the system temperature from ambient temperature to the temperature that system can produce the fuel cell quality hydrogen [24, 26, 29–32]. The results presented in Figure 3.2 shows the low start-up energy requirement of methanol.

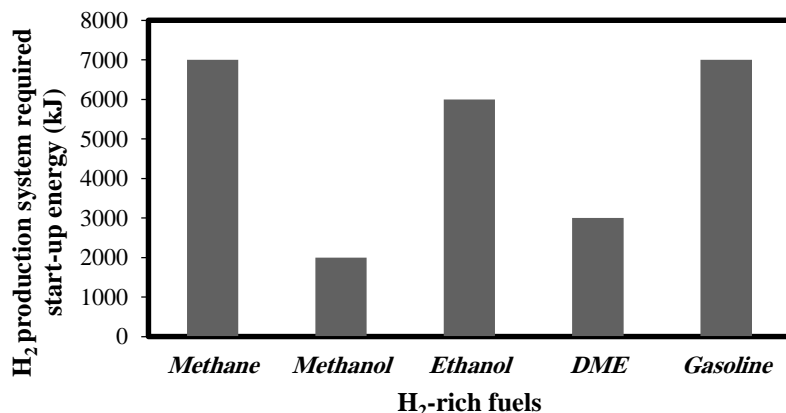
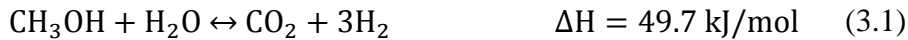


Figure 3.2. Required start-up energy of various feedstocks [33].

3.2. METHANOL STEAM REFORMING (MSR) REACTION PROCESS

There has been extensive research and study on methanol steam reforming process, recently. MSR process is a proper way to provide hydrogen with high yield for the fuel cell applications, while CO selectivity is very low. Two major catalyst groups are

proposed for this reaction; copper-based and group 8-10 metals. The overall reaction network of methanol steam reforming process can be described as follows:



The general operating conditions of this process are given in Table 3.2.

Table 3.2. *The general operating conditions of the MSR reaction.*

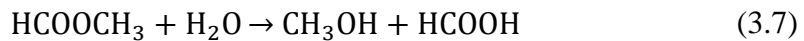
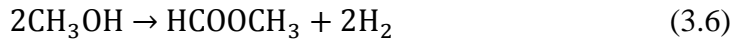
<i>Pressure</i>	1 bar
<i>Temperature</i>	250-300 °C
<i>Reactants molar ratio (MeOH/H₂O)</i>	1:1-1:1.3

It can be said that the methanol steam reforming reaction (3.1) comprises the combination of methanol decomposition (3.2) and water-gas shift (3.3) reactions. The main products of the process are hydrogen and carbon dioxide. However, trace amount of carbon monoxide is produced by the reverse water-gas shift reaction at high temperature, since the reaction is exothermic. It is found that the CO production is less than equilibrium predicted amount [24]. Peppley et. al reported that the methanol decomposition reaction rate is much lower than that of the steam reforming reaction. It is stated that adding water to the feed decreases the temperature that methanol decomposition begins [34, 35]. Moreover, it is also expressed that the absence of steam in the feed leads to coke formation [36]. Another study showed that there is no CO formation at low contact times [37].

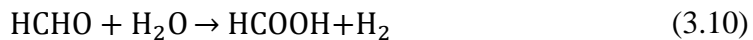
In spite of numerous investigations on MSR reaction process, the reaction mechanism is still a controversial issue due to the reaction complexity. Two other reaction

mechanisms, rather than methanol decomposition followed by water-gas shift reaction, have been postulated also which are described as follows:

(A) via methyl formate:



(B) via formaldehyde:



Jiang et. al suggested that the mechanisms (A) and (B) are the main reaction routes over copper-based catalysts which was confirmed afterwards by Takezawa et. al [28, 38]. R. Thattarathody et al. expressed that the side reactions of (3.6) and (3.9) and the corresponding mechanisms occur with high MeOH/steam ratio [36]. The mechanism study of MSR reaction over the group 8-10 catalysts was done by a few research groups as well. Those studies showed that the reaction mechanism is similar to the mechanism (B) [28]. To the extent of our knowledge, a detailed MSR mechanism study has not been done yet. Consequently, the controversy still remains on the mechanism of this process.

3.3. THERMODYNAMICS OF MSR

Thermodynamics is the best tool to predict the product equilibrium concentrations and afterwards other important parameters, such as the desired product yield, reactants conversion, and product selectivity. The Gibbs energy is the most commonly used function to determine the equilibrium compositions. The approach is to minimize the total Gibbs energy. The total Gibbs energy of the system is calculated using equation (3.12):

$$G^t = \sum_{i=1}^N n_i \bar{G}_i = \sum_{i=1}^N n_i \mu_i = \sum n_i G_i^o + RT \sum n_i \ln \frac{\hat{f}_i}{f_i^o} \quad (3.12)$$

The following assumptions can be made for reaction equilibria in the gas phase; $\hat{f}_i = y_i \hat{\Phi}_i P$, $f_i^o = P^o$ and $G_i^o = \Delta G_{f_i}^o$. By applying these assumptions and also the Lagrange multiplier method (a mathematical optimization strategy), the minimum Gibbs energy of each gaseous species and total system, equations (3.13) and (3.14), can be found.

$$\Delta G_{f_i}^o + RT \ln \frac{y_i \hat{\Phi}_i P}{P^o} + \sum_k \lambda_k a_{ik} = 0 \quad (3.13)$$

$$\sum_{i=1}^N n_i \left(\Delta G_{f_i}^o + RT \ln \frac{y_i \hat{\Phi}_i P}{P^o} + \sum_k \lambda_k a_{ik} \right) = 0 \quad (3.14)$$

with equation (3.15) as the constraining equation:

$$\sum_i n_i a_{ik} = A_k \quad (3.15)$$

In order to estimate the equilibrium state of the methanol steam reforming process, reactions (3.1)-(3.3) are considered. Considering the coke formation during the process in the calculations makes the results more realistic. Equation (3.16) shows the applying of the vapor-solid equilibrium to the solid carbon Gibbs energy.

$$\bar{G}_{C(g)} = \bar{G}_{C(s)} = G_{C(s)} \approx \Delta G_{fC(s)}^o = 0 \quad (3.16)$$

Applying equations (3.13) and (3.16), for gaseous and solid species respectively, to equation (3.12) leads to equation (3.17).

$$\sum_{i=1}^{N-1} n_i \left(\Delta G_{f_i}^o + RT \ln \frac{y_i \hat{\phi}_i P}{P^0} + \sum_k \lambda_k a_{ik} \right) + (n_c \Delta G_{fC(s)}^o) = 0 \quad (3.17)$$

The equilibrium product distribution of MSR was calculated using Gaseq, a software for equilibrium calculations, at 1 bar with respect to different temperatures (Figure 3.3).

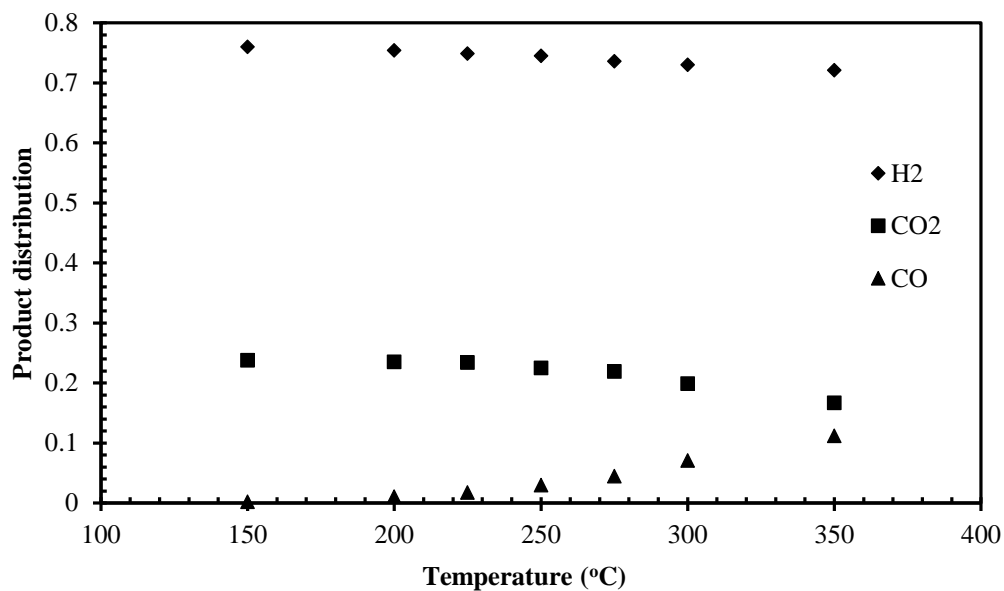


Figure 3.3. Equilibrium product distribution of MSR (1 atm, MeOH/H₂O molar ratio of 1).

This calculation was performed considering the formation of CO₂, CO, and H₂. As it is clear, the operating temperature does not significantly affect the product distribution. However, CO composition in the product stream slightly increased as the temperature went up in the range of 200-300 °C. With increasing the temperature to

400 °C, CO increase was significant. In average, it can be said that the product stream of MSR (at 1 bar with the feed molar ratio of 1) consists of 4% CO, 22% CO₂, and 74% H₂, which is in agreement with the literature [39]. Consequently, the MSR operating condition was decided as 250°C, 1 bar, and methanol to steam ratio of 1.

CHAPTER 4

CATALYSTS

A catalyst is a substance that accelerates chemical transformations by creating temporary bonds with reactant molecules. So the reactants can react to produce product molecules. Afterward, the produced molecules leave the bonds with the catalyst and leave the catalyst unchanged. This chemical process is called “Catalysis”. Catalysis is all about the kinetics of a reaction. In other words, it just changes the route to reach the equilibrium which is defined by thermodynamics and cannot be influenced by kinetics. According to The International Union of Pure and Applied Chemistry (IUPAC) definition, “*catalyst is a substance that increases the rate of a reaction without modifying the overall standard Gibbs energy change in the reaction*” [40].

Catalysis is a key field of chemistry. The development of chemical industry in the 20th century cannot be imagined without the catalysis primary role. More than 75% of chemical industrial products is produced with the aid of the catalysts. Production of plastics, resins, pharmaceuticals, pigments, fertilizers, dyes, and synthetic fibers is possible merely by catalytic processes. Similarly, a majority of processes in crude oil processing and petrochemistry involve catalytic processes [41]. A brief history of the catalysis development and its effect on industrial chemistry is represented in Table 4.1.

The catalysis is a phenomenon becoming understandable as time passes, although the humankind was familiar with it since ancient times. Noah and Sumerian men managed to produce their wine and beer by fermentation (and therefore catalytic) processes [42]. The early recognition of modern catalysis was done by Davi in 1816 before Berzelius could define it around 1835. In the early 20th century, the systematic

experiments of Mittasch gave the catalysis an empirical basis. In the mid-1920s, the Langmuir-Hinshelwood kinetics triggered catalytic mechanism studies. The advent of infrared spectroscopy followed by the other characterization techniques made the surface investigations feasible in the late 1950s. By the end of that century, surface parameters and bond strengths calculations became easier by advancements in computational programs and methods [43]. Figure 4.1 depicts the development of practical catalysis and understanding level of this phenomenon timeline.

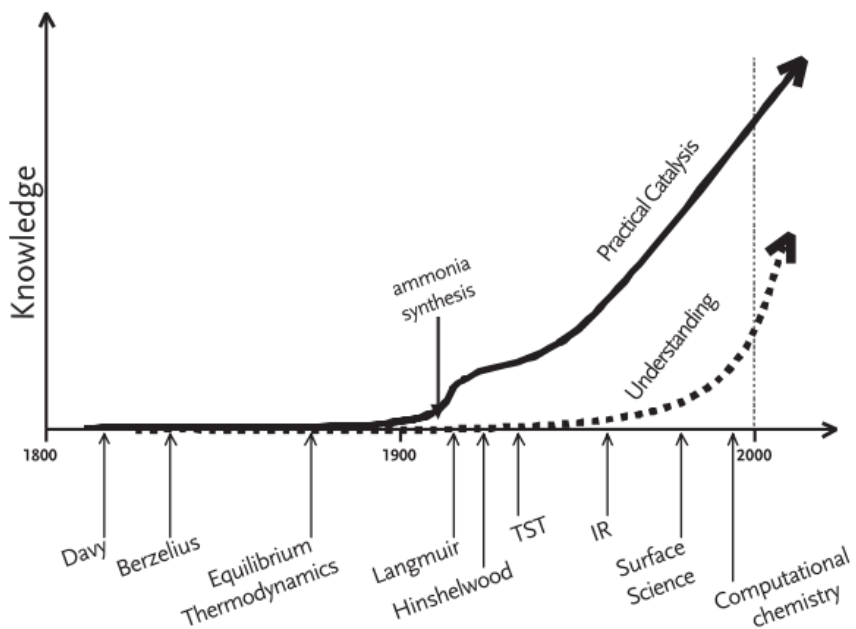


Figure 4.1. The timeline of catalysis knowledge development, reprinted from [43].

Table 4.1. *History of the catalysis of industrial processes [41].*

Catalytic reaction	Catalyst	Discoverer or company/year
Sulfuric acid (lead-chamber process)	NO_x	Désormes, Clement, 1806
Chlorine production by HCl oxidation	CuSO_4	Deacon, 1867
Sulfuric acid (contact process)	Pt, V_2O_5	Winkler, 1875; Knietsch, 1888 (BASF)
Nitric acid by NH_3 oxidation	Pt/Rh nets	Ostwald, 1906
Fat hardening	Ni	Normann, 1907
Ammonia synthesis from N_2 , H_2	Fe	Mittasch, Haber, Bosch, 1908; Production, 1913 (BASF)
Hydrogenation of coal to hydrocarbons	Fe, Mo, Sn	Bergius, 1913; Pier, 1927
Oxidation of benzene, naphthalene to MSA or PSA	V_2O_5	Weiss, Downs, 1920
Methanol synthesis from CO/H_2	$\text{ZnO/Cr}_2\text{O}_3$	Mittasch, 1923
Hydrocarbons from CO/H_2 (motor fuels)	Fe, Co, Ni	Fischer, Tropsch, 1925
Oxidation of ethylene to ethylene oxide	Ag	Lefort, 1930
Alkylation of olefins with isobutane to gasoline	AlCl_3	Ipatieff, Pines, 1932
Cracking of hydrocarbons	$\text{Al}_2\text{O}_3/\text{SiO}_2$	Houdry, 1937
Hydroformylation of ethylene to propanal	Co	Roelen, 1938 (Ruhrchemie)
Cracking in a fluidized bed	aluminosilicates	Lewis, Gilliland, 1939 (Standard Oil)
Ethylene polymerization, low-pressure	Ti compounds	Ziegler, Natta, 1954
Oxidation of ethylene to acetaldehyde	Pd/Cu chlorides	Hafner, Smidt (Wacker)
Ammonoxidation of propene to acrylonitrile	Bi/Mo	Idol, 1959 (SOHIO process)
Olefin metathesis	Re, W, Mo	Banks, Bailey, 1964
Hydrogenation, isomerization, hydroformylation	Rh-, Ru complexes	Wilkinson, 1964
Asymmetric hydrogenation	Rh/chiral phosphine	Knowles, 1974; L-Dopa (Monsanto)
Three-way catalyst	Pt, Rh/monolith	General Motors, Ford, 1974
Methanol conversion to hydrocarbons	Zeolites	Mobil Chemical Co., 1975
α -olefines from ethylene	Ni/chelate phosphine	Shell (SHOP process) 1977
Sharpless oxidation, epoxidation	Ti/ROOH/tartrate	May & Baker, Upjohn, ARCO, 1981
Selective oxidations with H_2O_2	titanium zeolite (TS-1)	Enichem, 1983
Hydroformylation	Rh/phosphine/aqueous	Rhône-Poulenc/Ruhrchemie, 1984
Polymerization of olefines	zirconocene/MAO	Sinn, Kaminsky, 1985
Selective catalytic reduction SCR (power plants)	V, W, Ti oxides/monolith	~1986
Acetic acid	Ir/I ⁻ /Ru	„Cativa“-process, BP Chemicals, 1996

4.1. CATALYST CLASSIFICATIONS

Catalysts can be classified according to their state of aggregation (Figure 4.2). Homogeneous and heterogeneous catalysts are the two main groups. In homogeneous catalysis, all of the reaction components are in the same phase, a uniform gas or liquid. The molecular dispersion of the homogeneous catalyst and the reactants in the reaction medium makes the reaction happen. Heterogeneous catalysis includes several phases. Normally, the heterogeneous catalyst is a solid and the reactants are in gas or liquid state. However, an intermediate form also exists.

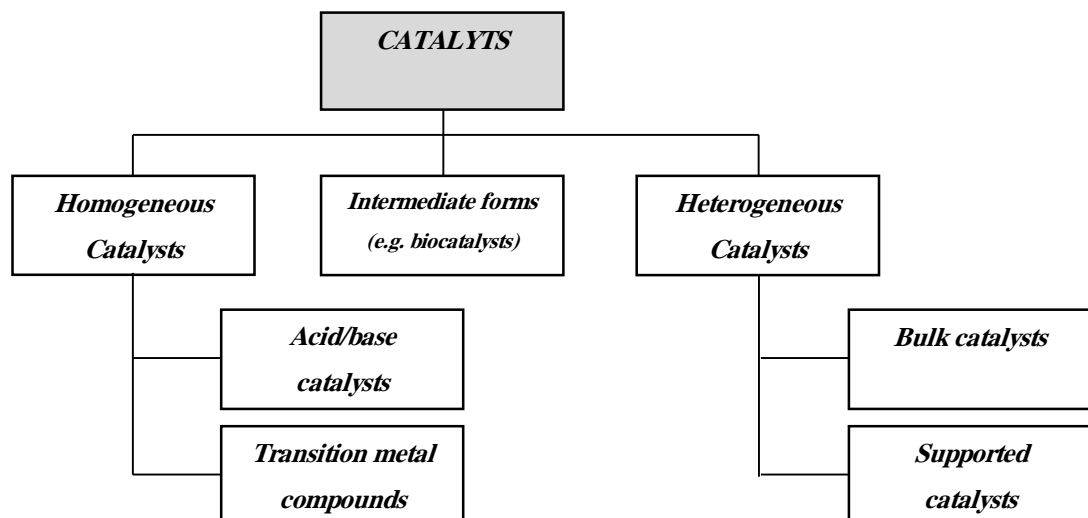


Figure 4.2. Classification of the catalysts [41].

The performance of a catalyst in a process is judged mainly by three parameters; activity, selectivity, and stability. Activity measures the reaction rate increase caused by the catalyst. Selectivity indicates the catalyst strength to conduct the reaction to produce the desired product(s). Stability determines the catalyst lifetime in the reactor, since the catalyst may become deactivated due to several factors, such as coking, poisoning, and decomposition [41]. Although these parameters are important, they do not necessarily guarantee that the catalyst would perform successfully. In addition to

these main parameters, there are other properties should be taken into consideration, too; possibility to regenerate, adequate thermal stability against sintering or structural change, reproducible preparation, high mechanical stability and resistance [44].

4.2. HETEROGENEOUS CATALYSTS

Heterogeneous catalysts are the most important type of the catalysts. In more than 85% of all catalyzed processes, heterogeneous catalysts are involved. This shows the substantial contribution of heterogeneous catalysts to the chemical industries. Moreover, wide range of operating conditions can be applied to the heterogeneously catalyzed processes. The most key point that makes them favored is ease of separation, as opposed to the homogeneous catalysts [45]. Heterogeneous catalysis has a significant role in producing petrochemicals and chemical industries. In the last three decades, it has dominated production of pharmaceuticals and also clean energy applications due to the advancements of “green chemistry”.

In a typical heterogeneous reaction, a packed bed reactor is used. Gaseous reactants enter the reactor, so the reactant molecules diffuse through the catalyst pores. The catalyst surface, where active sites are located, adsorbs the reactant molecules and therefore the reaction takes place. Finally, the products leave the catalyst surface to the gas phase. Figure 4.3 illustrates this process schematically.

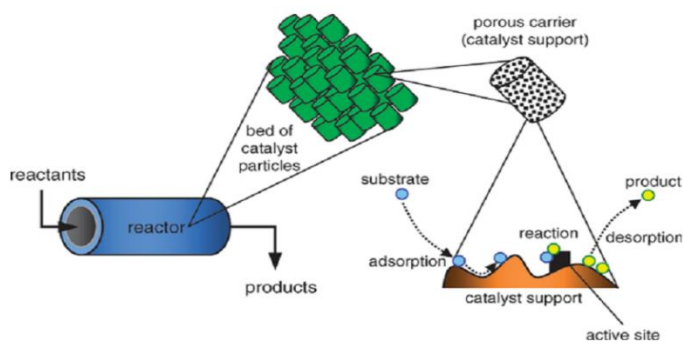


Figure 4.3. A heterogeneous catalysis at various levels, reprinted from [46].

Two main mechanisms for a heterogeneous catalyzed reaction, $A + B \rightarrow C$, are available (Figure 4.4). In the first mechanism, both **A** and **B** are adsorbed on the catalyst surface. After the molecules reach each other, the reaction occurs on the surface and **C** is desorbed. The second option includes only adsorption of **A** on the catalyst surface. Afterwards, **B** reacts with **A** and **C** is formed. These mechanisms are entitled as *Langmuir-Hinshelwood* and *Eley-Rideal*, respectively [46].

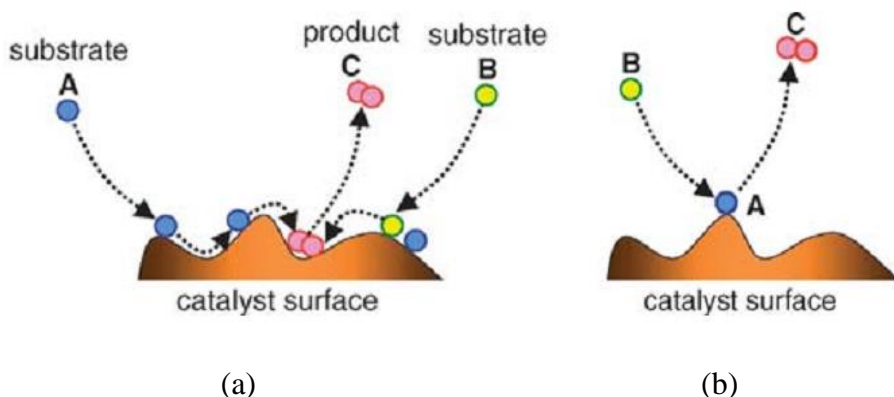


Figure 4.4. Two main mechanisms of heterogeneous catalysis: (a) Langmuir-Hinshelwood , (b) Eley-Rideal, reprinted from [46].

4.2.1. HETEROGENEOUS CATALYSTS PREPARATION

Catalyst preparation is a complicated task, since it is not possible to specify the complete and detailed reaction scheme. The heterogeneous catalysts are prepared by several different procedures that can easily affect the catalyst properties and performance. Most of the preparation techniques can be considered as a series of unit operations. Table 4.2 shows all the unit operations might be used in catalysts preparation. A brief description of each unit operation is given in this section.

Table 4.2. *Unit operations in heterogeneous catalyst preparation [47]*

<i>1. Gelation</i>	<i>5. Drying</i>	<i>9. Precipitation</i>
<i>2. Hydrothermal transformation</i>	<i>6. Calcination</i>	<i>10. Impregnation</i>
<i>3. Filtration, centrifugation</i>	<i>7. Activation</i>	<i>11. Mixing</i>
<i>4. Washing</i>	<i>8. Forming operations</i>	

Gelation is a process to reticulate the micelles of a hydrophilic colloidal solution and to form a hydrogel, a 3-D network imprisoning water molecules. The micelle formation is a result of polymerization or polycondensation reactions. The hydrothermal transformation contains modifications in precipitates or gels by means of temperature, under aging, or aging in the mother liquid. These modifications include textural or structural modifications. Filtration and centrifugation separate the solid from the mother liquid. Washing is then required to remove the impurities and the mother liquid thoroughly. Drying is a usual procedure to vaporize and eliminate water or other solvents from the solid pores. Calcination is a heat treatment process in air, typically at higher temperatures than catalyst formation reaction. The other heat treatments being performed in special atmospheres are considered as activation operations like reduction. During the calcination, active phase generation, structural modification, and mechanical stabilization take place. In order to obtain the catalyst with a desired shape and size, forming operations are done. The catalyst shape and size can have a significant effect on catalytic activity, particles strength, the pressure drop, and synthesis cost. Crushing, grinding, granulation, extrusion, and dry tableting are some of forming operations. Impregnation and precipitation are processes to prepare supported catalysts. In the former, the active particles are impregnated on the support by contacting the support with impregnating solution. However, during the latter, a solid is precipitated from a liquid solution into the support pore structure. It occurs in three main steps; supersaturation, nucleation, and growth [47].

4.2.2. SUPPORTED CATALYSTS

These catalysts comprise a substance which is catalytically active and a support material. The main purpose of using supported catalysts is to provide a combination of high dispersion and high thermostability of active substance. The active substance loaded on the support material can be roughly any type of material, such as oxides, metals, nitrides, salts, acids, etc. The support material is usually a porous material like zeolites, mesoporous materials, clays, etc. The porous structure provides the material a higher total surface area than its external surface. It can be either inert or catalytically active. The support function is quite simple; to form large particles of catalyst consisting of very small dispersed catalytic agent crystals. The support selection is done by considering the following criteria [47]:

- | | |
|---|--|
| <i>1. Inertness</i> | <i>4. Surface area (high surface area)</i> |
| <i>2. Mechanical properties</i> | <i>5. Porosity (average pore size)</i> |
| <i>3. Stability under reaction conditions</i> | <i>6. Low cost</i> |

Among a wide variety of possible materials, only a few of them show preferable combination of the mentioned criteria to be a proper support. Nanomaterials are considered as one of the most appropriate materials to be used as the catalyst support. The field of catalyst synthesis had significant advancements after the discovery of nanosized materials. In fact, nanomaterials have opened new era of catalyst synthesis.

A material with at least one dimension between 1 nm to 100 nm is called Nanomaterial [48]. Two fundamental factors made them significantly different from other materials; high surface area and quantum effects. These factors enhance some properties like reactivity and mechanical characteristics [49]. The porous structure of these materials makes them able to fit different areas of use. Moreover, their scientific interest and technological value have been raised because of their ability to interact with other components not only on the external surface, but throughout the bulk of the material.

According to IUPAC, nanomaterials are classified based on their pore diameter; microporous (<2 nm), mesoporous (2-50 nm), and macroporous (>50 nm) [20, 24].

There are many different kinds of nanoporous materials being studied in the literature; such as zeolites, carbon nanotubes, clays, anodic alumina, and porous carbon materials [50]. Figure 4.5 illustrates some examples of each category.

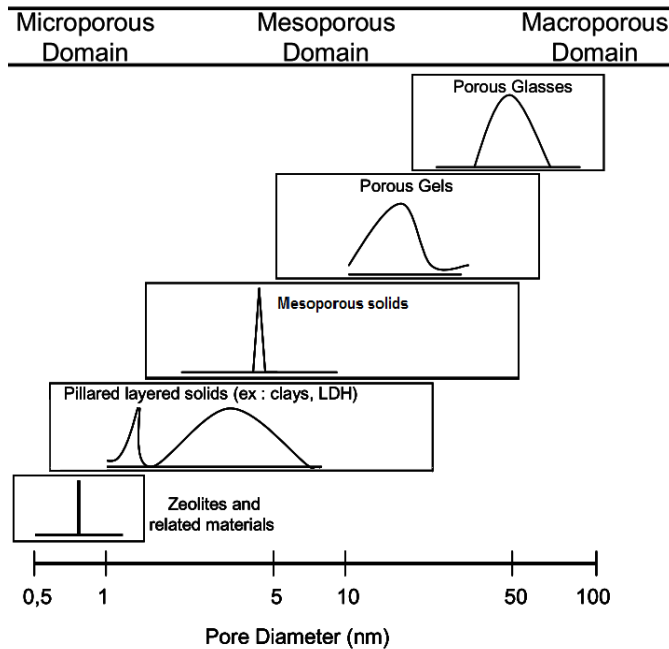


Figure 4.5. Examples of nanoporous materials showing pore size domains, reprinted from [24].

4.2.2.1. ORDERED MESOPOROUS MATERIALS

Ordered mesoporous materials have adjustable pore size and structure. The main advantage of these materials is that the uniform pore size distribution and ordered structure make the processes controllable. Moreover, they are not subject to mass transfer limitations as opposed to microporous materials [50]. Major advancements in the ordered mesoporous materials have been seen in the two past decades. Their application areas have been broaden from traditional fields of use, such as catalysis, adsorption, and ion exchange, to brand-new areas like liquid chromatography, macromolecule separation, diagnostic magnetic resonance imaging (MRI),

microlaser, electrode materials, and microelectronics due to their superior properties [51].

Although, preparation of low-density silica, as the first mesoporous material, was reported in a patent for the first time in 1969, obtaining ordered structure and uniform pore distribution was not achieved until the 1990s due to lack of analysis. Synthesis of pillared clay was the starting point of mesoporous material development in the 1980s. In 1992, a new field of research was opened up by Mobil Oil Corporation as a result of discovering a new type of silica, MCM-41 (Mobil Composition of Matter No.41), made of highly ordered hexagonal arrays. It was followed by the fabrication of MCM-48 and MCM-50. These materials possess tunable pore sizes of 2-10 nm and surface area of $600\text{-}1300 \text{ m}^2\text{g}^{-1}$. At the same time, a new group of ordered mesoporous materials were proposed. These highly ordered materials were synthesized from silicates and aluminosilicates via intercalation of a surfactant into silicate sheets and denoted as FSM-*n* (Folded Sheet mesoporous Material) [20, 40, 50, 52].

The first synthesized ordered mesoporous material (MCM-41) was a major advancement in the field of porous materials. It was synthesized by a synthesis method called templating. The main idea of this method is based on the interaction between a silica template and a surfactant. Since then many other ordered mesoporous materials were developed by this method and from different silica sources and surfactants. Additionally, there is another pathway to synthesize new mesoporous materials so-called nanocasting method. It is based on using an already formed ordered mesoporous material as a hard template. A brief comparison between possible methods of ordered mesoporous material synthesis is demonstrated in Table 4.3. The comparison is done considering the silica template used and also interactions between the template inorganic species (I) and the surfactant species (S).

Table 4.3. Possible pathways of the ordered mesoporous materials synthesis [50].

Template	Interaction		Synthesis condition	Examples
Ionic surfactant	<i>Direct</i>	$IS^{+} \sim \sim \sim$	<i>Basic</i>	<i>MCM-41, MCM-48, MCM-50, FSM-16</i>
		$I^{+}S^{-} \sim \sim \sim$	<i>Neutral-basic</i>	(Al, Fe, Pb oxides, etc.), AMS
	<i>Intermediated</i>	$I^{+}X^{+}S^{+} \sim \sim \sim$	<i>Acidic</i>	<i>SBA-1, SBA-2, SBA-3, HMS, TLCT</i>
		$IX^{+}S^{-} \sim \sim \sim$	<i>Basic</i>	(Al, Zn oxides etc.)
Non-ionic surfactant	<i>Non-ionic</i>	$I^0S^0 \sim \sim \sim$		HMS
Co-polymer	<i>Non-ionic</i>	$I^0N^0 \sim \sim \sim$	<i>Acidic</i>	<i>MSU, TLCT, SBA-15</i>
Ligand assisted	<i>co-valent bond</i>			<i>Nb-TMS, Ta-TMS</i>
Nanocasting	-	-	-	<i>CMK-n</i>

The synthesis of the mesoporous materials began using ionic surfactants and forming electrostatic interactions between inorganic and organic species. As a result of this interaction, the surfactant (S^{+}) and silicate (I^{-}) species become positively and negatively charged, respectively. Afterward, this mechanism was extended to reversed form, $I^{+}S^{-}$, and using an intermediate with counter charge, $I^{+}X^{-}S^{+}$ and $IX^{+}S^{-}$. Two other approaches were later added both relied on forming interactions between inorganic and non-ionic organic species. For this purpose, neutral surfactants and triblock co-polymers are used. In the ligand assisted method, covalent bonding occurs between inorganic species and organic surfactant molecules. The mechanisms explained so far all are based on the inorganic-surfactant species interactions. In fact, this co-operative interaction forms mesoporous composites. An entirely different method was introduced by Ryoo group called nanocasting in 1999. In this method, the hard template is the pore structure of an ordered mesoporous silica material, which is already synthesized. Therefore, there is no longer need of using the surfactant template. As the result of this method, the porous carbon materials were born [50].

Figure 4.6 reveals that different types of porous carbon materials can be obtained by nanocasting method from different silica sources and the template pore network defines that of the synthesized carbon material.

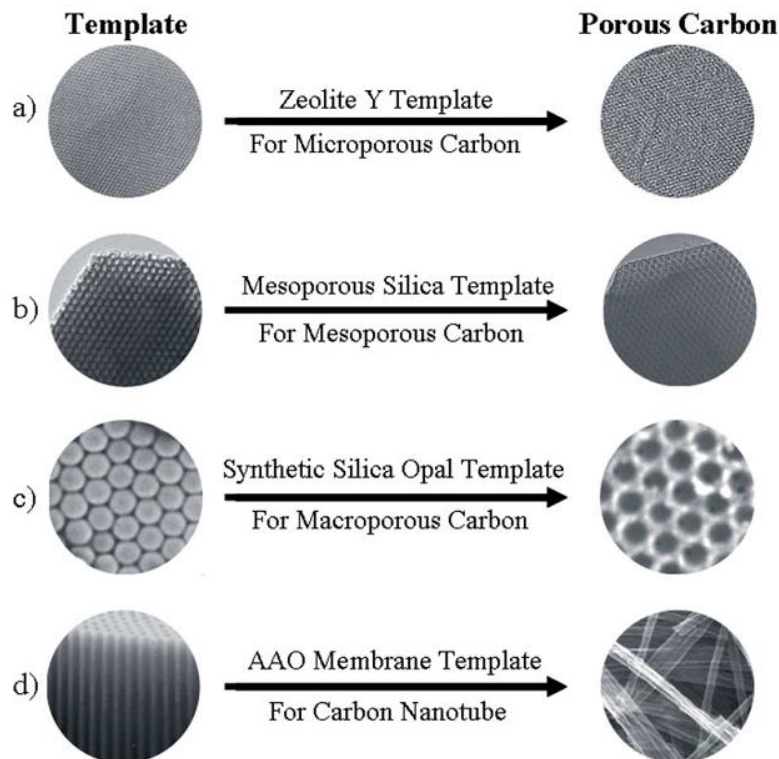


Figure 4.6. Synthesis of different types of porous carbon materials by nanocasting method, reprinted from [53].

4.2.2.2. ORDERED MESOPOROUS CARBON MATERIALS

Ordered mesoporous carbon (OMC) materials have received a considerable attention due to their superior properties like high chemical stability, electrical and thermal conductivities, and wide availability. Furthermore, their scientific importance is high because of high surface area, uniform pore size and pore volume, tunable porosity, low price, and high stability in both acidic and basic environments. These significant attributes of ordered mesoporous carbon materials made them a good choice to be

used as the catalyst support, adsorbents, energy and H₂ storage materials capacitors, and batteries and fuel cells electrode materials [54–58].

As it is mentioned in the previous section, the synthesis method of these materials is nanocasting. The concept of this method is exactly same as the method used for fabricating a ceramic jar, which is also called “casting”. However, in this case, it is scaled down to the nanometer scale. To cast a jar, a piece of wood is firstly prepared as a mold with the desired shape of the jar. Clay is then poured on the external surface of the mold. After heating, the clay is transformed and the ceramic jar is formed. The wooden mold is burned during the process and an empty void is created inside the jar [53]. This process is depicted schematically in Figure 4.7. Generally, the nanocasting procedure includes four main steps: (1) ordered mesoporous silica preparation as the hard template, (2) infiltrating the channels of template with carbon precursor, (3) the resulting composite carbonization at high temperature, and (4) the silica template elimination with NaOH or HF [50, 59].



Figure 4.7. Schematic representation of nanocasting concept, reprinted from [53].

Consequently, the spaces inside the template structure become pores of the synthesized ordered mesoporous carbon material. Generally to perform a successful synthesis using nanocasting technique, having interconnected and 3-D porous structure is necessary for the template [53]. The template pore structure, particularly pore wall thickness, has an important and undeniable effect on the resultant material pore size [59]. It is obvious that altering the mesoporous silica template leads to producing different types of mesoporous carbon materials [60].

According to the synthesis conditions, two types of ordered mesoporous carbon materials are obtainable. If the carbon precursor fills the template pores completely, rod-type mesoporous carbon is generated. On the other hand, tube-type mesostructured carbon can be achieved due to a thin film coating of carbon on the template pore walls [61]. The synthesis strategy of the ordered mesoporous carbon materials is shown in Figure 4.8.

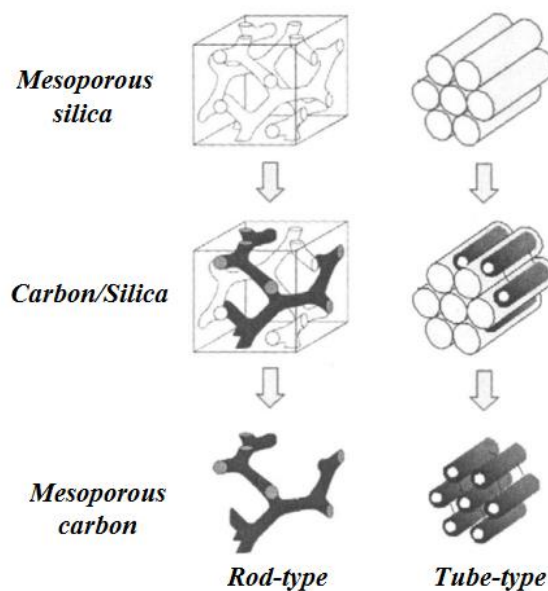


Figure 4.8. A schematic diagram of the ordered mesoporous carbon materials synthesis strategy, reprinted from [61].

The first member of highly ordered mesoporous carbon materials family, CMK-1, was discovered by the pioneer work of Ryoo research group, in 1999. These materials were named “CMK-*n*” (Carbon Mesostructured by KAIST, *n*=1-9) [62]. A brief study on this family is demonstrated in Table 4.4.

Table 4.4. *The ordered mesostructured carbon materials (CMK-n) [20, 61, 63].*

CMK-<i>n</i>	Silica template	Morphology
CMK-1	<i>MCM-48</i>	cubic <i>I4₁/a</i> , combination of rod-type and tube-type
CMK-2	<i>SBA-1</i>	cubic <i>Pm3n</i> , rod-type
CMK-3	<i>SBA-15</i>	2-D hexagonal <i>P6mm</i> , rod-type
CMK-4	<i>MCM-48</i>	cubic <i>Ia3d</i> , combination of rod-type and tube-type
CMK-5	<i>SBA-15</i>	2-D hexagonal <i>P6mm</i> , tube-type
CMK-6	<i>SBA-16</i>	cubic <i>Im3m</i> , rod-type
CMK-7	<i>SBA-16</i>	cubic <i>Im3m</i> , tube-type
CMK-8	<i>KIT-6</i>	cubic <i>Ia3d</i> , rod-type
CMK-9	<i>KIT-6</i>	cubic <i>Ia3d</i> , tube-type

The main role of carbon sources in the synthesis of the mesoporous carbon materials is to form the carbon framework inside the silica template structure. In the literature, various types of carbon sources are reported, such as sucrose [62], furfuryl alcohol, phenolic resin [64], polypyrrole [53], styrene, acetonitrile [65], naphthalene, anthracene, pyrine, acenaphthene, and oil pitch [66]. The carbon precursor molecular structure has a significant effect on mesoporous carbon material structure and pore size. Some of them have loose molecular structure, for example, sucrose or furfuryl alcohol. Employing such materials normally leads to a mesoporous structure with micropores on the pore walls. As a result of the micropores presence in the carbon framework, the resultant mesoporous carbon material exhibits large BET surface area and pore volume. By contrast, utilizing aromatic precursors (e.g. pyrine, acenaphthene, oil pitch, etc) leads to synthesizing a mesoporous material with smaller BET surface area, pore size and volume, and high mechanical strength [57]. All of the carbon precursors used so far, except sucrose, contain toxic solvents (e.g. aromatic hydrocarbons). In addition, their procedures are time-consuming and multi-stage. Therefore, it seems that sucrose is a preferable choice due to low cost and wide availability as well as the mentioned reasons [54].

CMK-3 was firstly introduced by Ryoo group using mesoporous hexagonal SBA-15 silica (Santa Barbara Amorphous-15) as the silica template and sucrose as the carbon source, in 2000. SBA-15 comprises of very large mesoporous channels and thick framework walls. The long cylindrical channels are interconnected with micropores. These interconnections increase the stability of the material and lead to the synthesis of a highly ordered material as well. It is reported that CMK-3 maintains the mesostructural of the hard template completely. It is an exact negative replica of the hard template, while no structural transformation occurs during the silica removing step. In general, highly ordered arrays of carbon nano-rods in a hexagonal pattern interconnected by micropores bridges is a complete description of CMK-3 structure [20, 57, 61–63]. As is shown by Figure 4.9(a), the average pore size of CMK-3 becomes narrower than SBA-15 due to nanocasting process. The average pore size of CMK-3 is in the range of 4-5 nm which is around 4 nm less than that of SBA-15. Moreover, the capillary condensation occurs at lower pressures inside the CMK-3 pores compared to SBA-15. The highly ordered channels of CMK-3 are clearly shown in Figure 4.9(b).

Two other synthesis procedures were also reported for CMK-3 in the literature. It was claimed that employment of Al-SBA-15 as the silica template and adjusting the aging temperature enhance the CMK-3 textural properties [67]. In addition, the synthesis of CMK-3 was done by chemical vapor deposition (CVD) using SBA-15 as the silica matrix [65].

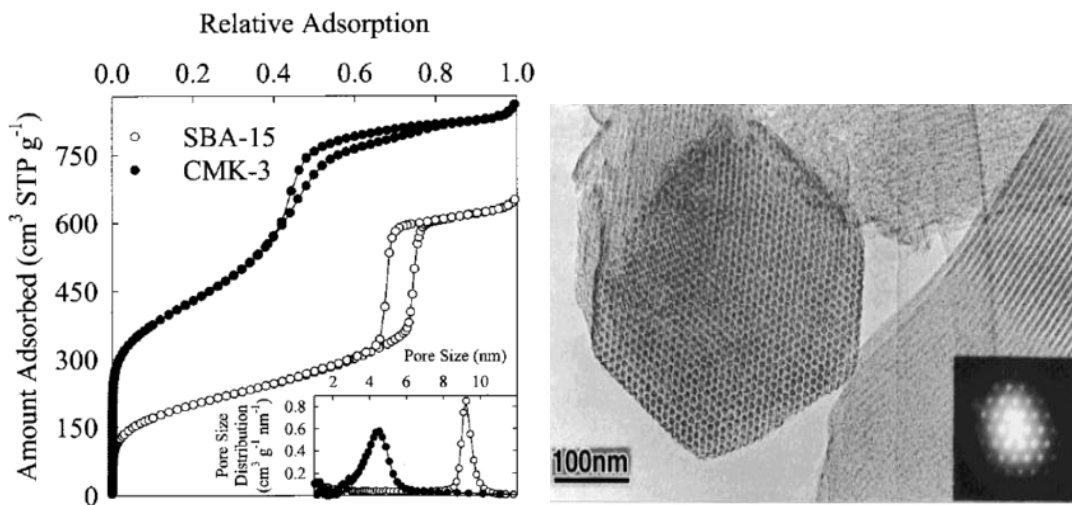


Figure 4.9. (a) N_2 adsorption-desorption isotherm at 77 K and pore size distribution of CMK-3 and SBA-15, (b) TEM images of highly ordered mesoporous channels of CMK-3, reprinted from [62].

4.3. MSR CATALYSTS

As it is discussed in section 3-2, methanol steam reforming is a heterogeneously catalyzed reaction. Copper-based and group 8-10 catalysts are two common types of catalysts used in this process which the main active components are copper and group 8-10 metals, respectively. However, in order to enhance the activity of copper-based catalysts and prevent the copper from sintering, the copper catalysts are promoted with various types of metal oxides. Finally, the promoted copper or group 8-10 metals are loaded on a catalyst support. A comprehensive literature survey on different types of catalysts used in MSR is done and represented Table 4.5.

The copper-based catalysts are the most conventional type of catalysts used in MSR process because of their high activity, high selectivity, and also low cost. However, some disadvantages are attributed to them, such as pyrophoricity, change in oxidation state, deactivation due to sintering, and coke deposition. The copper-based catalysts are highly prone to sintering at a temperature higher than 300 °C. Nevertheless, it is proved that the process temperature in MSR should not exceed 260 °C.

Table 4.5. *MSR catalysts literature survey.*

Catalyst	Loading (%)	T (°C)	Activity ($\mu\text{molH}_2 \text{ gcat}^{-1} \text{ s}^{-1}$)	X _{MeOH} (%)	H ₂ yield (%)	S _{CO} (%)
<i>CuZnO/Al₂O₃</i> (commercial) [28]	-	250	109	97.3	-	1
<i>Cu/MCM-41</i> [68]	5	250	-	30.7	-	10.3
<i>Cu/MCM-41</i> [68]	10	250	-	67.8	-	5.6
<i>Cu/MCM-41</i> [68]	15	250	-	72.3	-	0.8
<i>Cu/MCM-41</i> [68]	20	250	-	69.6	-	1.0
<i>Cu/CMK-3</i> [24]	11	250	-	-	9	-
<i>Cu/CMK-3</i> [24]	22	250	-	-	18	-
<i>CuZnO/CMK-3</i> [24]	<i>Cu:22, Zn:4</i>	250	-	-	13	-
<i>Cu/CMK-5</i> [24]	15.3	250	-	-	12	-
<i>Cu/CMK-5</i> [24]	22.9	250	-	-	25	-
<i>CuZnO/CMK-5</i> [24]	<i>Cu:22, Zn:4</i>	250	-	-	25	-
<i>Cu/γ-alumina</i> [69]	15	300	144	78	-	1.1
<i>CuZn/γ-alumina</i> [69]	<i>Cu:12, Zn:3</i>	300	139	75	-	1.3
	<i>Cu:9, Zn:6</i>	300	180	97	-	1.3
	<i>Cu:6, Zn:9</i>	300	185	100	-	1.2
	<i>Cu:3, Zn:12</i>	300	157	85	-	1.3
<i>Zn/γ-alumina</i> [69]	15	300	11	6	-	0.5
<i>CuCr/γ-alumina</i> [69]	<i>Cu:12, Cr:3</i>	300	83	45	-	1.2
	<i>Cu:9, Cr:6</i>	300	94	51	-	1.6
	<i>Cu:6, Cr:9</i>	300	117	63	-	1.1
	<i>Cu:3, Cr:12</i>	300	113	61	-	1.6
<i>Cr/γ-alumina</i> [69]	15	300	6	3.4	-	0.32
<i>CuZr/γ-alumina</i> [69]	<i>Cu:12, Zr:3</i>	300	81	44	-	0.88
	<i>Cu:9, Zr:6</i>	300	76	41	-	0.71
	<i>Cu:6, Zr:9</i>	300	81	44	-	0.75
	<i>Cu:3, Zr:12</i>	300	76	41	-	0.72
<i>Zr/γ-alumina</i> [69]	15	300	3.9	2.1	-	0.21
<i>Ni/SiO₂</i> [70]	10.6	220	2.03	-	-	1.1
<i>Pt/SiO₂</i> [70]	2.1	220	0.42	-	-	25.6
<i>Pd/SiO₂</i> [70]	1.4	220	0.38	-	-	0.0
<i>Pd/Al₂O₃</i> [70]	13	220	1.86	-	-	1.4
<i>Pd/Nb₂O₅</i> [70]	20	220	1.56	-	-	4.2
<i>Pd/Nd₂O₃</i> [70]	25	220	3.71	-	-	7

All of these drawbacks motivated searching for an alternative type of catalyst. Although group 8-10 catalysts exhibit better thermal and longer stability, their activity is low. In the other words, they produce less amount of hydrogen than the copper-based catalysts. The activity of palladium, the most commonly used metal of this group, in MSR process is reported 14 times lower than that of the copper-based catalysts. Moreover, group 8-10 metals are considerably expensive. In conclusion, employing the copper-based catalysts is economically preferred. The copper

dispersion and the support surface area affect the catalyst performance. It is the main parameter should be considered to have a highly active catalyst and hence fulfill the main aim of the MSR process which is producing the fuel cell quality hydrogen with high yield. To enhance the copper status as well as the catalyst performance, different promoters have been utilized and reported in the literature. It is reported that addition of alumina (Al_2O_3) and chromium oxide (Cr_2O_3) increases the catalyst surface area and improves copper dispersion. Furthermore, a better copper status and less CO formation can be achieved due to usage of zirconia (Zr) and/or ceria (CeO_2). Zinc is also effective in increasing the catalyst stability and methanol conversion [24, 28, 32, 38, 70, 71]. There are numerous studies on heterogeneous bulk catalysts employed in MSR process in the literature, while only a few works have studied the supported catalysts. Therefore, it is required to concentrate more on the porous material supported-catalysts, due to their remarkable capability to increase the catalyst total surface area and copper dispersion.

Loading of copper on ordered mesoporous MCM-41 and its usage in methanol steam reforming reaction system was studied. The best catalytic performance was obtained with 15%Cu/MCM-41 at 300 °C. With this catalyst, methanol conversion of 89% was achieved. It was also noted that using a catalyst support with high surface area significantly enhanced the stability of the catalyst [68].

In a recent study, high surface area silica aerogel was selected as the MSR reaction catalyst support. The catalyst with 15% copper loading into silica aerogel support had a methanol conversion of 92%, average hydrogen yield of 2.75, and coke formation of 3.6% with steam to methanol molar ratio of 2.2 at the operating temperature of 280 °C. Moreover, capturing of CO_2 from the product stream was also investigated using hydrotalcite [39].

CHAPTER 5

MICROWAVE-ASSISTED MSR

The present study concentrates on an endothermic process, methanol steam reforming (MSR). The economic feasibility of an endothermic process is a highly crucial issue which can be achieved by providing high temperature, while the energy input is low. Microwave heating is a potential method to generate high temperature and uniform temperature distribution with low energy input compared to the conventional heating methods.

5.1. HISTORY OF MICROWAVE

In 19th century, the development of radio waves resulted in the invention of RADAR (Radio Detection and Ranging). Radar was a huge contribution to the technology, especially in navigation. In 1946, when the Second World War was extremely heated up, Dr. Percy LaBaron Spencer noticed melting the candy bar he had in his pocket while he was standing close to a radar active set during a research project. The system was generating microwave signals. Therefore, he decided to examine his scientific idea and finally could prove it. The idea was simple; microwaves can cook foods [72, 73]. The microwave development and evolution trend can be summarized in Table 5.1.

Table 5.1. *The microwave development and evolution history [73].*

1946	<i>The discovery of microwave heating method, filing as a patent by the Raytheon Company</i>
1947	<i>Building the first commercially microwave oven by the Raytheon Company; about 350 kg and US \$5000 (~\$53,000 in today's dollars)</i>
1955	<i>Introduction of the first home microwave oven by Tappan Stove company of Mansfield, Ohio; about US \$1295 (~\$11,500 in today's dollars)</i>
1965	<i>Introduction of the first countertop home model by Amana; about US \$495 (~\$3500 in today's dollars)</i>
1978	<i>Establishment of the first microwave laboratory by CEM Corporation, USA to analyze solids moisture</i>
1983-85	<i>Employment of the microwave radiation for chemical analysis</i>
1986	<i>Publishing the first paper about microwave radiation in chemical synthesis by Robert Gedy et. al,</i>
1990	<i>Making the first high pressure MW vessel</i>
1992-96	<i>Development of an effective batch microwave system reactor</i>
1997	<i>Compilation of the reference book: "Microwave-enhanced chemistry-fundamentals, sample preparation, and applications"</i>
1990s	<i>Emerging the microwave promising applications in chemical reactions</i>
2000 onwards	<i>Broadening the prosperity of microwave-assisted reactions</i>

5.2. MICROWAVE HEATING

The electromagnetic waves with a wavelength range of 0.01-1 meters are categorized as “microwaves” (Figure 5.1). In order to avoid any probable interference with other frequencies (especially telecommunication), a particular frequency of 2.45 GHz (12.24 cm) is allocated to all microwave ovens, both domestic and chemical reactor types. At this frequency, microwave photon energy (approximately 1 J/mol) is much lower than the energy of any types of the bonds available in a material, as well as the Brownian motion (Table 5.2). Consequently, microwave irradiations are not able to break the chemical bonds and hence begin the chemical reactions.

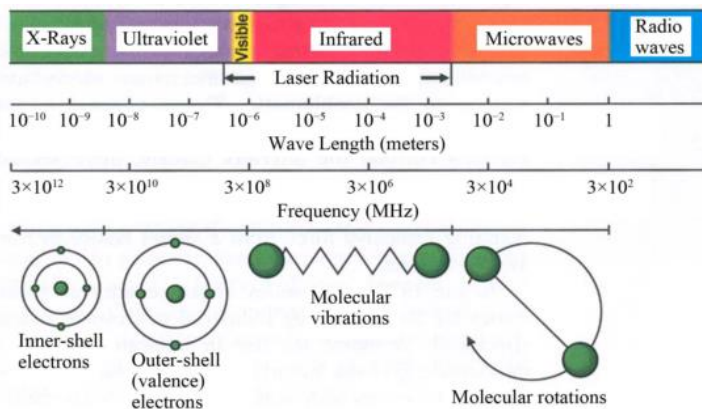


Figure 5.1. The electromagnetic spectrum, reprinted from [73].

Table 5.2. Energetic comparison of different bonds and microwave radiation at 2.45 GHz [74].

	Brownian motion	Hydrogen bonds	Covalent bonds	Ionic bonds	Microwave photons
Energy in eV	0.025 (at 200K)	0.04-0.44	5.0	7.6	10^{-5}
Energy in kJ/mol	1.64	3.8-4.2	480	730	10^{-3}

The materials under the microwave irradiations are heated by dielectric heating phenomenon which mainly depends on their characteristics. The dielectric properties of the materials define their ability to absorb the microwave irradiations and finally convert it into heat. The electromagnetic waves have an electric component. When a material is under exposure of the electromagnetic waves, an electric field is applied which make the electrons freely move. The electric field oscillates quickly and due to this fast oscillation, the polarization occurs. It is a phenomenon that realigns and then separates the positive and negative charges of dielectric materials. As a result of this quick orientation of the dipoles and hence the occurred molecular friction, energy dissipates in form of heat. The dielectric loss tangent (δ) is an indicative parameter to measure the ability of a material to convert electromagnetic waves into heat. The higher dielectric loss tangent, the higher heating can be supplied by microwave irradiations. Table 5.3 shows the dielectric loss tangent of some materials and

classifies them based on their microwave absorbing strength. The dielectric loss tangent consists of real permittivity (ϵ' , dielectric constant) and imaginary permittivity (ϵ'' , dielectric loss factor) terms; $\tan(\delta) = \epsilon''/\epsilon'$. The former determines the amount of reflected and absorbed microwaves and the latter indicates the amount of converted electric energy to heat within the material [73–75].

Table 5.3. *Loss factors ($\tan \delta$) of different materials at 2.45 GHz and 20 °C [73].*

Microwave absorbing strength	Material	$\tan \delta$
<i>High ($\tan \delta > 0.5$)</i>	<i>Ethanol</i>	0.941
	<i>Formic acid</i>	0.722
	<i>Methanol</i>	0.659
	<i>1-butanol</i>	0.571
<i>Medium ($0.1 < \tan \delta < 0.5$)</i>	<i>2-butanol</i>	0.477
	<i>Acetic acid</i>	0.174
	<i>Water</i>	0.123
	<i>Chlorobenzene</i>	0.101
<i>Low ($\tan \delta < 0.1$)</i>	<i>Chloroform</i>	0.091
	<i>Acetone</i>	0.054
	<i>Toluene</i>	0.040
	<i>Hexane</i>	0.020

The materials generating heat by absorbing microwaves are called “microwave absorbers”. It can be concluded from Table 5.3 that methanol and water, the reactants of methanol steam reforming reaction, absorb the microwaves and produce heat effectively. It is also widely reported in the literature that the carbon materials are strong microwave absorbers (Table 5.4) [74]. Due to this fact, study on microwave absorbing properties of carbon materials has been growing recently. Figure 5.2 demonstrates the rising number of published articles reporting the researches done on

the microwave-assisted processes of the carbon materials by 2010. The high absorbing rate of microwaves by the carbon materials strongly supports the idea of utilizing them as the catalyst support for endothermic microwave-assisted reactions.

Table 5.4. Loss factors ($\tan \delta$) of the carbon materials at 2.45 GHz and 20 °C [75].

Carbon material	$\tan \delta$	Carbon material	$\tan \delta$
Coal	0.02-0.08	Carbon black	0.35-0.83
Carbon foam	0.05-0.20	Activated carbon	0.57-0.80
Charcoal	0.11-0.29	Carbon nanotube	0.25-1.14

Microwave heating is an alternative to conventional heating methods which are mainly by electrical or thermal sources. Microwave and conventional heating methods are compared in many respects and the differences are summarized in Table 5.5. In addition to all of the remarkable advantages which microwave heating exhibits, there are still a few limitations requiring further efforts, such as lack of scalability, safety hazards, and health risks [73].

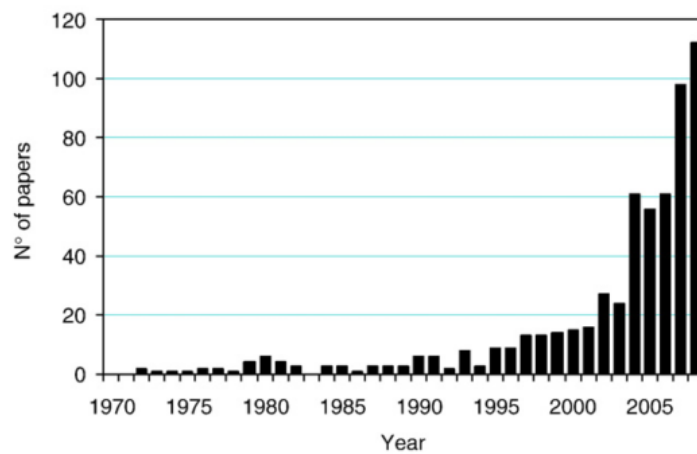


Figure 5.2. Research papers published related to microwave-assisted processes of the carbon materials, reprinted from [75].

Table 5.5. Comparison of the conventional and microwave heating methods [73].

	Conventional Heating	Microwave Heating
Heating source	<i>Thermal or electrical</i>	<i>Electromagnetic waves</i>
Heating direction	<i>From the inside surface of the reaction container</i>	<i>Directly inside the material</i>
Physical contact with the container	<i>The reaction vessel and the heating source</i>	<i>No physical contact</i>
Heating mechanism	<i>Heat conduction</i>	<i>Dielectric polarization</i>
The highest achievable temperature	<i>Boiling point of the material</i>	<i>Higher than the boiling point of the material</i>
Heating selectivity	<i>Equal heating of all components</i>	<i>Specific heating based on the dielectric characteristics</i>
Heating rate	<i>Low</i>	<i>High (10-1000 times higher)</i>

5.3. MICROWAVE APPLICATORS

The microwave ovens are usually categorized into two main classes; mono-mode and multi-mode. The mono-mode microwave ovens are operating by creating a standing wave model (Figure 5.3) by interfering different fields. The microwave energy intensity is zero at the nodes, and maximum at the antinodes. It is very important to locate the sample vessel in a proper distance from the magnetron. The proper location for the sample vessel is at the anti-nodal position of the wave pattern (Figure 5.4). In mono-mode microwave applicators, high rate, effective, and homogeneous heating can be obtained. However, the number of irradiated vessels is limited to only one at a time.

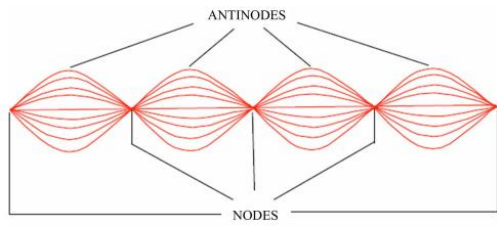


Figure 5.3. The wave pattern created by mono-mode applicators, reprinted from [73].

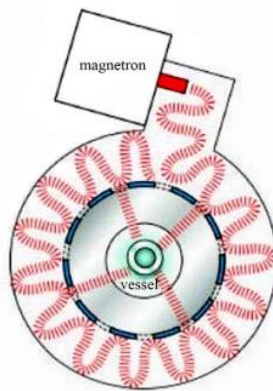


Figure 5.4. The mono-mode applicators heating mechanism, reprinted from [73].

Initial microwave ovens and the ovens currently used in houses are multi-mode microwave ovens. In this type of the applicators, the standing wave pattern is not generated deliberately in order to generate chaos inside the microwave cavity (Figure 5.5). The generated chaos helps to have more effective heating zone by increasing the radiation dispersion. Lack of temperature uniformity and hence poor heating control are the main drawbacks of multi-mode applicators. In contrast to mono-mode ovens, more than one sample can be heated in multi-mode ovens at the same time. Moreover, multi-mode ovens always occupy a larger volume. Due to these disadvantages, mono-mode ovens are used for laboratory experimental set-up, especially heterogeneous catalysis [73, 74, 76].

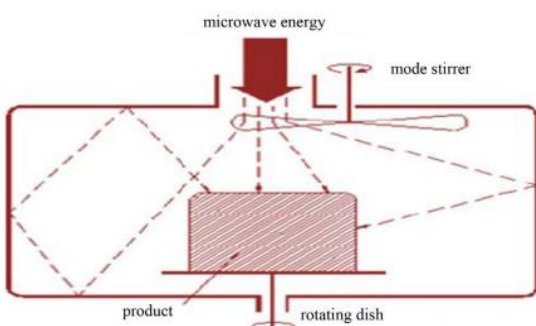


Figure 5.5. The multi-mode applicators heating mechanism, reprinted from [73].

5.4. MICROWAVE APPLICATIONS

In recent years, use of microwave has been extensively investigated in wide directions; including material processing, plasma processes, waste remediation, and catalytic reactions. Despite the major efforts on microwave development and being a clean, fast, cheap, environmentally friendly, and efficient technique, this technology is still in the laboratory stage [73, 76]. In this section, the focus is on the microwave applications in chemical reactions and processes, particularly in chemical synthesis and heterogeneous catalysis.

5.4.1. MICROWAVE-ASSISTED CHEMICAL SYNTHESIS

Microwave heating was firstly used in a chemical synthesis reaction by R. Gedye. Afterward, a large number of studies have been reported synthesis of different organic materials by the means of microwave irradiations. Few examples of these reports are summarized in Table 5.6 to show the microwave significant potential in different chemicals synthesis and its major success.

Table 5.6. A survey on reported microwave-assisted chemical processes [73, 77].

<i>Acetylation reaction</i>	<i>Deacetylation reaction</i>	<i>Michael reaction</i>
<i>Alkylation reaction</i>	<i>Dimerization reaction</i>	<i>Organometallics</i>
<i>Alkynes metathesis</i>	<i>Esterification reaction</i>	<i>Oxidation reaction</i>
<i>Amination reaction</i>	<i>Free radicals</i>	<i>Phosphorylation synthesis</i>
<i>Assymmetric reactions</i>	<i>Glycosylation reaction</i>	<i>Photochemistry</i>
<i>Claisen-Smith reaction</i>	<i>Halogenation reaction</i>	<i>Reduction reaction</i>
<i>CO insertions</i>	<i>Heck reaction</i>	<i>Ring closing synthesis</i>
<i>Coupling reaction</i>	<i>Heterocycle synthesis</i>	<i>Sonogashira reaction</i>
<i>Cynation reaction</i>	<i>Kumada reaction</i>	<i>Suzuki reactions</i>
<i>Cyclo-addition reaction</i>	<i>Mannich reaction</i>	<i>Ullman condensation reaction</i>

5.4.2. MICROWAVE AND HETEROGENEOUS CATALYSIS

The most significant advantage of using microwave heating in heterogeneously catalyzed reactions is to provide the catalyst active sites at a higher temperature (hot spot formation) than the bulk. In the conventional heating, the catalyst active sites are heated by heat conduction from the bulk, so the temperature can be optimistically equal to the bulk temperature. However, in microwave heating, the active sites are quickly heated to a temperature higher than the bulk temperature by microwave irradiations. Consequently, the higher temperature of the active sites increases the reaction rate. It also causes the reaction to reach the thermodynamic equilibrium with less energy. In the beginning, the microwave effect on reaction rates was a controversial issue. It was unknown whether the microwave irradiations have thermal effect on substrates, or there is a non-thermal interaction between microwave irradiations and the reactants. Afterward, several studies acknowledged that there is not any non-thermal and molecular effect of microwave on components of neither homogeneous nor heterogeneous reactions [72, 78].

Wan research group did the first attempt to utilize microwave heating in a chemical reaction by adding excellent microwave absorbers, ferromagnetic catalysts, in the early 1980s. As the result of microwave heating, a better temperature control was reported as well as the secondary reaction minimization [74].

Decomposition of H₂S was studied over MoS₂/γ-Al₂O₃ catalysts. Microwave heating resulted in higher conversion of this endothermic reaction than that of estimated by both thermodynamic and the previous experiments done by conventional heating methods. X-ray diffractograms proved that the main reason of the higher conversion is hot spots formation. Temperature at those hot spots was approximately 100-200 °C higher than the catalyst bulk material which increased the reaction rate [72, 74].

In another study, microwave-assisted pyrolysis of crude glycerol from biodiesel waste was examined to produce energy. In this study, a carbonaceous catalyst was selected due to its high microwave absorbing strength. It was affirmed that the microwave heating provides a rapid and efficient heating [79]. In a similar fashion, microwave-assisted pyrolysis was studied on soapstock to produce hydrocarbon-rich bio-oil with different types of catalysts. Ease of operation and maintenance, rapid and efficient heating, and simple system were the observed advantages of the microwave heating in pyrolysis process [80].

The effect of microwave heating on carbon dioxide reforming of methane over Pt catalysts was investigated. As a result, the reaction rate was accelerated due to microwave usage. Moreover, higher methane conversion and production selectivity were observed under microwave conditions compared to that with conventional heating method at the same temperature. These values were reported also to be higher than the values estimated by thermodynamic equilibrium [78].

Another study was done on a strongly exothermic reaction, hydrodesulphurization of thiophene over a commercial catalyst (BP-C2634). Studying the microwave heating effect on an exothermic reaction has been less examined compared to endothermic reactions so far in the literature. In this study, the thiophene conversion was reported

consisting of three stages. Firstly, it went up with temperature up to 300 °C. In this stage, the thiophene conversion under microwave conditions was higher than both equilibrium and the conversion under conventional heating condition. Secondly, the conversion was almost close to the equilibrium value (~100%) and no considerable difference between the heating methods was observed. Finally, the increase in temperature decreased the conversion. In this stage, the conversion of conventionally heated process remained closer to the equilibrium value, as opposed to the microwave heated reaction. Therefore, it was concluded that for an exothermic reaction, however, the hot spot formation can increase the reaction rate, it may cause an undesirable shift in the thermodynamic equilibrium [78].

5.4.2.1. MICROWAVE-ASSISTED HYDROGEN PRODUCTION

This area is less developed than the other application fields of microwave heating. Lack of documentation in the literature caused this category of microwave-assisted heterogeneous catalysis remains immature. However, it is drawing the attention of researchers due to the growing interest in hydrogen production methods and also microwave heating potential to be a reliable heating source.

Oxidation of methane over cobalt and nickel loaded catalysts supported by ZrO₂ and La₂O₃ was studied in order to produce hydrogen. The methane conversion and hydrogen selectivity were evaluated and compared under both conventional and microwave heating conditions. The results showed the higher values of methane conversion and hydrogen selectivity under microwave heating for all catalysts types. It was also observed that the same methane conversion as the conventional heating could be obtained with the microwave heating at a temperature almost 200 °C lower [72].

Another study investigated microwave heating effect on hydrogen production from water-gas shift reaction. For this purpose, Fe-Cr-based catalyst (Sud-Chemie SHT4) was used. It was strongly affirmed that the reaction performance was much better

under microwave irradiation than conventional heating methods. A smooth increase in CO conversion was observed under microwave heating condition as a result of either temperature or steam/CO ratio increase, unlike conventional heating methods. It was attributed to steam and catalyst efficient energy absorption. Furthermore, a faster and more efficient heating was provided by microwave irradiation as well as the less needed space [81].

Hydrogen generation from ammonia decomposition was another study to compare microwave and conventional heating performances. The aim of this research was the fuel cell quality hydrogen generation using iron incorporated mesoporous carbon catalysts. Complete ammonia conversion was obtained at 600 °C and 450 °C with conventional and microwave heating methods, respectively. The catalyst characterizations revealed that iron carbide crystals were formed under microwave irradiation which was postulated to be a decisive factor in ammonia decomposition. While, the catalysts used in conventionally-heated reactor system contained metallic iron [82].

Microwave-assisted ethanol steam reforming reaction over Co-Mg/mesoporous alumina was also reported. The most important observations of this investigation were the higher stability, better energy utilization, and lower coke formation in comparison to conventional heating methods [83].

Methanol steam reforming reaction heated by microwave over the most commonly used catalyst, Cu/ZnO/Al₂O₃, was examined. It was reported that microwave double absorption by the reactants and the catalyst provides a quick heating and the process begins in a short time. The methanol conversion with microwave heating at 250 °C was higher than that with conventional heating method at the same temperature. According to the results of this study, increasing the steam/methanol ratio has opposite effect on methanol conversion due to the increasing water microwave absorption than that of methanol [84].

This process was also kinetically investigated. The study on both Cu/ZnO catalyst pellet and reactor scales, confirmed that the energy generated by microwave heating is homogeneously distributed. Moreover, it was mentioned that there is not any considerable difference on kinetics parameters under microwave and conventional heating methods. The same performance as conventionally-heated reactor was obtained by microwave-heated system at a temperature of 20 °C lower [85].

A comprehensive study was done on methanol steam reforming reaction over both common catalysts, CuZnO/Al₂O₃ and PdZnO/Al₂O₃, heated by microwave and electrical methods. A higher methanol conversion (~10%) was always observed with microwave heating either at a same catalyst bed temperature with electrical heating or when the electrically-heated catalyst bed temperature is considerably higher. No change in products distribution was noticed. Moreover, a lower heat input by microwave was needed to achieve the same methanol conversion [86].

To best of our knowledge, microwave-assisted methanol steam reforming process has not been investigated using a mesoporous carbon supported catalyst so far. As is mentioned before, the carbon materials are strong microwave absorbers. This fact causes a better and more efficient energy transfer by microwave irradiations, due to the catalyst double microwave absorption by both the support and the loaded metals. As the result, the process becomes more economically feasible.

5.5. OBJECTIVES OF THE STUDY

According to the literature survey done for MSR process, it was concluded that using the mesoporous carbon materials as the catalyst support of methanol steam reforming reaction was very rarely discussed. The main aim of the presented work is to produce high purity CO-free hydrogen from the methanol steam reforming process to feed the on-board fuel cell system. For this purpose, an active and stable catalyst was designed and synthesized. The catalyst activity was tested in both conventional and microwave-heated reaction setups. As far as the author is aware, no work was dedicated to the

usage of this catalyst support in the microwave-focused methanol steam reforming process. In conclusion, the following issues were covered:

- Synthesis of Cu-Zn catalysts supported by CMK-3.
- Catalysts characterization using different methods, such as N₂ adsorption/desorption (BET method), XRD, thermogravimetric analysis (TGA), Raman spectroscopy, and SEM.
- Analyzing the catalyst performance in conventionally-heated and microwave reactor systems.

CHAPTER 6

EXPERIMENTAL

This chapter comprises the detailed description of materials synthesis procedures and characterization conditions, as well as the complete explanation of methanol steam reforming reaction systems.

6.1. MATERIAL PREPARATION

CMK-3 was selected as the catalyst support of the reaction studied in this work due to its superior properties that were completely explained in Chapters 4 and 5. In this section, the synthesis procedures of CMK-3 and its silica template, SBA-15, are described followed by the active components loading procedure by wet impregnation method.

6.1.1. SBA-15 SYNTHESIS

A solution of 2 M hydrochloric acid fuming 37 % (HCl, Merck) was first prepared by mixing 25 ml HCl and 125 ml deionized (DI) water. 4.0 g Pluronic P-123 (Poly(ethylene glycol)-block-poly(propylene glycol)-block-poly(ethylene glycol)) (Aldrich) was dissolved in the solution. It was stirred by a magnetic stirrer at the room temperature for 3 h until a clear solution was obtained. The mixture was gradually heated to 40 °C. 8.2 g Tetraethylorthosilicate (TEOS, Merck) was then added to the mixture dropwise under the continuous stirring. To begin the hydrothermal synthesis, the mixture was placed and kept inside an oven at 90 °C for 24 h. After cooling the mixture, it was filtered and washed with an adequate amount of DI water until the pH reached to 7. The resultant white paste was then put into the oven to be dried at 40 °C

for 2 h. The dried material was calcined at 600 °C in a tubular furnace with a heating rate of 1 °C/min for 6 h under dry air with a flow rate of 60 cc/min. Finally, the obtained material is SBA-15 [87]. Figure 6.1 depicts the scheme of SBA-15 formation.

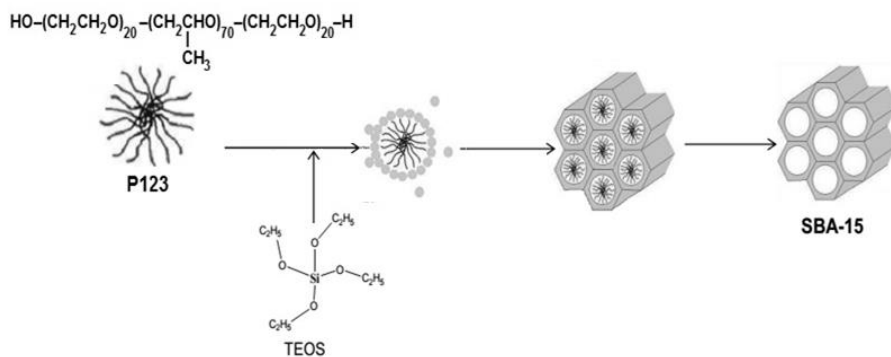


Figure 6.1. Scheme of SBA-15 synthesis [20].

6.1.2. CMK-3 SYNTHESIS

For CMK-3 synthesis, the original synthesis procedure published by Ryoo research group [62] was modified. Firstly, 1.25 g sucrose (Torku Şeker) was added in a mixture of 0.14 g sulfuric acid (95-98 %) (H_2SO_4 , Merck) and 5 ml DI water. Then 1 g synthesized SBA-15 was added to the mixture. After 1 h stirring by a magnetic stirrer, the mixture was placed in an oven in order to commence the carbon precursor infiltration. Two different ways were followed for carbon formation reaction. In the first way, carbon formation reaction temperature was kept at 100 °C for 6 h, then it was increased to 160 °C and kept at that temperature for 6 h. In the second way, the carbon formation reaction temperature was kept at 160 °C for 12 h. Afterward, a solution of 0.8 g sucrose in 0.09 g H_2SO_4 and 5 ml DI water was added to the resulting solid. The same heating step was applied to the mixture. The resulting material was pyrolyzed at 900 °C in the tubular furnace with a heating rate of 5 °C/min under nitrogen atmosphere with a flow rate of 75 cc/min for 6 h. After the pyrolysis, the silica template had to be removed completely from the carbonaceous material. In order

to remove the silica template, two etching agents were used, NaOH and HF. In case of using NaOH, the sample was added to 1 M NaOH solution (50:50 vol% ethanol-H₂O) at its boiling point (90 °C in the experiment condition) which was prepared by solving 24 g sodium hydroxide (NaOH, Merck) in 300 ml DI water and 300 ml ethanol. After stirring for 2 h at the constant temperature, it was filtered and treated again with another 1 M NaOH solution. The mixture was then filtered, washed with 1 L boiling absolute ethanol ($\geq 99.8\%$) (Aldrich), at almost 78 °C, and then dried at 100 °C for 4 h. On the other hand, a different procedure was followed for HF. By mixing 24 ml hydrofluoric acid (48 %) (HF, Aldrich) and 100 ml DI water, a 10 wt% solution of hydrofluoric acid was prepared. The pyrolyzed material was added to the solution and stirred for 45 minutes at the room temperature in plastic tubes. Then it was centrifuged in a centrifuge (TG19-WS) at 6000 rpm for 3 minutes, filtered and washed with DI water. Finally, the template-free CMK-3 was dried at 100 °C for 4 h. A brief information about the studied parameters in the CMK-3 synthesis and the corresponding synthesized CMK-3 materials is given in Table 6.1. The scheme of CMK-3 is represented in Figure 6.2.

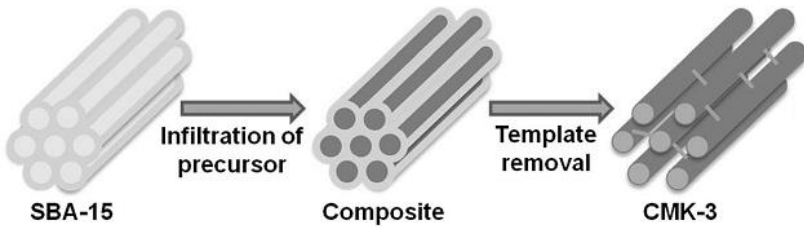


Figure 6.2. Scheme of CMK-3 synthesis [20].

Table 6.1. *Investigated parameters in the synthesis of CMK-3.*

	Reaction Temperature of Carbon Formation Reaction	Silica Removing Agent	Name
CMK-3	<i>160 °C (12 hours)</i>	<i>NaOH</i>	<i>CMK-3/1-NaOH</i>
	<i>100 °C (6 hours) + 160 °C (6 hours)</i>		<i>CMK-3/2-NaOH</i>
	<i>160 °C (12 hours)</i>	<i>HF</i>	<i>CMK-3/1-HF</i>
	<i>100 °C (6 hours) + 160 °C (6 hours)</i>		<i>CMK-3/2-HF</i>

6.1.3. METAL LOADING INTO CMK-3

The final step in the catalyst preparation was loading of the active metal and the desired promoters into the synthesized catalyst support (CMK-3) by wet impregnation method [20]. In this study, copper and zinc were impregnated into the catalyst support with different specifications. Table 6.2 summarizes the catalysts and the parameters tested in the MSR process for this study. It is worth mentioning that the synthesized catalysts were entitled based on their synthesis condition as XCuYZn/CMK-3/Z, where X and Y indicate the impregnated copper and zinc mole percentage, respectively, and Z shows the catalyst calcination temperature.

The detailed calculations related to required amounts of each copper salt, copper (II) nitrate trihydrate (Merck), and zinc salt, zinc nitrate tetrahydrate (Merck), is given in Appendix A. The results of these calculations are shown in Table 6.3.

Table 6.2. *The studied parameters and catalysts used for the MSR reaction in the conventionally-heated reactor.*

Studied Parameter	Catalyst	Calcination Temperature, (°C)	Total Metal Loading, (%)	Cu/Zn	Reaction Temperature, (°C)
<i>Calcination Temperature</i>	12Cu6Zn/CMK-3/300	300	18	2	250
	12Cu6Zn/CMK-3/450	450			
<i>Cu/Zn</i>	9Cu9Zn/CMK-3/300	300	18	1	250
	12Cu6Zn/CMK-3/300			2	
	13.5Cu4.5Zn/CMK-3/300			3	
<i>Total Metal Loading</i>	13.5Cu4.5Zn /CMK-3/300	300	18	3	250
	18.75Cu6.25Zn/CMK-3/300		25		
<i>Reaction Temperature (°C)</i>	18.75Cu6.25Zn/CMK-3/300	300	25	3	200
					225
					250
					275
					300

Table 6.3. *The required amount of metal precursors for 0.3 g CMK-3.*

Catalyst	Total metal loading, (%)	Cu/Zn	Cu	Zn
9Cu9Zn/CMK-3/300	18	1	0.102 g	0.108 g
12Cu6Zn/CMK-3/300		2	0.134 g	0.074 g
13.5Cu4.5Zn/CMK-3/300		3	0.154 g	0.054 g
18.75Cu6.25Zn/CMK-3/300	25	3	0.214	0.075 g

In order to prepare each catalyst, the specified amount of the corresponding salt was dissolved in 5 ml DI water. After adding 2 ml DI water, the mixture was poured into 0.3 g CMK-3 dropwise by a dropper. The mixture was stirred for 24 h and then dried at 45 °C in a water bath. The dried material sample was heated to 300°C at a heating rate of 5°C/min in a quartz tubular reactor and under nitrogen flow of 100 ml/min. The resultant material was also reduced with pure hydrogen flow of 40 ml/min at 250 °C at a heating rate of 5 °C/min for 150 minutes to activate it for the reaction. The reduction step was carried out carefully with a slow heating ramp and a temperature lower than 300 °C to prevent catalyst sintering. During this process, CuO was reduced to Cu⁰ [88].

6.2. MATERIAL CHARACTERIZATION

Physical and chemical properties of the synthesized materials were investigated using different characterization techniques. Several characterization methods were applied to the catalysts, such as, N₂ adsorption/desorption (BET method), X-ray diffraction (XRD), thermogravimetric analysis (TGA), chemical adsorption (TPD), Raman spectroscopy, scanning electron microscopy (SEM).

6.2.1. NITROGEN ADSORPTION/DESORPTION

Nitrogen physisorption is a mighty and widely used technique to determine the textural properties of porous materials, particularly surface area, pore diameter, and pore volume. These properties were determined using Micromeritics Tristar II 3020 instrument available in METU Chemical Engineering department after degassing the samples at 150 °C for 3 h. The nitrogen gas temperature was 77 K. This characterization analysis was performed for all synthesized samples prior to proceeding to other techniques.

6.2.2. X-RAY DIFFRACTION (XRD)

This technique is a unique tool to identify the material crystalline phase and to determine the crystallite size of porous materials. The synthesized samples were analyzed using Rigaku Ultima-IV X-Ray diffraction device with nickel filtered CuK α 1 radiation in METU central laboratory with the following conditions: scanning rate of 0.1 °/min for 2 θ values of 0.5°-2°, and 2 °/min for 10-90° at 40 kV and 30 mA.

6.2.3. THERMOGRAVIMETRIC ANALYSIS (TGA)

TGA tests were done using Shimadzu Simultaneous TGA/DTA Analyzer DTG-60H in METU Chemical Engineering department in order to check thermal stability of the support and the fresh catalysts. The analysis was performed at a temperature range of 25-900 °C with the heating rate of 10 °C/min under dry air flow of 60 cc/min.

6.2.4. RAMAN SPECTROSCOPY

In order to identify the synthesized materials, Raman spectroscopy is a useful characterization technique that gives structural fingerprint of the materials. The Raman spectra of samples were recorded using Bruker FRA 106/S FT-Raman instrument with a laser (532 nm) as excitation source and liquid N₂-cooled detector was also used.

6.2.5. SCANNING ELECTRON MICROSCOPY (SEM)

The synthesized samples were imaged using QUANTA 400F Field Emission with the microscope resolution of 1.2 nm in METU Central Laboratory. They were coated by Au-Pd in order to increase intensity of the signals coming from electrons.

6.3. ACTIVITY TESTS FOR MSR PROCESS

The most crucial stage after designing and synthesizing a catalyst was to test its activity in the MSR reaction. In this work, the catalytic activity tests were conducted in two different reactor setups; conventionally-heated flow and focused-microwave. The systems were composed of two main streams, one for catalyst reduction and the other for hydrogen production.

6.3.1. HYDROGEN PRODUCTION SYSTEM

6.3.1.1. CONVENTIONALLY-HEATED REACTOR SYSTEM

The conventionally-heated flow reactor system is schematically shown on Figure 6.3. A syringe pump, evaporator, electrically-heated tubular furnace, fixed bed flow reactor, condenser and gas chromatograph (Agilent Technologies 6850) were the components of the system. In the hydrogen production unit, the syringe pump (Cole Palmer TW-74905- 02) fed the reactants to the system. The reactants were already prepared in form of a liquid feed. In the evaporator, argon gas was used as the carrier gas to carry the reactants and also to pressurize the GC valve. Argon was supplied flowing through globe valve, and a mass flow controller. The gas mixture entered the reactor after leaving the evaporator. The reaction took place in a quartz tubular reactor (1/4" diameter) which has a porous quartz filter in the middle to retain catalyst particles. The reactor was filled with catalyst and placed inside the electrically heating tubular furnace (Carbolite MTF 12/38/250). The furnace has a temperature controller that can adjust the reaction temperature. The tubes connected to the reactor were heated by heating tapes to prevent the reactant and product condensation. In order to separate condensable components of the stream leaving reactor, a condenser was connected to a chiller water bath (Wise Circu). The gaseous stream was analyzed using on-line GC with 1/8" Alltech Porapak S packed column (Agilent Technologies 6850

Network GC System). GC parameters and the method information are tabulated in Tables 6.4-6.5. After the GC, the gas flow was measured using a soap bubble meter and then the gas mixture was vented.

Table 6.4. *GC parameters and their setting values*

Parameter	Value
Inlet heater temperature (°C)	200
Total flow (ml/min)	5
Detector temperature (°C)	200
Reference flow (ml/min)	40
Makeup flow (ml/min)	5

Table 6.5. *Temperature program for liquid and gas analyses*

Initial Temperature, (°C)	Final Temperature, (°C)	Temperature Ramp, (°C/min)	Time, (min)
38	38	-	3
38	175	24.1	7
175	175	-	15.64

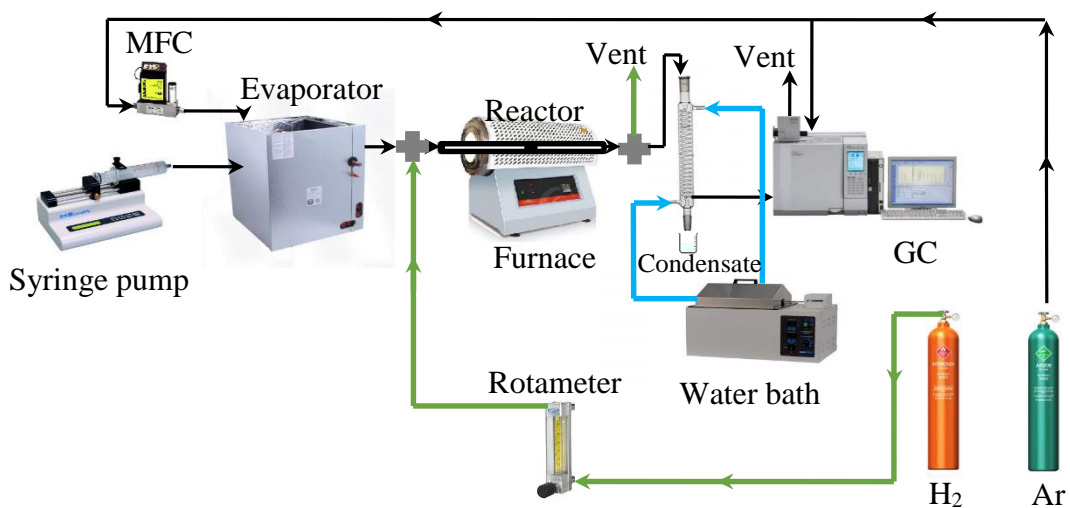


Figure 6.3. Conventionally-heated reactor system.

6.3.1.2. FOCUSED-MICROWAVE HEATED REACTOR SYSTEM

In order to make use of the focused-microwave system, it was replaced with the electrically heating furnace. The only difference between the focused-microwave and the conventionally-heated reactor systems was the heating supply device. Therefore, all the procedures described in section 6.3.1.1 for both catalyst reduction and hydrogen production units were applied to this system as well. As it is shown in Figure 6.4, the focused-microwave heated reactor (Sairem) comprised a generator, a magnetron, tuners, and an applicator. The generator was able to generate power up to 2000 W. The direct current coming from the generator was switched to microwave by the magnetron. The tuners were reflecting paddles directing the microwave onto the catalyst bed in the reactor. The reaction took place in a quartz reactor located on the applicator. There was also a piston on the top of the applicator which reflects the microwave not absorbed by the material to the catalyst bed. The water circulation between the generator and the magnetron was due to sensitive components of the magnetron protection, like filaments, from the unabsorbed microwave. The catalyst

bed temperature was measured using an infrared pyrometer located in front of the catalyst bed within a distance of 2 cm.

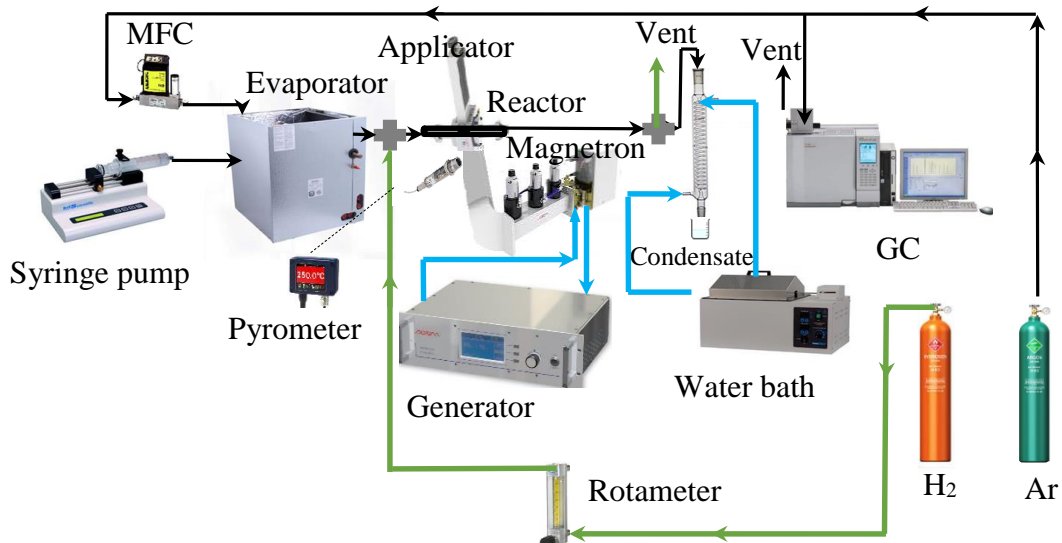


Figure 6.4. Microwave-focused reactor system.

6.3.2. EXPERIMENTAL PROCEDURE

0.15 g catalyst was weighed in each experiment. Ar flow rate was set to 30 ml/min and the water bath was adjusted to -15 °C. The effluent total flow rate was measured using a soap bubble meter before venting. The tubular furnace was set to the desired reaction temperature and heated at a heating rate of 7°C/min. After reaching to the desired reaction temperature, hydrogen gas at 2 bar with a flow of 40 mL/min was fed to the reactor for 150 min to make the synthesized catalysts active and ready for the reaction. It was then vented after passing through the soap bubble meter. After the reduction step, the evaporator was set to 130 °C. Heating tapes were wrapped on the pipelines at the furnace inlet and outlet. They were also set to 130°C. The syringe pump, containing methanol and water in a molar ratio of 1, fed the reactants to the system at the constant flow rate of 0.9 ml/h. The gaseous stream leaving the furnace

was analyzed by GC, for every 20 min before passing through the soap bubble meter, where the flow was measured, and venting. At the end of 5 hours, the syringe pump was turned off and the GC was shut down. After 1 hour, the evaporator and the furnace were switched off. Heating the heating tapes was stopped and the argon mass flow controller was closed.

CHAPTER 7

RESULTS AND DISCUSSION

This section involves the characterization results of both support material and the synthesized catalysts. The support material, CMK-3, was synthesized at one step and two step reaction temperature using two different silica removing agents, HF and NaOH. The metal-loaded catalysts were prepared with different calcination temperatures (300 °C and 450 °C), Cu/Zn ratios (1,2, and 3), and metal loading amounts (18% and 25%). Afterward, the catalytic performance results of the metal-loaded catalysts in the conventionally-heated, at the reaction temperature range of 200-300 °C, and the focused-microwave heated reactor, at the reaction temperature range of 250-300 °C, are given in catalytic activity result part.

7.1. CHARACTERIZATION RESULTS OF CATALYST

Various characterization techniques were applied on the synthesized materials, such as N₂ adsorption/desorption (BET method), XRD, thermogravimetric analysis (TGA), Raman spectroscopy, and SEM. Firstly, the characterization results of the support material are given in this section. Secondly, the results of the metal-loaded catalysts are discussed.

7.1.1. CHARACTERIZATION RESULTS OF THE SUPPORT

As it was explained thoroughly, the catalyst support (CMK-3) was synthesized using a silica template, SBA-15. Furthermore, the effects of one and two step reaction temperature, as well as the silica removing performance of HF and NaOH, on the physical properties of CMK-3 were investigated by characterizing the materials.

Based on the obtained characterization results, the best and optimum conditions of synthesis were determined. It is worth mentioning that the materials were synthesized and characterized numerous times to test the reproducibility of the results.

7.1.1.1. XRD RESULTS

Low-angle XRD pattern of SBA-15 is shown in Figure 7.1. The presence of three reflection peaks at 1° , 1.8° , and 2.3° is a sign of well-ordered structure of SBA-15. Figure 7.2 represents the XRD patterns of the synthesized CMK-3 samples. The low angle XRD patterns of the materials (Figure 7.2 (a)) reveal existence of three reflection peaks at 0.82° , 0.94° , and 1.04° corresponding to the (100), (110) and (200) reflections. It was observed that the well-ordered mesoporous structure of the SBA-15 was preserved in the synthesized samples [89]. Figure 7.2 (b) displays the wide-angle XRD patterns of these samples which all exhibit two broad diffraction peaks at 23° and 43° (PDF card no.: 411487 given in Appendix B). These peaks can be assigned to the (002) and (100) diffraction peaks of graphite, respectively. However, there were four peaks in the XRD pattern of CMK-3/1-NaOH at 2θ values of 30.24° , 34.66° , 38.14° , and 39.88° . These peaks correspond to sodium carbonate (PDF card no.: 01-077-2082). The XRD patterns proved that the synthesized material was carbon and well-ordered structure of SBA-15 was also preserved in the carbon material. Therefore, the synthesized material was CMK-3. Comparing the XRD patterns of the materials synthesized with different synthesis conditions, it was evident that the ordered structure of the material was not affected by changing the reaction temperature steps and/or using different silica removing agents. The XRD patterns are consistent with the XRD pattern of CMK-3 in the literature [89].

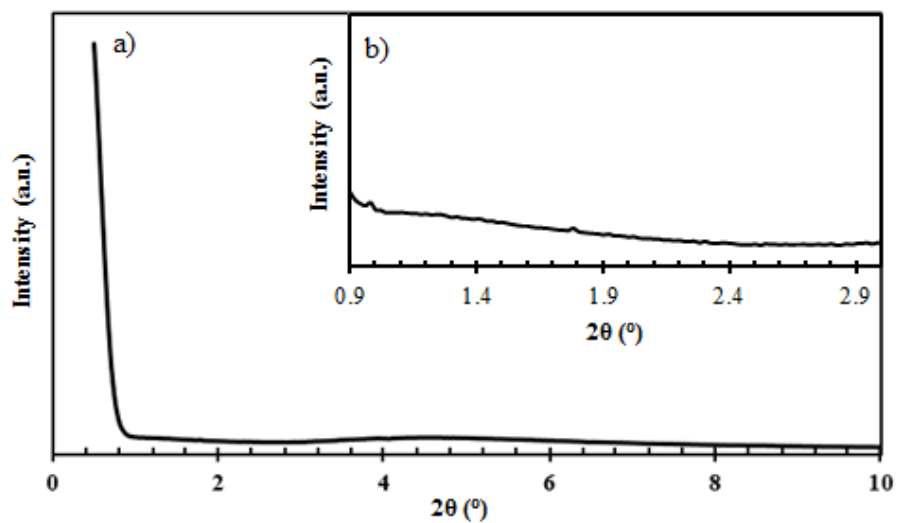


Figure 7.1. (a)Low-angle and (b)enlarged low-angle XRD patterns of the synthesized SBA-15.

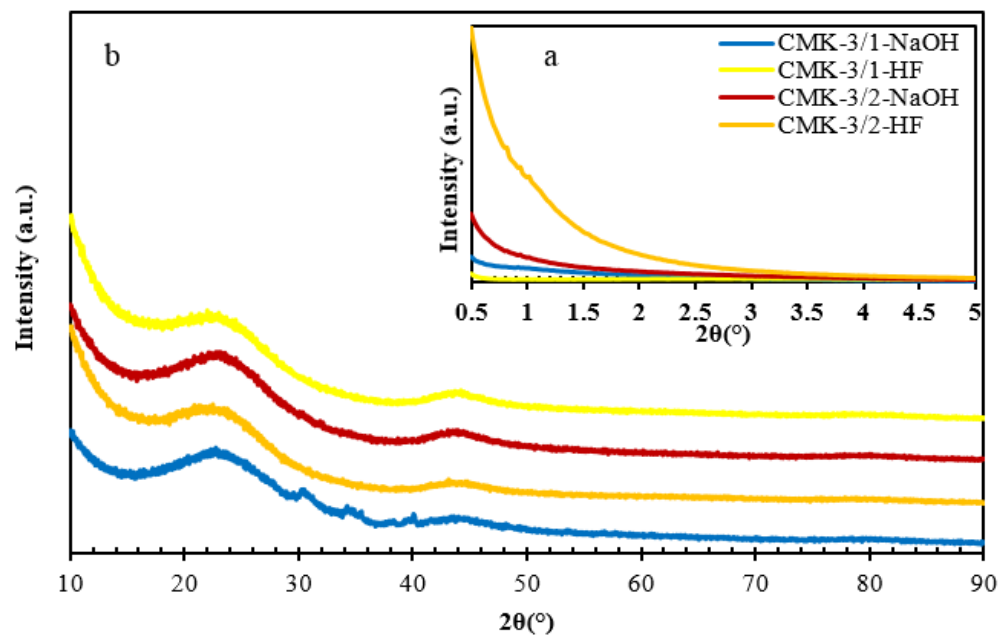


Figure 7.2. XRD patterns of the synthesized CMK-3 materials; (a) low angle and (b)wide-angle.

7.1.1.2. RAMAN SPECTROSCOPY RESULTS

Raman spectra of the synthesized CMK-3 samples are shown in Figure 7.3. Two Raman bands at 1339 cm^{-1} and 1588 cm^{-1} for both samples which are associated with the graphite-like structure of CMK-3 in the literature [60]. The former represents the D band that shows the disordered carbonaceous products and structural defects of the material. However, the latter shows the G band which generally appears in the graphite materials. The Raman results were in good agreement with the XRD results. It can be concluded that using different silica removing agent did not influence the material structure.

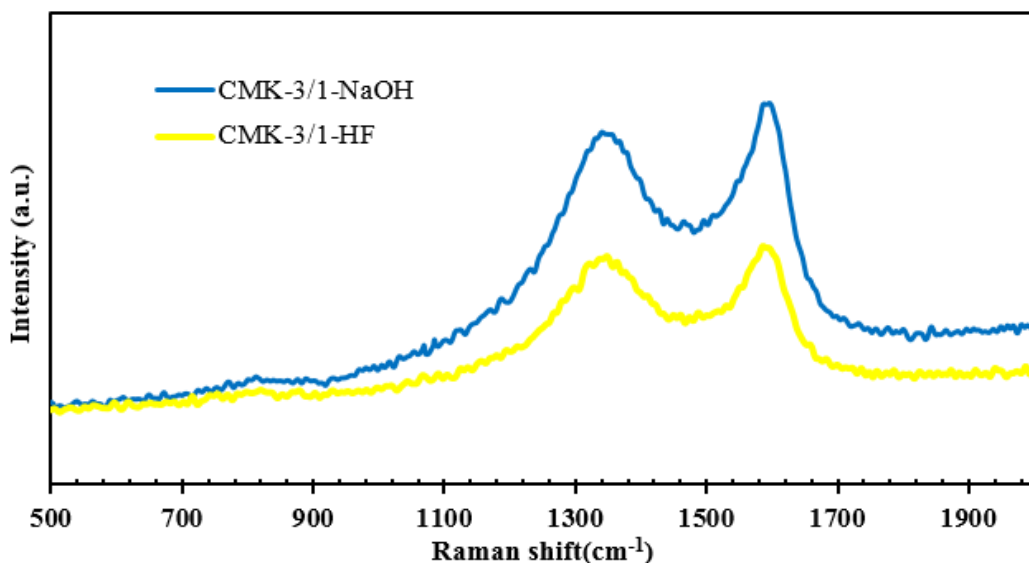


Figure 7.3. Raman spectra of the synthesized CMK-3 materials with different silica removing agents.

7.1.1.3. N₂ ADSORPTION/DESORPTION RESULTS

Figure 7.4 shows N₂ adsorption/desorption isotherms of SBA-15 and CMK-3 samples. Isotherm Type IV with H1 hysteresis (according to IUPAC classification) was observed in SBA-15 which is in good agreement with the literature [90]. SBA-15 has

uniform cylindrical mesopores with narrow pore size. However, all CMK-3 samples exhibited isotherm Type IV with H₂ hysteresis loop. This type of isotherm is the characteristic of mesoporous materials having cylindrical pore and non-uniform size. The physical properties of the materials are also tabulated in Table 7.1. It was observed that the surface area, pore volume, and pore diameter of the carbon materials synthesized in single step reaction temperature were higher than those of the materials synthesized in two step reaction temperature. The HF-utilized samples possess a higher average pore volume than those of the samples treated with NaOH. The larger pore volume was indication of effective silica removing from the carbon materials. Nevertheless, N₂ absorbed volume in the samples treated with HF at the low relative pressures (~0.01) was increased compared to that of SBA-15 and also the other CMK-3 samples which show the larger amount of micropores. A capillary condensation step was observed in the CMK-3 materials at a relative pressure range of 0.45–0.95 and in SBA-15 at a relative pressure range of 0.5–0.75, which indicates the uniform pore size distributions of the samples. The pore size distributions of the materials, calculated by BJH method from the desorption branch, are demonstrated in Figure 7.5. The mesoporous nature of the synthesized materials can be affirmed by a unimodal pore size distribution which can be easily observed in the mesopore range. Moreover, the pore range starts from 2 nm to 11 nm for each material. Narrow pore size distribution was observed in SBA-15 compared to all mesoporous carbon materials. The pore size distributions of the synthesized materials show a good agreement with their N₂ adsorption isotherms. It can be concluded that the single step reaction temperature in the formation of the silica/carbon composite leaded to a larger surface area, pore diameter, and pore volume. It caused less microporosity, too. Moreover, HF had a more effective performance in removing the silica matrix from the carbonaceous material compared to NaOH.

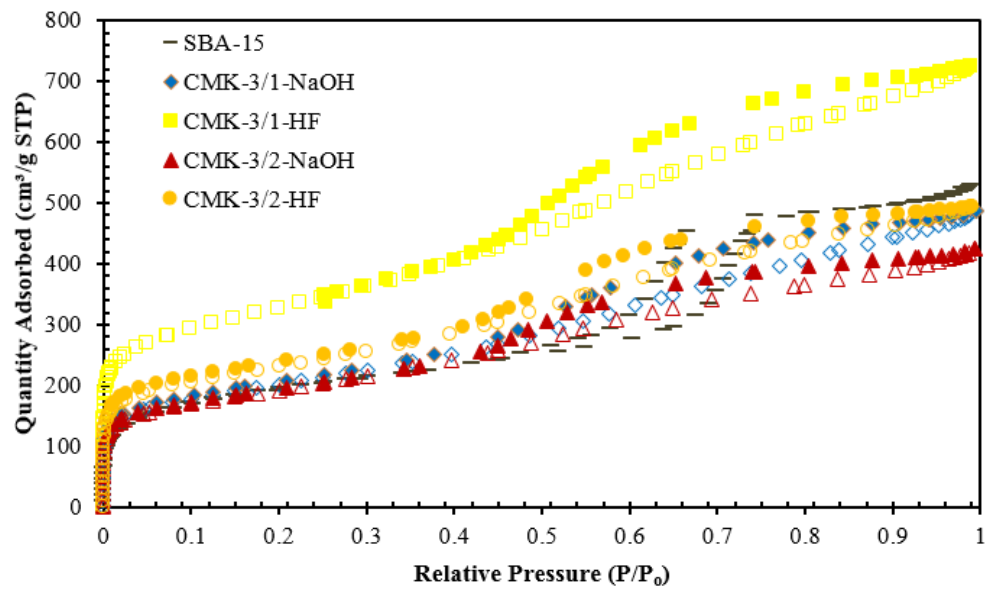


Figure 7.4. N_2 adsorption/desorption isotherms of the synthesized materials (The hollow and filled markers indicate adsorption and desorption branches, respectively).

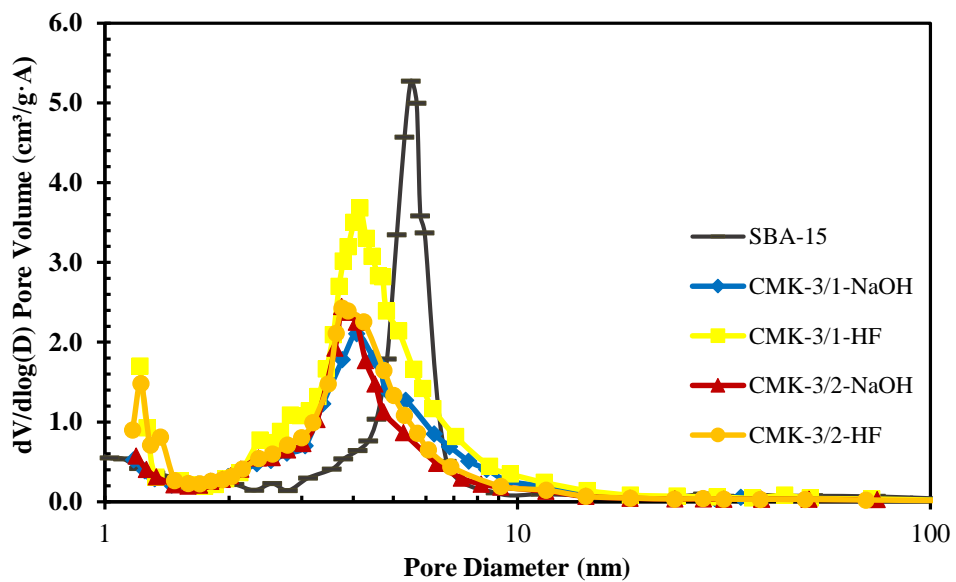


Figure 7.5. Pore size distributions of SBA-15 and CMK-3 materials.

Table 7.1. *Physical properties of the synthesized CMK-3 materials and the silica template.*

Material	S_{BET}^a, (m²/g)	Average Pore Volume^b,(cm³/g)	Average Pore size^b,(nm)	Microporosity, (%)
SBA-15	670	0.85	3.5	22
CMK-3/1-NaOH	696	0.78	3.7	30
CMK-3/1-HF	1120	1.19	3.7	34
CMK-3/2-NaOH	665	0.70	3.4	33
CMK-3/2-HF	790	0.83	3.2	35

^a Multipoint BET surface area is evaluated in the range of relative pressures of 0.00002-0.99
^b Pore volume and pore size are calculated by BJH method from desorption branch

7.1.1.4. TGA RESULTS

The TGA results of the synthesized CMK-3 materials are illustrated in Figure 7.6. The weight loss at the temperature range of 25-100 °C was due to moisture present in the pores of CMK-3. The second weight loss in the temperature range of 350°C-400°C was due to combustion of the carbon in the CMK-3 materials treated with NaOH. However, the HF-washed CMK-3 materials had the second major weight loss at around 550°C which demonstrates their higher thermal stability. The observed residual mass of the NaOH-treated samples is 7% which is higher than that of the samples etched by HF (=5%). HF removed silica from the CMK-3 structure effectively compared to NaOH. In other words, the performance of HF in removing silica from the carbon materials showed that HF was the best silica removing agent.

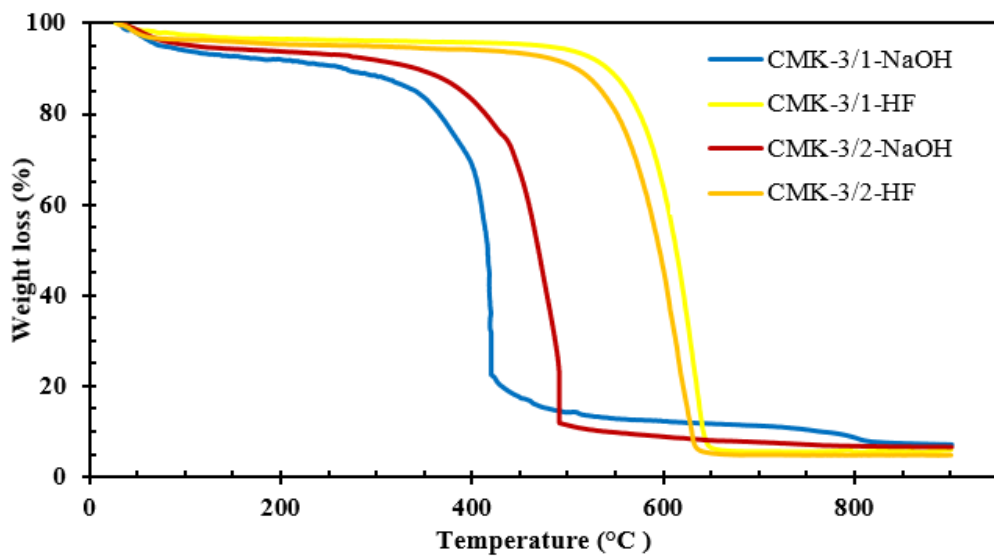


Figure 7.6. TGA results of the CMK-3 materials, performed under air.

7.1.1.5. SEM RESULTS

SEM images of SBA-15 are shown in Figure 7.7 with different magnifications. From the SEM images, formation of SBA-15 rod-like particles is visible. The agglomeration of hexagonal particles can also be observed easily.

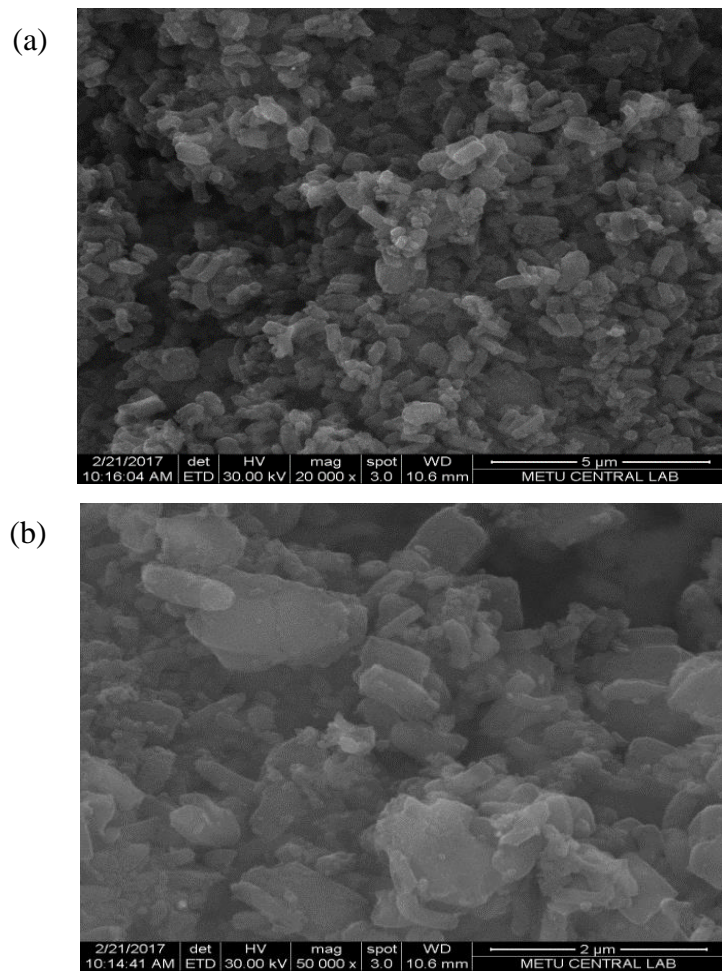


Figure 7.7. SEM images of SBA-15 at a)20000X and b)50000X magnifications.

Figure 7.8 represents SEM images of CMK-3 materials. Their morphology was different than SBA-15. In the CMK-3 materials synthesized in one step reaction temperature (Figure 7.8 (a) and (b)), there is only one uniform morphology. However, the samples synthesized in two step reaction temperature (Figure 7.8 (c) and (d)) have non-uniform morphology, shown in white and yellow circles. The presence of the sodium in the CMK-3/1-NaOH support, in the form of fibers, can be seen easily. It is also visible in the CMK-3/2-NaOH as white dots. Energy-dispersive X-ray spectroscopy results of the materials treated with NaOH and HF are given in Figure

7.9 (a) and (b), respectively. EDX results of the other synthesized carbon materials are given in Appendix C.

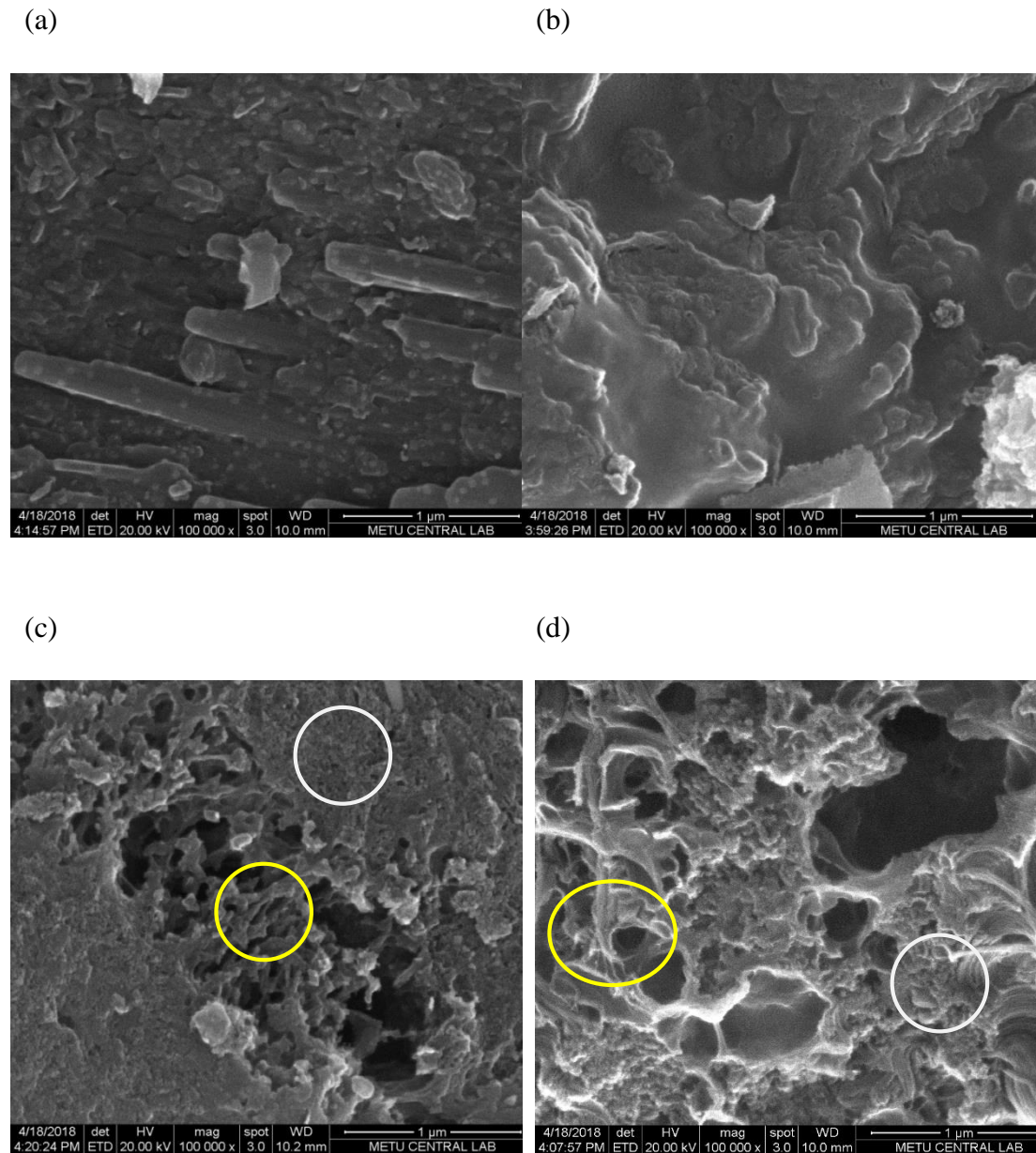


Figure 7.8. SEM images of a)CMK-3/1-NaOH, b)CMK-3/1-HF, c)CMK-3/2-NaOH, d)CMK-3/2-HF, at 100000X magnification.

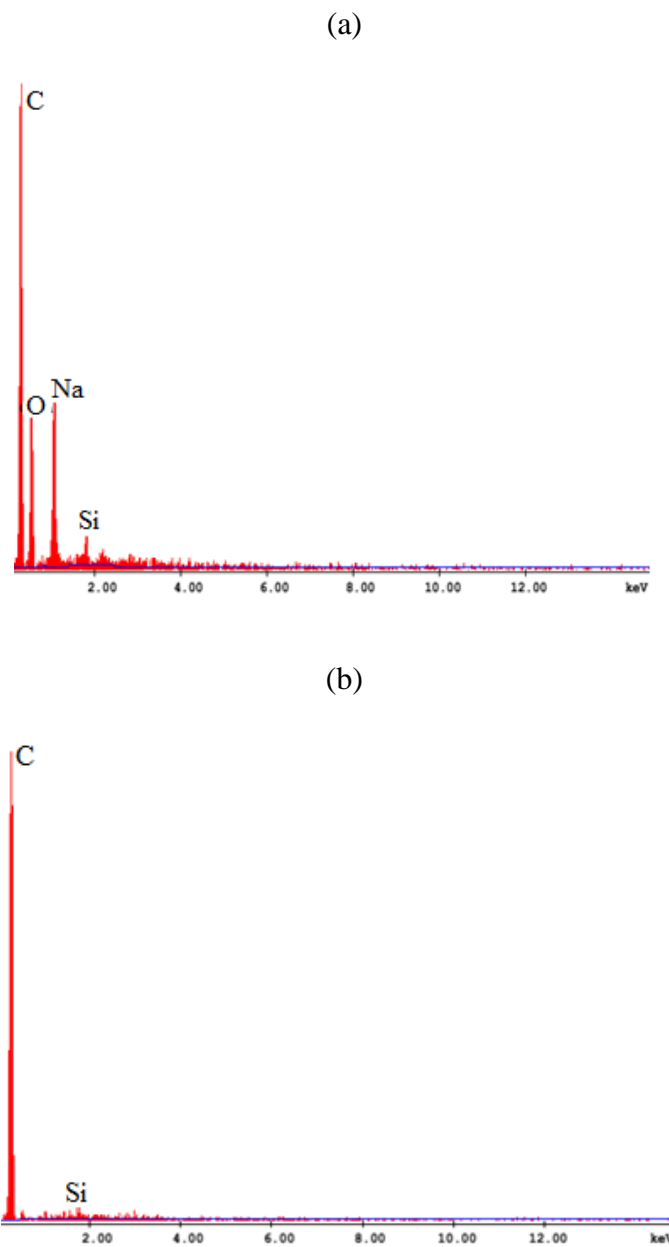


Figure 7.9. EDX analysis results of (a) CMK-3/I-NaOH and (b) CMK-3/I-HF.

The EDX results of the CMK-3 samples clarified that HF removed the silica template more efficiently than NaOH. There was higher amount of remained silicon in the samples washed with NaOH. Additionally, Na residue in the samples showed that

NaOH elimination from the material was not performed completely, too. Presence of sodium, as a result of using NaOH to remove the silica template, can be also seen from the SEM images of the CMK-3 materials (Figures 7.8 a and c).

All the points considered, the support CMK-3/1-HF has better and desirable properties. This fact was confirmed by the results obtained from each of the characterization tests, which are sufficiently discussed above. In conclusion, its synthesis route was selected as the main procedure to produce the best catalyst support.

7.1.2. CHARACTERIZATION RESULTS OF THE METAL-LOADED SUPPORT

Various catalysts were prepared and characterized in order to examine different parameters in the MSR process. The catalysts 12Cu6Zn/CMK-3/300 and 12Cu6Zn/CMK-3/450 were utilized to investigate the effect of catalyst calcination temperature. 9Cu9Zn/CMK-3/300, 12Cu6Zn/CMK-3/300, and 13.5Cu4.5Zn/CMK-3/300 were the synthesized catalysts in order to examine effect of Cu/Zn ratio on the catalytic performance. The effect of total metal loading amount was studied with the 13.5Cu4.5Zn/CMK-3/300 and 18.75Cu6Zn/CMK-3/300 catalysts. The MSR reaction temperature was also studied with 18.75Cu6Zn/CMK-3/300 in temperature range of 200-300 °C for the conventionally-heated reactor system and 250-300 °C for the focused-microwave heated reactor system.

7.1.2.1. XRD RESULTS

XRD patterns of all synthesized catalysts are given in Figure 7.10. The same trend in all of the patterns is visible including two broad peaks at approximately 22.8° and 43.18° corresponding to the carbon support material.

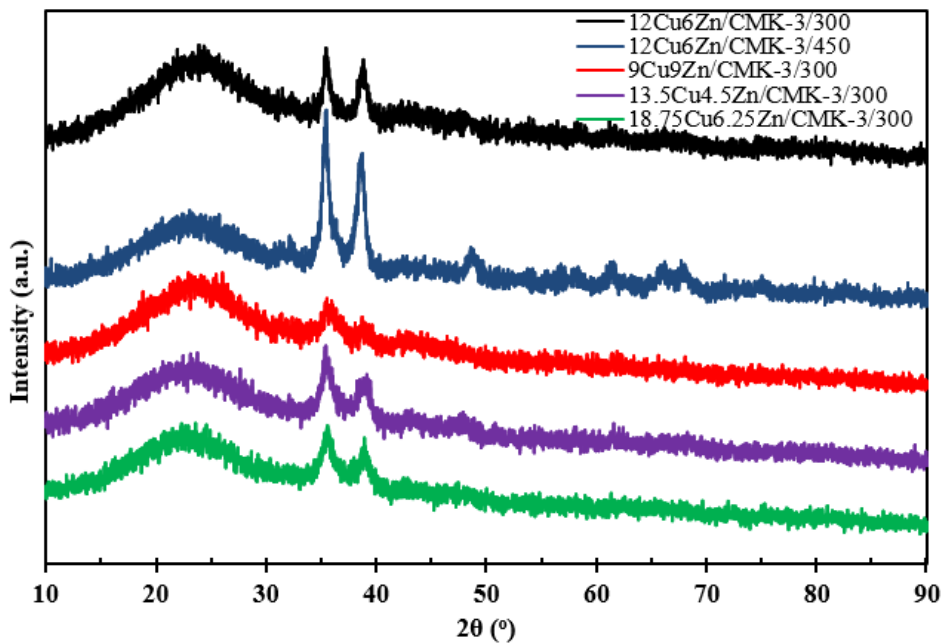


Figure 7.10. XRD patterns of all synthesized catalysts.

The XRD patterns of the catalysts with different calcination temperatures are shown in Figure 7.11. In the XRD pattern of 12Cu6Zn/CMK-3/450, the peaks at 2θ values of 35.29° , 35.50° , 38.76° , 38.76° , 39° , 48.74° , 58.04° , 61.56° , 65.58° , and 68.1° belong to CuO (PDF card no.: 10800076 given in Appendix B). Moreover, the peaks at 2θ values of 32.32° , 36.4° , 34.52° , 47.84° , and 57.06° were also observed which are attributed to ZnO (PDF card no.: 10751526 given in Appendix B). However, there were unassigned peaks at 66.3° , 67.78° , 72.5° , and 74.92° . In the XRD pattern of 12Cu6Zn/CMK-3/300 the peaks located at 2θ values of 32.41° , 35.48° , 35.71° , 38.72° , and 38.68° belong to CuO (PDF card no.: 10800076 given in Appendix B). It also contained the peaks at 2θ values of 32.15° , 34.55° , 36.74° , and 47.79° which are attributed to ZnO (PDF card no.: 10751526 given in Appendix B).

Calculation of crystallite sizes of 12Cu6Zn/CMK-3/300 and 12Cu6Zn/CMK-3/450 was determined using Scherrer equation, given in Appendix B. Results are summarized and presented in Table 7.2. 12Cu6Zn/CMK-3/450 has larger CuO

crystallite size with 51.54 nm, compared to that of 12Cu6Zn/CMK-3/300, which is attributed to the copper sintering because of its high calcination temperature. The larger crystallite size of 12Cu6Zn/CMK-3/450 can be also verified by the high and sharp peaks.

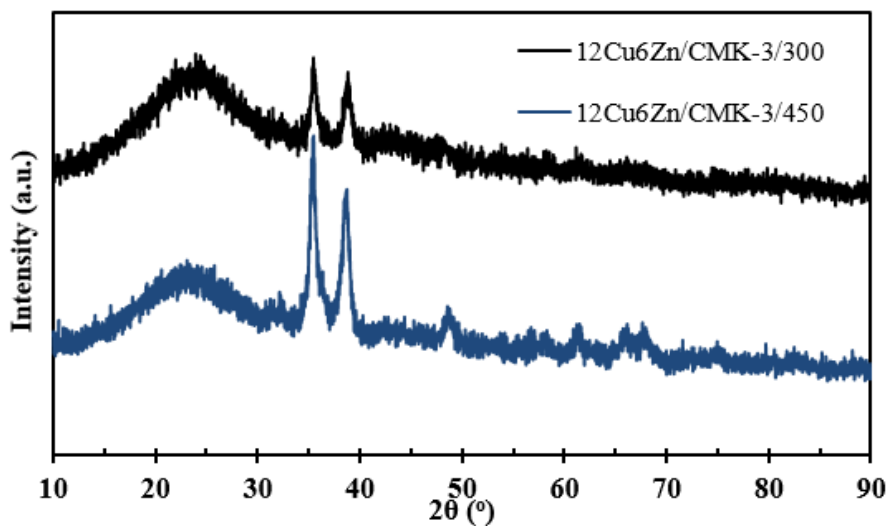


Figure 7.11. XRD patterns of the catalysts with different calcination temperatures.

Table 7.2. Copper crystallite sizes in the synthesized catalysts with different calcination temperatures

Catalyst	Cu crystallite size, (nm)
12Cu6Zn/CMK/300	37.49
12Cu6Zn/CMK/450	51.54

Furthermore, Figures 7.12-7.13 demonstrate the XRD patterns of the catalysts synthesized with different Cu/Zn ratio and metal loading amounts, respectively. In the XRD pattern of 13.5Cu4.5Zn/CMK-3/300, the peaks at 2θ values of 32.52° , 35.39° , 35.54° , 38.64° , and 38.97° correspond to CuO (PDF card no.: 10800076 given in

Appendix B). Moreover, the peaks at 2θ value of 32.36° , 36.42° , 34.57° , 47.81° , and 57.15° were also observed which are attributed to ZnO (PDF card no.: 10751526 given in Appendix B). In the XRD pattern of 9Cu9Zn/CMK-3/300, the peaks located at 2θ values of 32.47° , 35.43° , 35.78° , 38.76° , and 38.75° belong to CuO (PDF card no.: 10800076 given in Appendix B). It also contains the peaks at 2θ values of 32.39° , 36.46° , 34.58° , 47.89° , and 57.11° which are attributed to ZnO (PDF card no.: 10751526 given in Appendix B). The XRD pattern of 18.75Cu6.25Zn/CMK-3/300 shows the peaks at 2θ values of 32.5° , 35.5° , 35.8° , 38.81° , and 38.72° corresponding to CuO (PDF card no.: 10800076 given in Appendix B) and 32.4° , 36.41° , 34.51° , 47.88° , and 57.12° corresponding to ZnO (PDF card no.: 10751526 given in Appendix B).

The intensities of peaks for all catalysts are lower than that of the peaks for 12Cu6Zn/CMK-3/450. Therefore, any peaks at higher than 2θ values of 38.97° (for CuO) and 57.17° (for ZnO) were not observed. Moreover, the peaks intensity at 36.44° increased with an increase in Zn content.

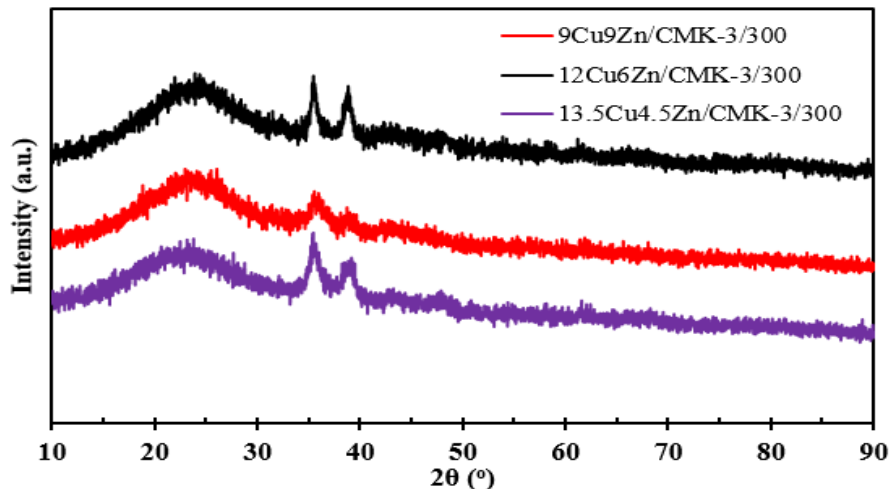


Figure 7.12. XRD patterns of the catalysts with different Cu/Zn ratio.

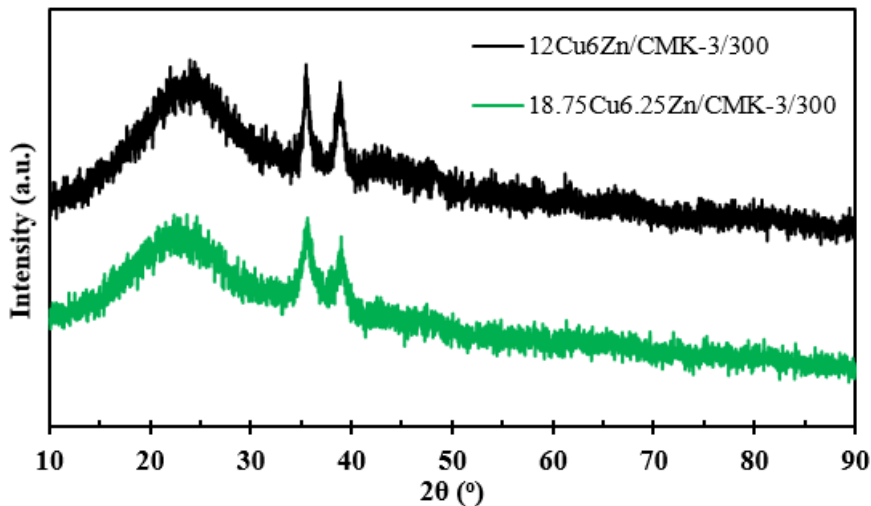


Figure 7.13. XRD patterns of the catalysts with different total metal loading amount.

The XRD patterns of the synthesized metal-loaded catalysts showed that copper and zinc oxides are the solid phases present in the materials, in addition to carbon phase.

7.1.2.2. N₂ ADSORPTION/DESORPTION RESULTS

The catalysts N₂ adsorption/desorption isotherms are given in Figure 7.14. Comparing to the CMK-3 isotherm, there is no difference between the isotherms of CMK-3 and the metal loaded supports. Comparatively, according to Table 7.3, it is clear that there was a decrease in the surface area, pore size, and pore volume of the support due to the metal loading on the support material. The capillary condensation for the catalysts occurred between the relative pressures of 0.48 and 0.97. The decrease in the textural properties by increasing the calcination temperature was caused by the metal particles sintering. The higher microporosity of 12Cu6Zn/CMK-3/300 compared to that of 12Cu6Zn/CMK-3/450 showed that metal particles were mostly loaded onto the mesopores. The increase in microporosity verified the successful impregnation of the metals onto the mesopores. On the other hand, altering Cu/Zn ratio indicated that the

optimum Cu/Zn ratio is 2 due to the larger surface area, pore volume, and pore size of 12Cu₆Zn/CMK-3/300 compared to those of 9Cu₉Zn/CMK-3/300 and 13.5Cu_{4.5}Zn/CMK-3/300.

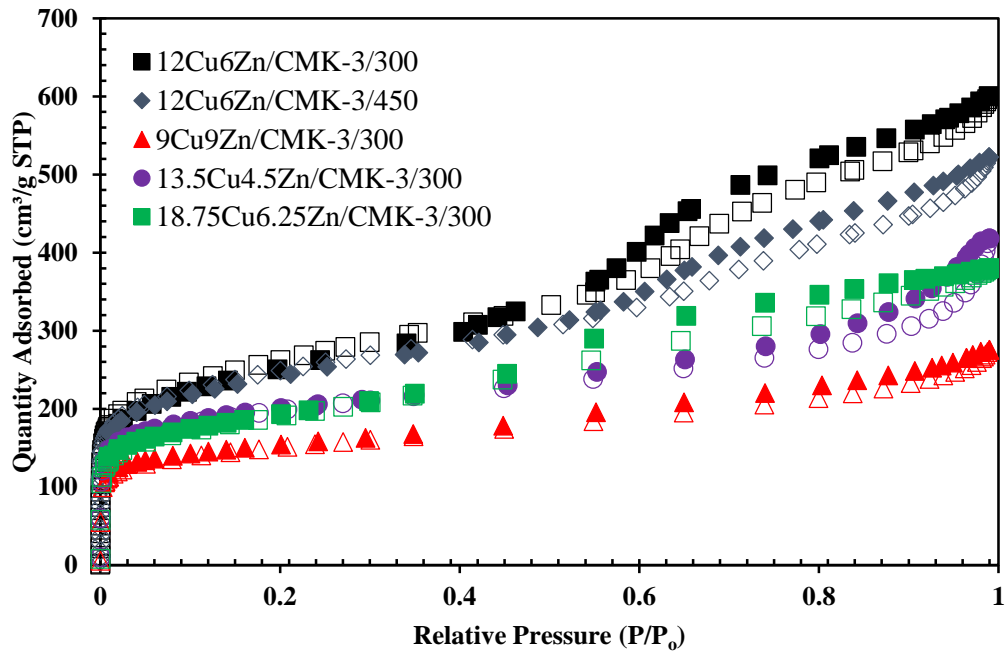


Figure 7.14. N₂ adsorption/desorption isotherms of the catalysts, (The hollow and filled markers indicate adsorption and desorption branches, respectively).

The catalysts pore size distributions are plotted in Figure 7.15. All samples had BJH desorption pore diameter in the range of mesopores which confirms their mesoporous structure. A slight decrease was observed in the support pore size due to the metal impregnation which is due to the occupation of uniform mesopores by metal impregnation. Additionally, increase in the metal loading amount and Cu/Zn ratio resulted in a less uniform pore size distribution and also smaller pore size. Moreover, the higher calcination temperature of 12Cu₆Zn/CMK-3/450 was the main reason of the less pore size distribution uniformity compared to the 12Cu₆Zn/CMK-3/300 catalyst.

Table 7.3. Physical properties of the synthesized catalysts.

Material	S_{BET}^a , (m ² /g)	Average Pore Volume ^b , (cm ³ /g)	Average Pore size ^b , (nm)	Microporosity, (%)
12Cu6Zn/CMK-3/300	870	0.99	3.40	32
12Cu6Zn/CMK-3/450	830	0.88	3.33	37
9Cu9Zn/CMK-3/300	580	0.54	3.22	47
13.5Cu4.5Zn/CMK-3/300	645	0.65	3.33	39
18.75Cu6.25Zn/CMK-3/300	690	0.81	3.31	38

^a Multipoint BET surface area is evaluated in the range of relative pressures of 0.00002-0.99

^b Pore volume and pore size are calculated by BJH method from desorption branch

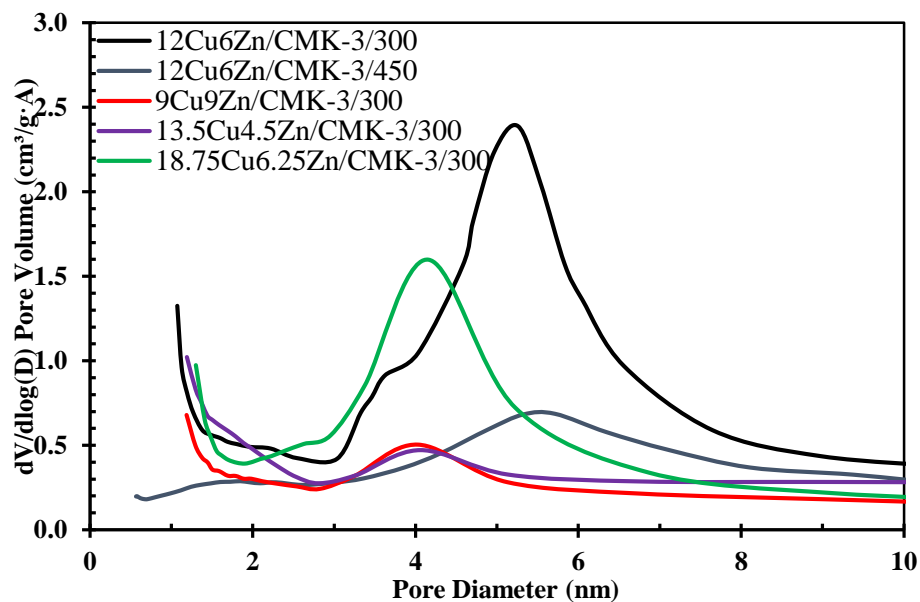


Figure 7.15. Pore size distribution of the catalysts.

7.1.2.3. TGA RESULTS

Fig 7.16 indicates TGA results of the synthesized catalysts. The first major weight loss can be observed by a common peak for all of the samples at around 80°C which the moisture starts to vaporize. The second weight loss gradually takes place at approximately 325°C where the amorphous carbon combustion begins. The metal-loaded catalyst has more thermal stability compared to the pure support material.

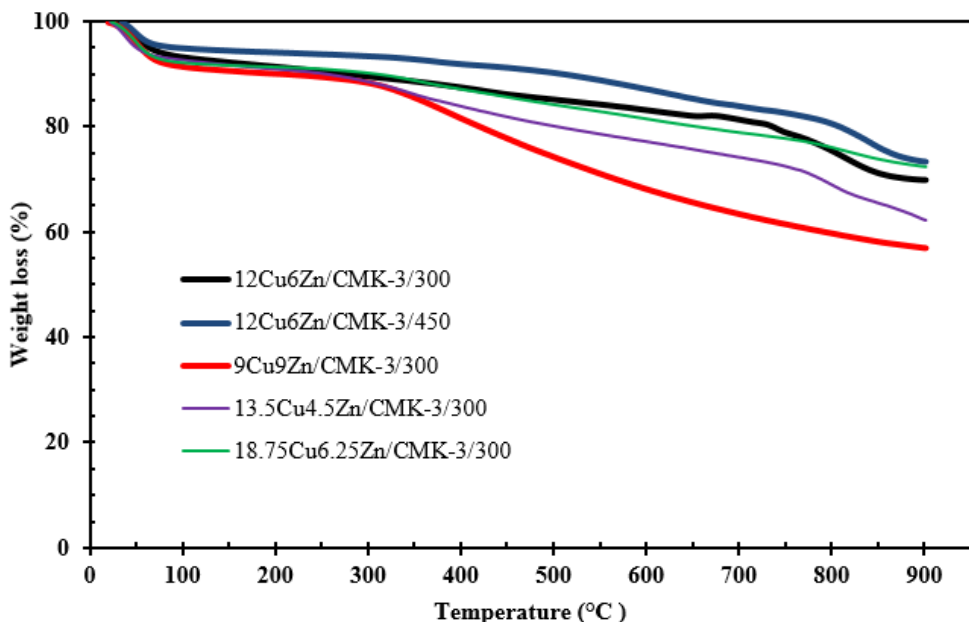


Figure 7.16. TGA results of the synthesized catalysts.

7.1.2.4. SEM RESULTS

Figure 7.17 shows the SEM images of fresh 12Cu6Zn/CMK-3/300 at the magnification of 10000X. The metal dispersion on the support surface is shown in Figure 7.17 (b) at 10000X by backscattering detector. The SEM and back scattered electron images of fresh 12Cu6Zn/CMK-3/450 are also demonstrated in Figure 7.18 at the same magnification to observe effect of increase in the calcination temperature.

In the images captured by backscattering detector, the white dots are the metals on the support material. The dispersion of the metals on the support surface was observed. Comparatively, the presence of larger white particles in the 12Cu6Zn/CMK-3/450 catalyst indicates the sintered metals due to its higher calcination temperature, while the copper dispersion on the 12Cu6Zn/CMK-3/300 catalyst is uniform. Moreover, it was observed that the CMK-3 morphology was preserved after the metal loading. The EDX results of 12Cu6Zn/CMK-3/300 (Figure 7.19(a)) and 12Cu6Zn/CMK-3/450 (Figure 7.19(b)) catalysts are indicating that these materials consist of C, O, Cu, and Zn.

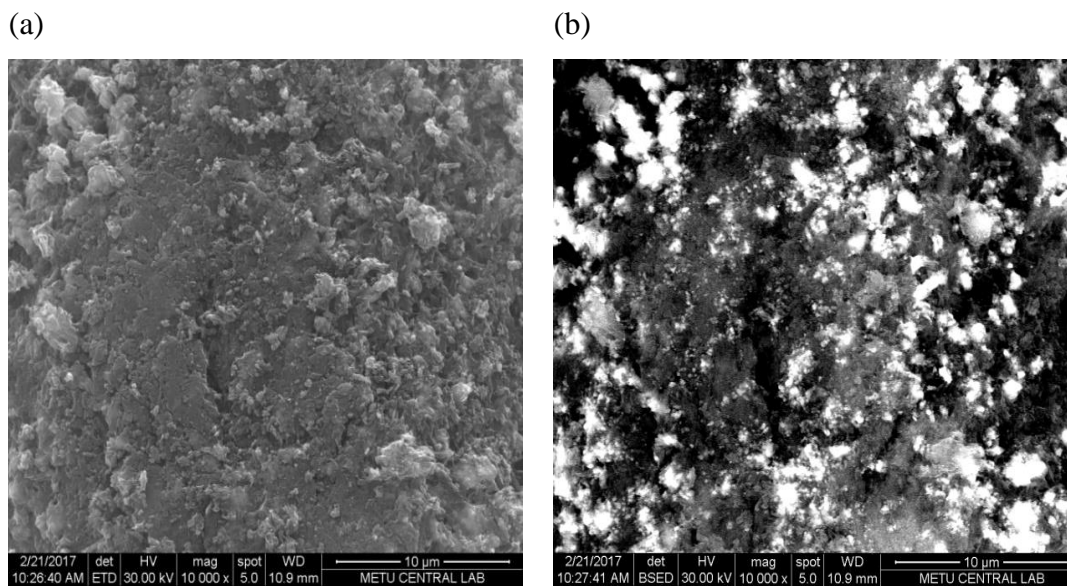


Figure 7.17. (a) SEM image and (b) back scattered electron image of fresh 12Cu6Zn/CMK-3/300 at the magnification of 10000X.

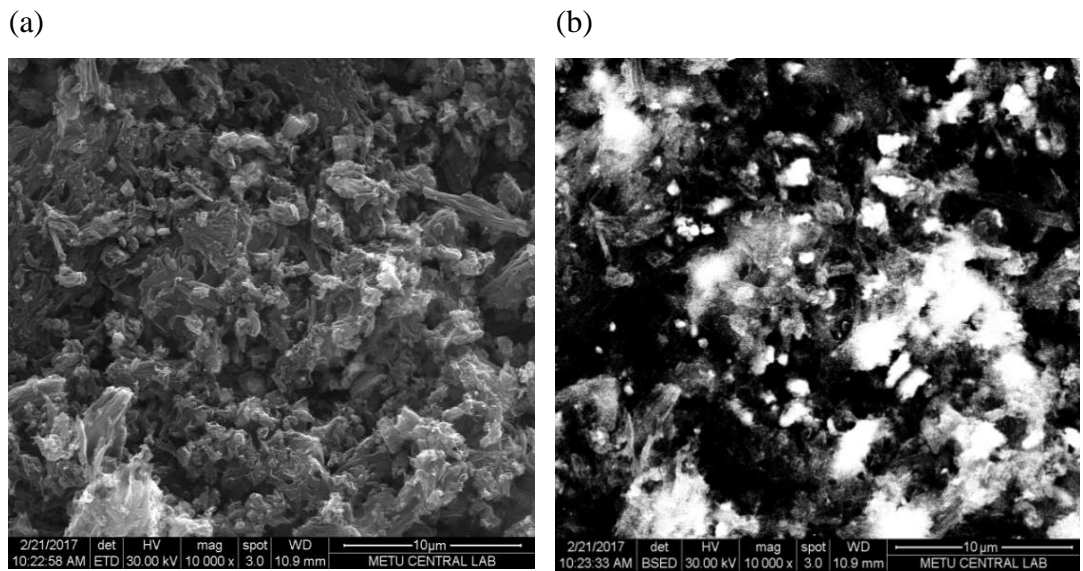


Figure 7.18. (a) SEM image and (b) back scattered electron image of fresh 12Cu6Zn/CMK-3/450 at the magnification of 10000X.

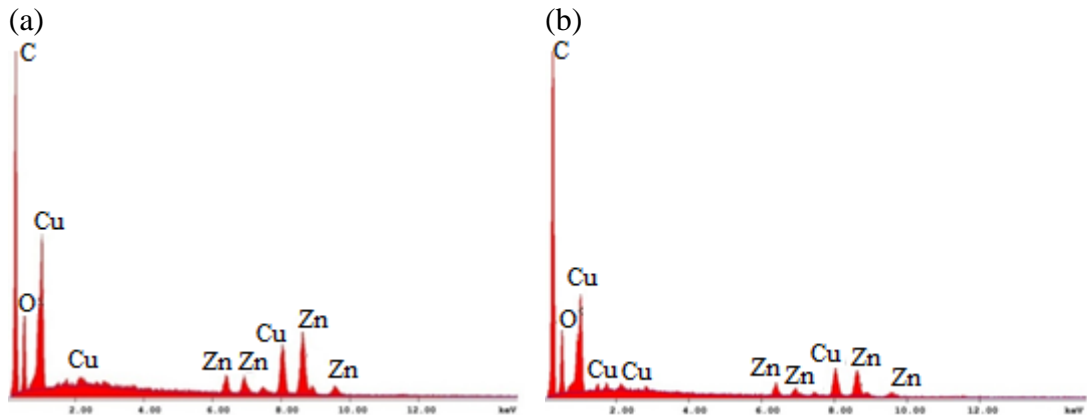


Figure 7.19. EDX spectrum of fresh (a) 12Cu6Zn/CMK-3/300 and (b) 12Cu6Zn/CMK-3/450.

The SEM images of 9Cu9Zn/CMK-3/300 are shown in Figure 7.20(a) and (b) at the magnifications of 20000X and 50000X, respectively. The CMK-3 morphology can be seen easily. The image captured by backscattering detector is also shown in Figure 7.20 (c) at 20000X magnification which indicates big clusters of metals, shown in red circles, and hence poor dispersion of metals on the support.

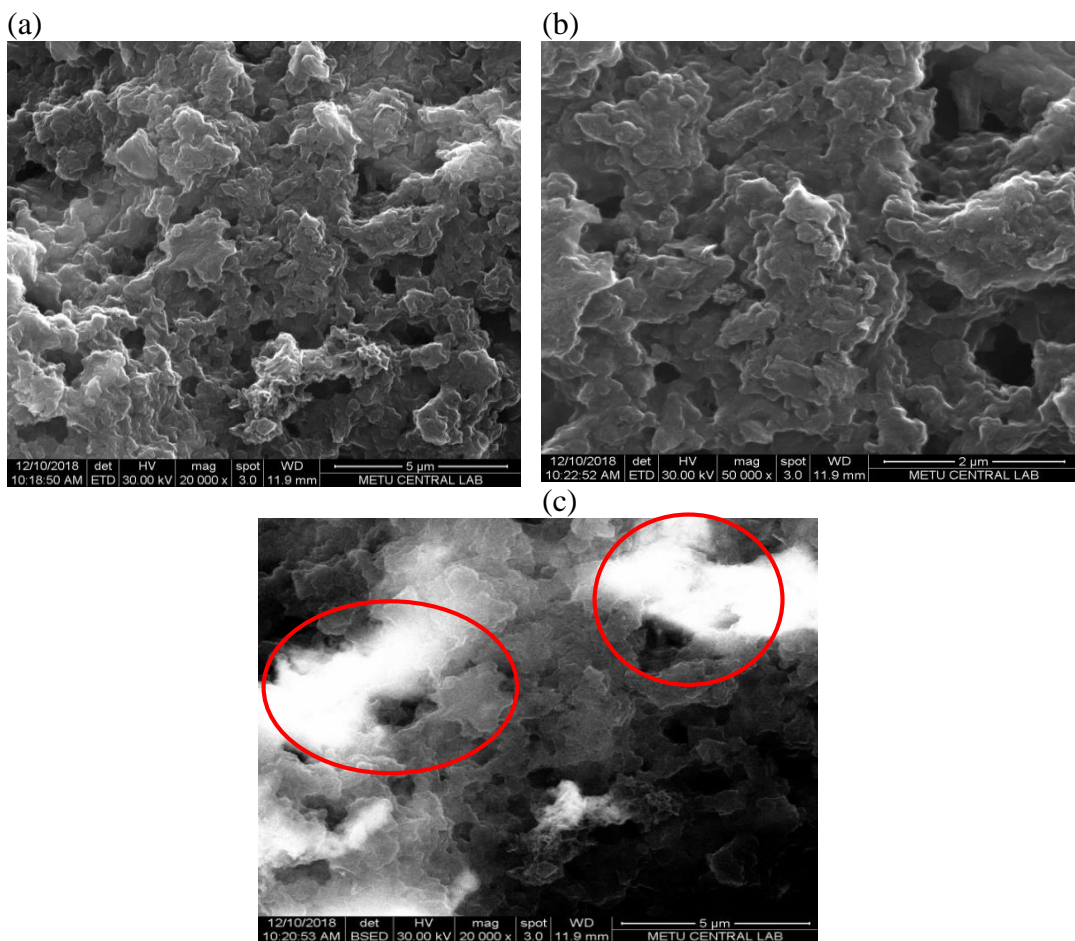


Figure 7.20. SEM images at the magnifications of (a) 20000X and (b) 50000X, and (c) back scattered electron image of fresh 9Cu9Zn/CMK-3/300 at 20000X magnification.

The SEM and back scattered electron images of fresh 13.5Cu4.5Zn/CMK-3/300 catalyst are demonstrated in Figure 7.21 at 20000X, 50000X, and 100000X magnifications. It was evident that CMK-3 morphology was preserved after the metal loading. As can be seen from the back scattered electron image, the metals dispersion is not uniform. Figure 7.21 (c) indicates the impregnated metals on the CMK-3 particles clearly (white dots marked by red circles).

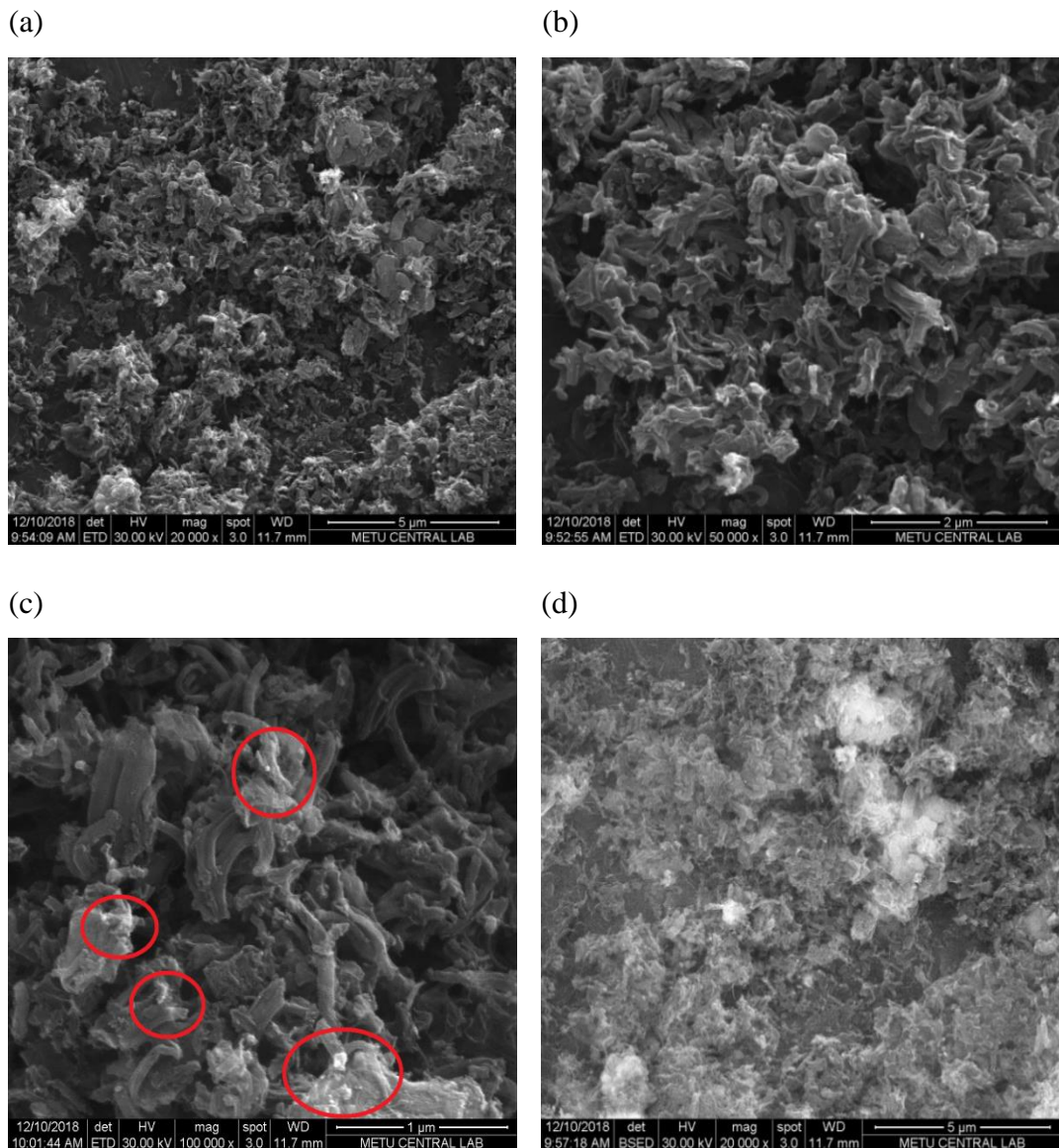


Figure 7.21. SEM images at the magnifications of (a) 20000X, (b) 50000X, (c) 100000X, and (d) back scattered electron image of fresh 13.5Cu4.5Zn/CMK-3/300 at 20000X magnification.

The SEM and back scattered electron images of fresh 18.75Cu6.25Zn/CMK-3/300 are shown in Figure 7.22 at the magnifications of 20000X, 50000X, and 100000X. The back scattered electron image (Figure 7.22(d)) demonstrates well and uniform dispersion of metals. Figure 7.22 (c) also shows the impregnated metals particles on the support particles (bright dots marked by red circles).

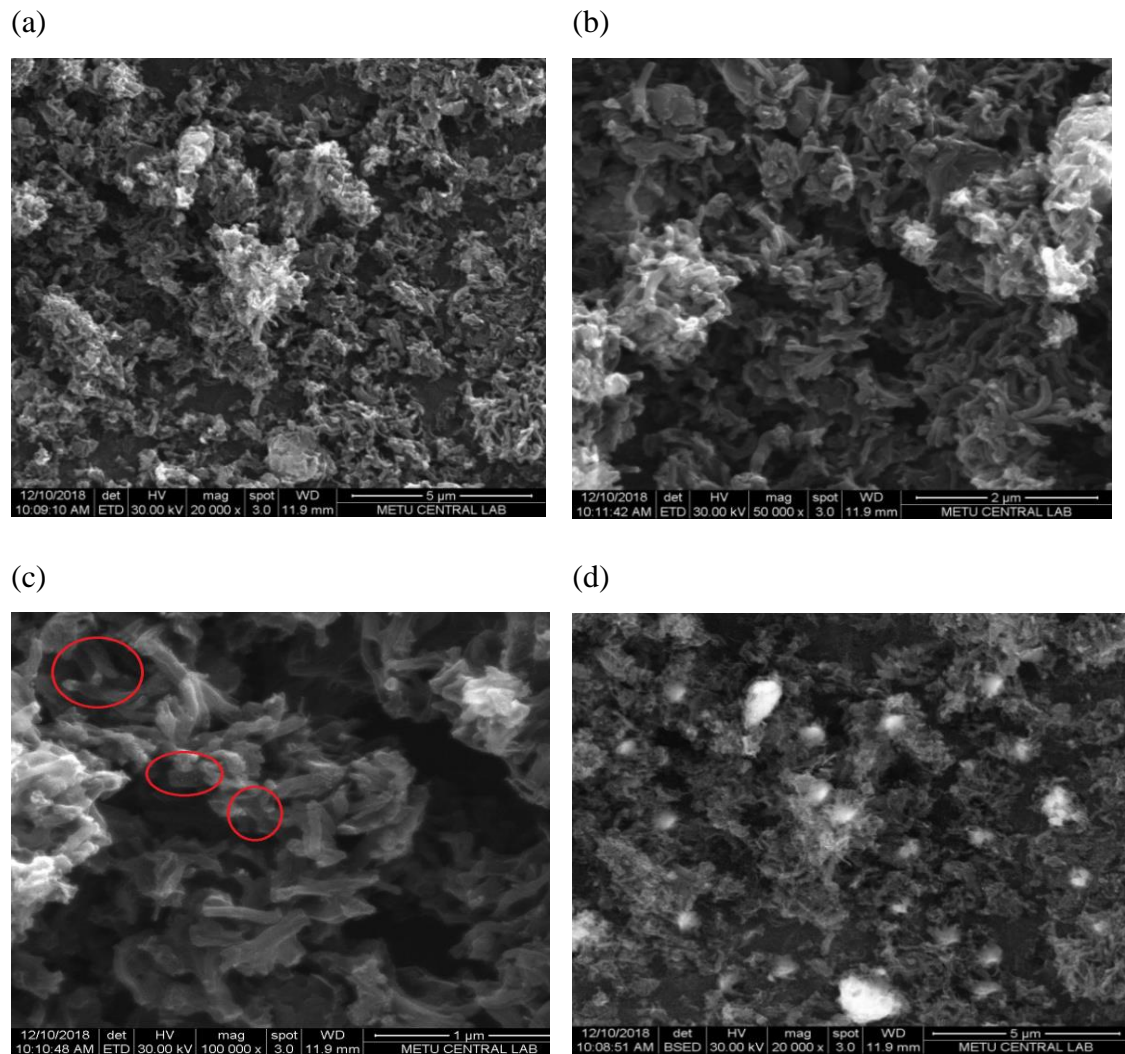


Figure 7.22. SEM images at the magnifications of (a) 20000X, (b) 50000X, (c) 100000X, and (d) back scattered electron image of fresh 18.75Cu6.25Zn/CMK-3/300 at 20000X magnification.

Briefly, it can be said that the catalysts, regardless of their configurations, maintained their similar morphologies to the lean CMK-3 (Figure 7.8). The EDX results of 9Cu9Zn/CMK-3/300, 13.5Cu4.5Zn/CMK-3/300, and 18.75Cu6.25Zn/CMK-3/300 catalysts (Figure 7.23) confirmed presence of C, O, Cu, and Zn in these materials. The EDX results of all synthesized catalysts are tabulated in Table 7.4. It was clear that Zn weight percentage in the metal-loaded catalysts was lower than the desired percentage. While, the Cu weight percentage was same as the desired value. This confirmed the

successfully impregnation of the metals into the support. Presence of C in the EDX results showed that the support was mainly made of carbon. Additionally, the present O in the materials revealed that the loaded metals were all in their oxide forms, since they were reduced with H₂ just before the reaction began.

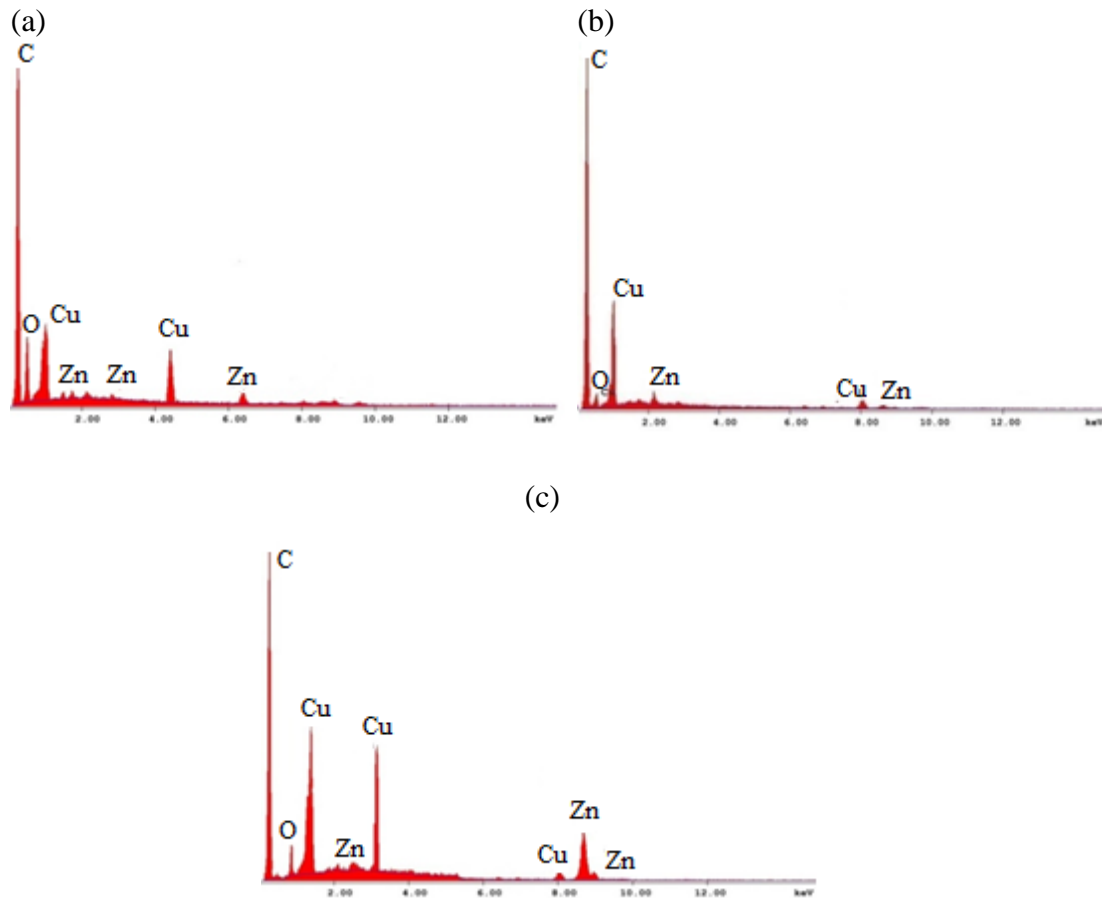


Figure 7.23. EDX spectrums of fresh (a) 9Cu9Zn/CMK-3/300, (b) 13.5Cu4.5Zn/CMK-3/300, and (c) 18.75Cu6.25Zn/CMK-3/300.

Table 7.4. EDX results summary of the synthesized catalysts

Catalyst	Weight Percentage (%)				Cu/Zn
	C	O	Cu	Zn	
12Cu6Zn/CMK-3/300	71.94	11.49	11.79	4.79	2.46
12Cu6Zn/CMK-3/450	71.16	14.67	10.25	3.92	2.61
9Cu9Zn/CMK-3/300	73.24	11.78	8.14	6.84	1.19
13.5Cu4.5Zn/CMK-3/300	72.49	11.86	12.10	3.55	3.41
18.75Cu6.25Zn/CMK-3/300	67.87	9.73	16.77	5.63	2.97

7.2. CATALYTIC ACTIVITY RESULTS

The catalytic activity of the Cu and Zn loaded CMK-3 catalysts was evaluated in methanol steam reforming process at a temperature range of 200-300 °C under argon atmosphere with a flow rate of 30 ml/min and 0.9 ml/min methanol water feed rate. A continuous flow packed column reactor was used in the MSR reaction. Each catalyst was reduced with hydrogen before performing the MSR reaction. Gas analysis of the reactor effluent stream was performed using GC by means of calibration gas mixture beta factors of each product (given in Appendix D). Effect of reaction temperature, metal loading amount, Cu/Zn ratio, the catalyst calcination temperature, and two different reactor systems on the hydrogen yield, methanol conversion, and product distribution was investigated. Methanol conversion and hydrogen yield were calculated using the GC data (Appendix E). In order to test reproducibility of hydrogen production experiments, experiments with the 12Cu6Zn/CMK-3/300 and 12Cu6Zn/CMK-3/450 catalysts were performed twice.

7.2.1. CONVENTIONALLY-HEATED REACTOR SYSTEM

The MSR tests were performed in the conventionally-heated reactor system in order to find the best catalyst configuration for the Cu and Zn loaded catalysts. Repeatability

results of the catalysts and reaction at atmospheric pressure and 250 °C with argon flow rate of 30 ml/min and the reactants flow rate of 0.9 ml/min are given in this section.

7.2.1.1. CATALYST CALCINATION TEMPERATURE EFFECT ON METHANOL CONVERSION AND HYDROGEN YIELD

The 12Cu6Zn/CMK-3/300 and 12Cu6Zn/CMK-3/450 catalysts were prepared at two different calcination temperatures (300°C and 450°C) and tested in the MSR reaction. The reactor effluent stream analysis results showed the presence of hydrogen and carbon dioxide gases. Presence of these gases revealed that steam reforming of methanol (3.1) took place in the reactor.



The product distribution, methanol conversion, and hydrogen yield in the MSR reaction with the 12Cu6Zn/CMK-3/300 catalyst are given in Figures 7.24-26. The system reached to a steady state at reaction time of 30 minutes. Average gas composition was 75.1% H₂, 24.9% CO₂, and 0% CO. Average methanol conversion and hydrogen yield were 90.5% and 91%, respectively.

One more experiment was carried out with the same catalyst under the same condition at different time. Average gas composition was 75.9% H₂, 24.1% CO₂, and 0% CO. Average methanol conversion and hydrogen yield were 89% and 93.2%, respectively.

The reactor outlet gas compositions were almost 75.5±0.4% H₂, 24.5±0.4% CO₂, and 0% CO. Average methanol conversion and hydrogen yield were 89.7±0.8% and 92.1±1.1%, respectively. These results showed that the experiments were reproducible.

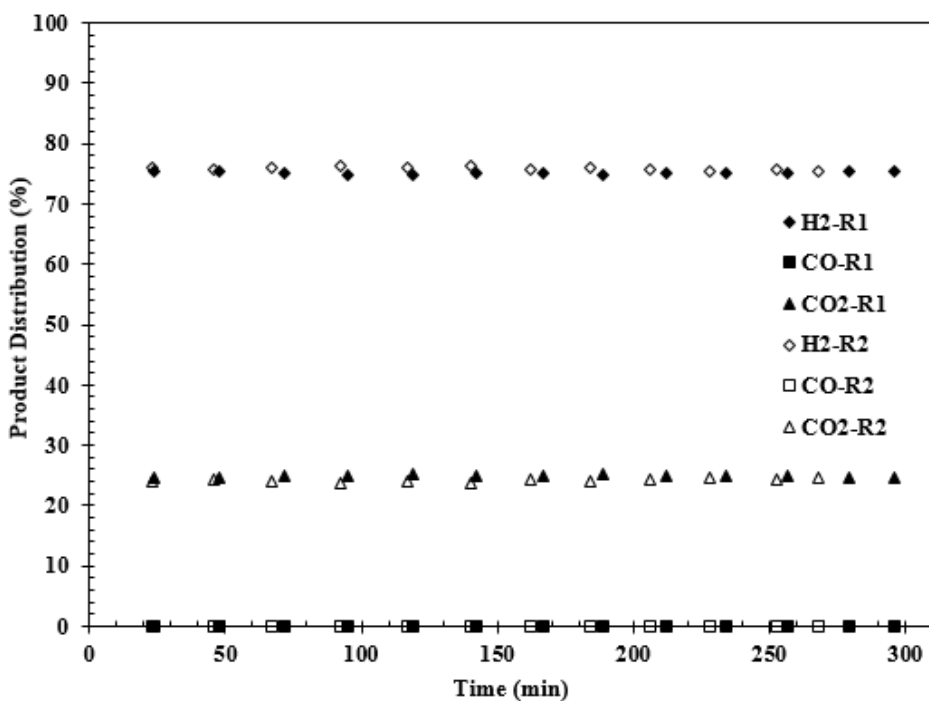


Figure 7.24. Product distribution of two reproducible MSR experiments with the 12Cu6Zn/CMK-3/300 catalyst ($P=1\text{ atm}$, $T=250^\circ\text{C}$, $\text{H}_2\text{O}/\text{CH}_3\text{OH}=1$).

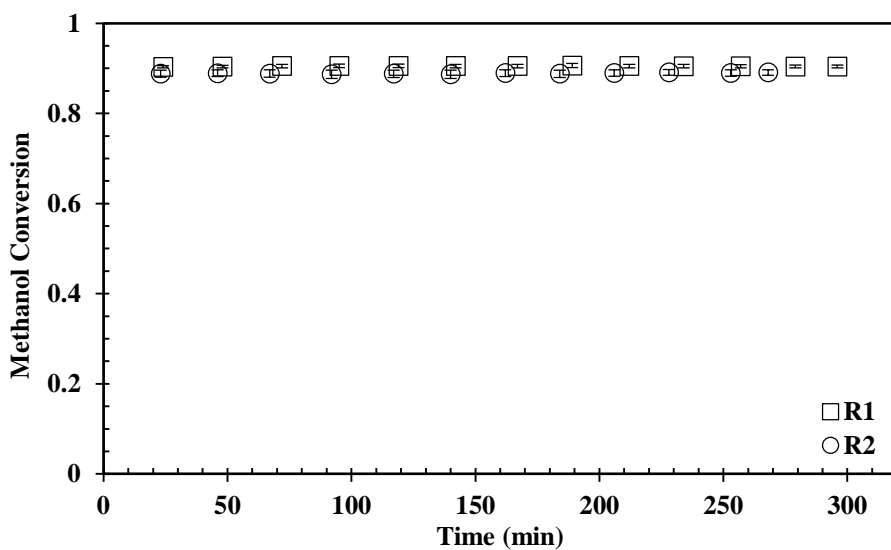


Figure 7.25. Methanol conversion of two reproducible MSR experiments with the 12Cu6Zn/CMK-3/300 catalyst ($P=1\text{ atm}$, $T=250^\circ\text{C}$, $\text{H}_2\text{O}/\text{CH}_3\text{OH}=1$).

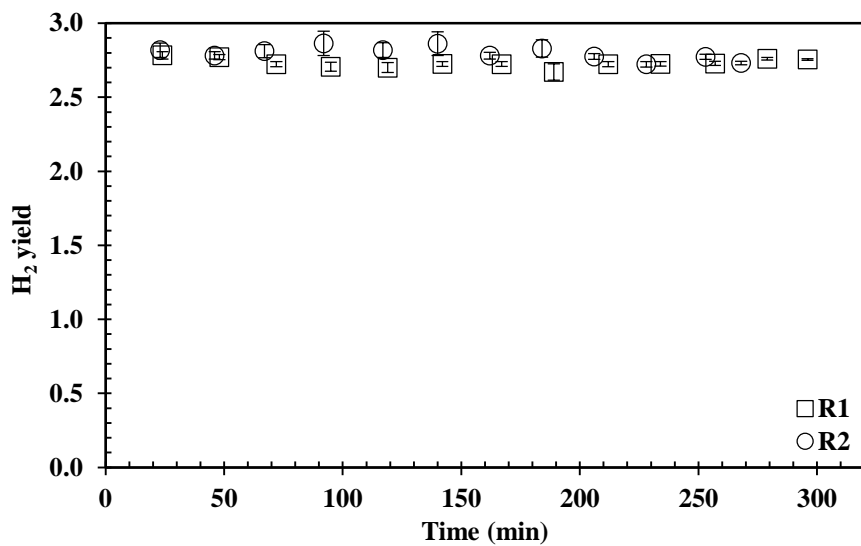


Figure 7.26. Hydrogen yield of two reproducible MSR experiments with the 12Cu6Zn/CMK-3/300 catalyst ($P=1\text{ atm}$, $T=250^\circ\text{C}$, $\text{H}_2\text{O}/\text{CH}_3\text{OH}=1$).

In the other words, a strong agreement was observed between the results of two experiments which shows repeatability of the experiments.

The product distribution, methanol conversion, and hydrogen yield of two experiments done at different times under the same conditions with the 12Cu6Zn/CMK-3/450 catalyst were also compared in Figures 7.27-29. The system reached to a steady state at reaction time of 30 minutes. The same gas products were observed. Average hydrogen, carbon dioxide, and carbon monoxide compositions were 75.5%, 24.4%, and 0%, respectively. Average mole fractions of hydrogen, carbon dioxide, and carbon monoxide for the second reaction were 77.3%, 22.7%, and 0%, respectively. Average methanol conversion of the first experiment was 71.8%, while that of the second experiment was 70.3%, which shows the reproducibility of the results. Furthermore, average hydrogen yield of two experiments were 73.5% and 73.8%. These two results are in good agreement with each other.

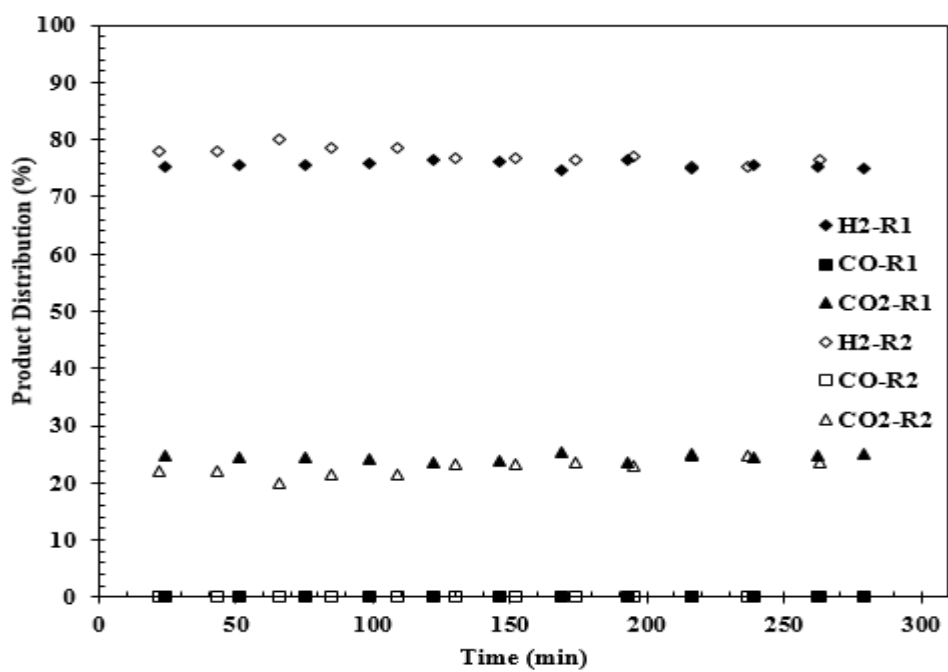


Figure 7.27. Product distribution of two reproducible MSR experiments with the 12Cu6Zn/CMK-3/450 catalyst ($P=1$ atm, $T=250^\circ\text{C}$, $\text{H}_2\text{O}/\text{CH}_3\text{OH}=1$).

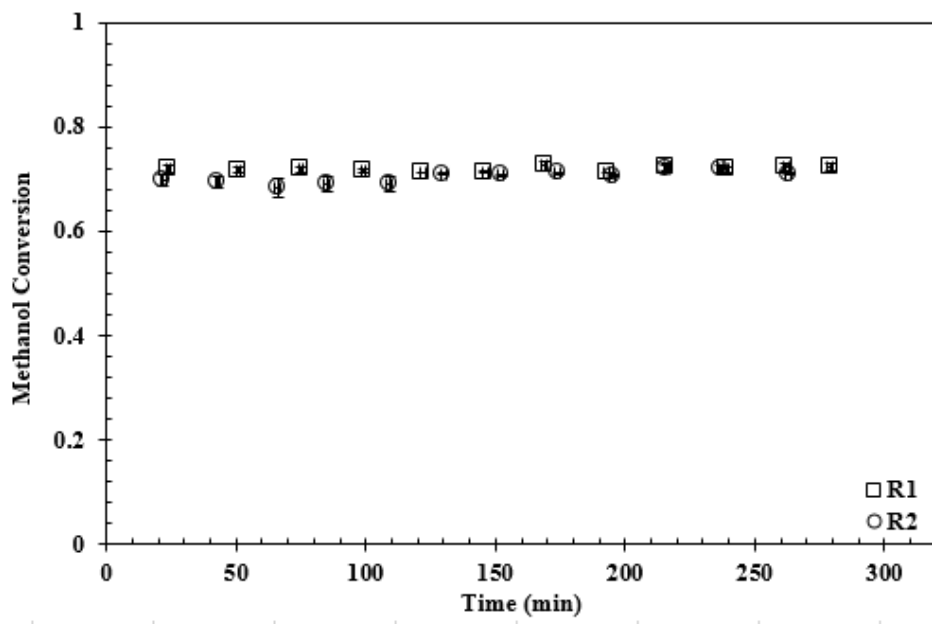


Figure 7.28. Methanol conversion of two reproducible MSR experiments with the 12Cu6Zn/CMK-3/450 catalyst ($P=1$ atm, $T=250^\circ\text{C}$, $\text{H}_2\text{O}/\text{CH}_3\text{OH}=1$).

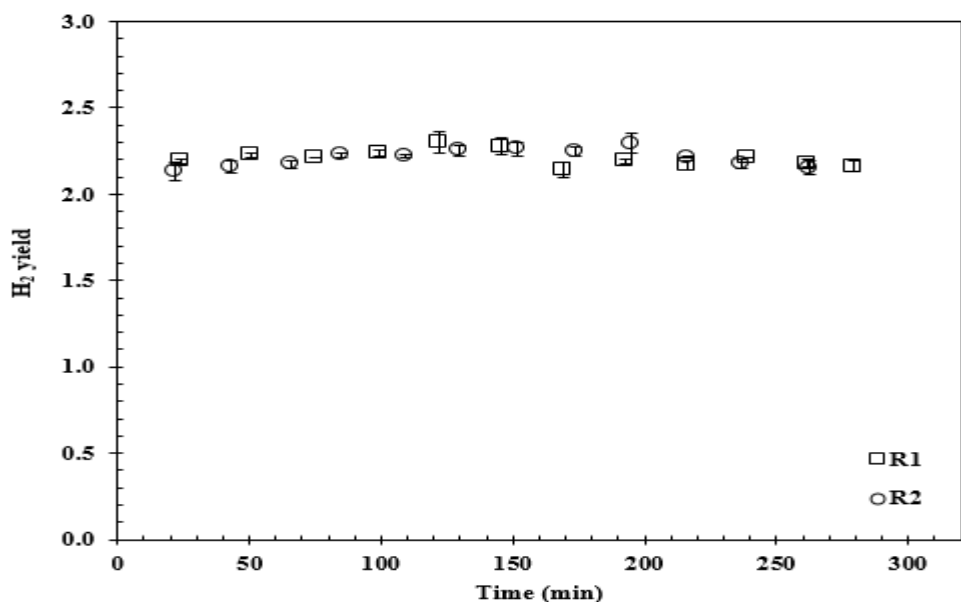


Figure 7.29. Hydrogen yield of two reproducible MSR experiments with the 12Cu6Zn/CMK-3/450 catalyst ($P=1$ atm, $T=250^\circ\text{C}$, $\text{H}_2\text{O}/\text{CH}_3\text{OH}=1$).

In other words, consistent results were also achieved from these reproducible experiments. The reactor outlet gas compositions were almost $76.4\pm0.5\%$ H₂, $23.6\pm0.9\%$ CO₂, and 0% CO. The average methanol conversion of $71.05\pm0.75\%$ and the average hydrogen yield of $73.65\pm0.15\%$ were achieved.

In order to investigate effect of the catalyst calcination temperature on methanol conversion and hydrogen yield, the average methanol conversion and hydrogen yield achieved with the 12Cu6Zn/CMK-3/300 and 12Cu6Zn/CMK-3/450 catalysts were compared in Figures 7.30 and 7.31.

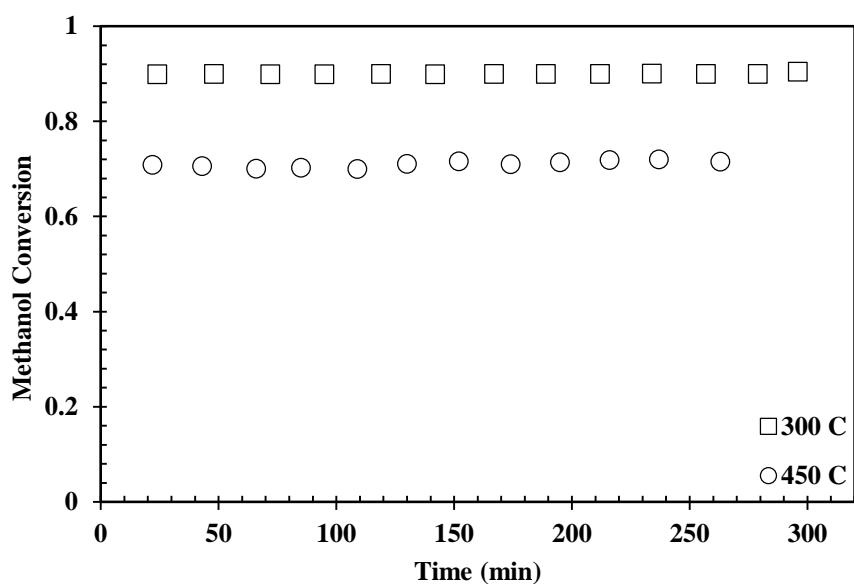


Figure 7.30. Methanol conversions of the $12\text{Cu}6\text{Zn}/\text{CMK-3}$ catalysts synthesized at different calcination temperatures ($P=1 \text{ atm}$, $T=250^\circ\text{C}$, $\text{H}_2\text{O}/\text{CH}_3\text{OH}=1$).

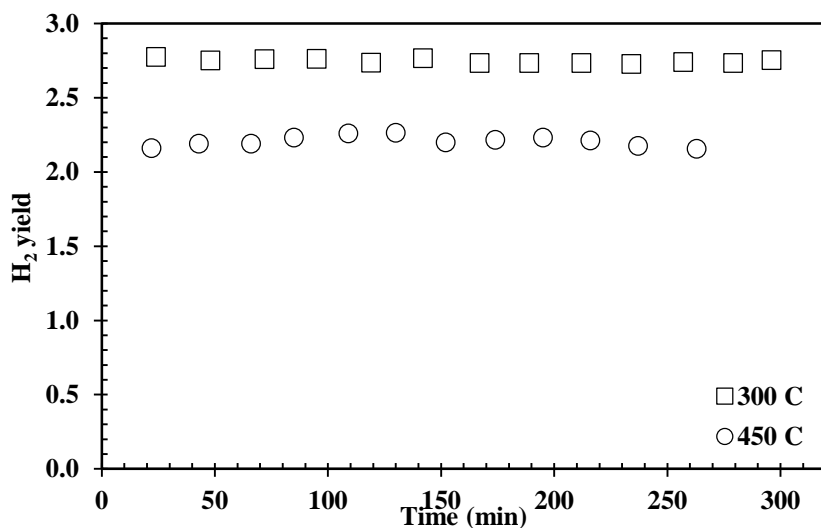


Figure 7.31. Hydrogen yields of the $12\text{Cu}6\text{Zn}/\text{CMK-3}$ catalysts synthesized at different calcination temperatures ($P=1 \text{ atm}$, $T=250^\circ\text{C}$, $\text{H}_2\text{O}/\text{CH}_3\text{OH}=1$).

The average outlet gas compositions obtained with the $12\text{Cu}6\text{Zn}/\text{CMK-3}/300$ catalyst were 75.5% H_2 , 24.5% CO_2 , and 0% CO . Average mole fractions of the gas product

with the 12Cu6Zn/CMK-3/450 catalyst were 76.4% H₂, 23.6% CO₂, and 0% CO. The average methanol conversion of 90% and 71% were achieved with the 12Cu6Zn/CMK-3/300 and 12Cu6Zn/CMK-3/450 catalysts, respectively. The average values of hydrogen yield for the 12Cu6Zn/CMK-3/300 and 12Cu6Zn/CMK-3/450 catalysts were 91.6% and 73.6%, respectively.

The average compositions of the products for both catalysts were nearly same. The catalyst calcined with the lower calcination temperature (12Cu6Zn/CMK-3/300) showed a higher activity. The higher activity in the 12Cu6Zn/CMK-3/300 catalyst can be attributed to the fact that copper sintering was observed at the temperatures higher than 300°C which may strongly diminish the catalyst activity [26]. This fact was confirmed by the CuO crystallite size as a result of increase in the calcination temperature and the SEM images. In other words, 300°C is the proper calcination temperature for the copper loaded catalyst. Therefore, in this study, the catalyst calcination temperature was chosen as 300°C.

7.2.1.2. EFFECT OF COPPER/ZINC RATIO ON METHANOL CONVERSION AND HYDROGEN YIELD

To determine the best catalyst configuration, the impregnated copper/zinc ratio was adjusted. For this purpose, three catalysts with three different ratios were prepared and their activity in the MSR reaction was evaluated at atmospheric pressure and 250 °C. Comparison of methanol conversion and hydrogen yield as a function of time was given in Figures 7.32-7.33.

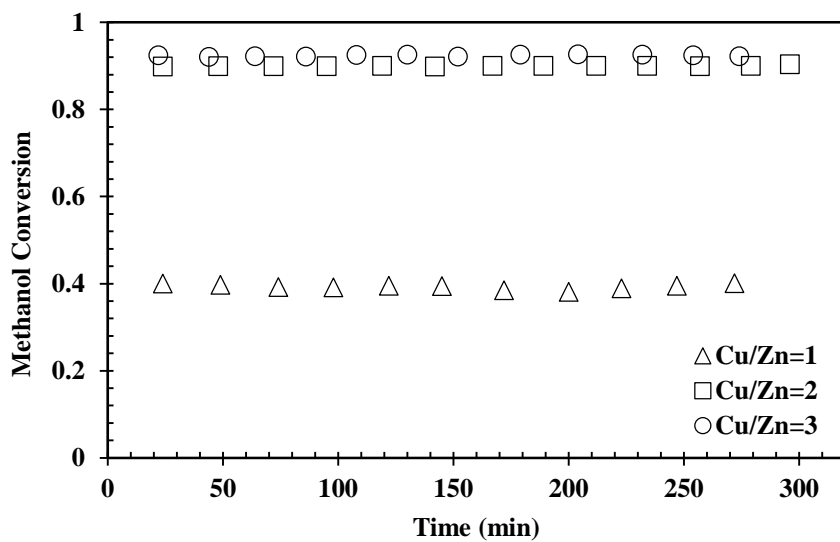


Figure 7.32. Effect of Cu/Zn ratio on the methanol conversion ($P=1$ atm, $T=250^\circ\text{C}$, $\text{H}_2\text{O}/\text{CH}_3\text{OH}=1$).

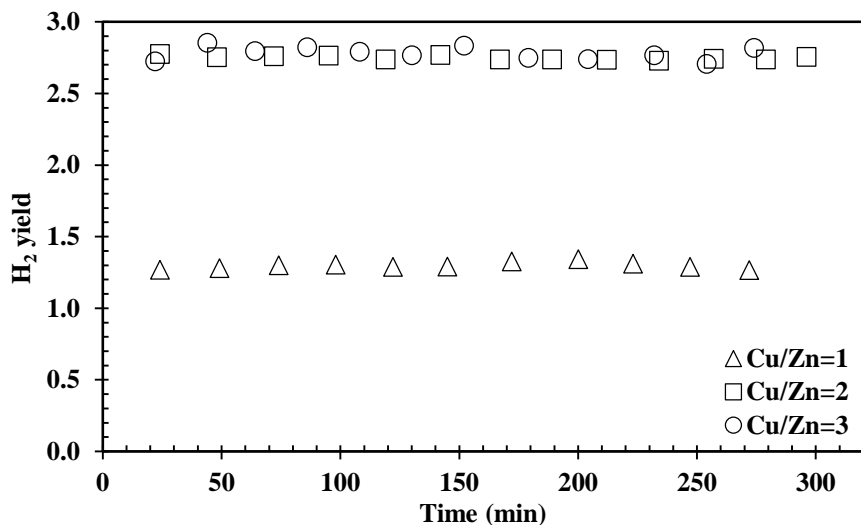


Figure 7.33. Effect of Cu/Zn ratio on the hydrogen yield ($P=1$ atm, $T=250^\circ\text{C}$, $\text{H}_2\text{O}/\text{CH}_3\text{OH}=1$).

The average methanol conversion and hydrogen yield obtained with the catalyst having $\text{Cu}/\text{Zn}=1$ was 39.3% and 43.2%, respectively. The catalyst with $\text{Cu}/\text{Zn}=2$ had average methanol conversion of 90.5% and average hydrogen yield of 90.8%. With the catalyst having $\text{Cu}/\text{Zn}=3$, average methanol conversion and hydrogen yield of

92.4% and 92.7% were obtained. Methanol conversion and hydrogen yield were increased with an increase in the copper content which plays the primary role in the catalyst activity. A slight increase was observed in methanol conversion and hydrogen yield when the Cu/Zn ratio was increased from 2 to 3. The slight increase can be due to the minor difference in the copper contents of these catalysts (~1.5%). Although the catalyst with Cu/Zn=1 had a considerably lower activity, the catalysts with Cu/Zn ratio of 2 and 3 had an almost similar performance. The low activity of the 9Cu9Zn/CMK-3/300 catalyst can be attributed to its lower copper content, as well as its lower textural properties compared to the 12Cu6Zn/CMK-3/300 and 13.5Cu4.5Zn/CMK-3/300 catalysts.

Furthermore, Table 7.5 represents the comparison of H₂, CO₂, and CO percentages, average methanol conversion, and average hydrogen yield values. The best Cu/Zn weight ratio was 3 with the highest yield.

Table 7.5. Average hydrogen production results from the catalysts with different Cu/Zn ratios.

Catalyst	Cu/Zn weight ratio	Gas Composition			Methanol Conversion, (%)	Hydrogen Yield, (%)
		y _{H₂} , (%)	y _{CO} , (%)	y _{CO₂} , (%)		
9Cu9Zn/CMK-3/300	1	76.7	0	23.3	39.3	43.2
12Cu6Zn/CMK-3/300	2	76	0	24.0	90.5	90.8
13.5Cu4.5Zn/CMK-3/300	3	75.2	0	24.8	92.4	92.7

7.2.1.3. EFFECT OF TOTAL METAL LOADING ON METHANOL CONVERSION AND HYDROGEN YIELD

Effect of the total metal loading amount on methanol conversion and hydrogen yield was investigated. Total metal loading amount was increased from 18% to 25% with keeping the Cu/Zn ratio as 3. Figures 7.34 and 7.35 illustrate methanol conversion and

hydrogen yield as a function of the reaction time, respectively. Moreover, in Table 7.6, the results obtained from different metal loading amounts were compared.

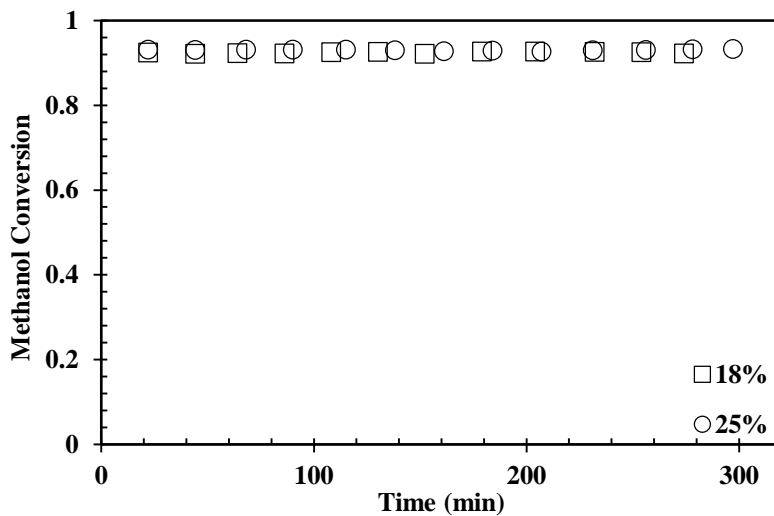


Figure 7.34. Effect of total metal loading amount on methanol conversion ($P=1\text{ atm}$, $T=250^\circ\text{C}$, $\text{H}_2\text{O}/\text{CH}_3\text{OH}=1$).

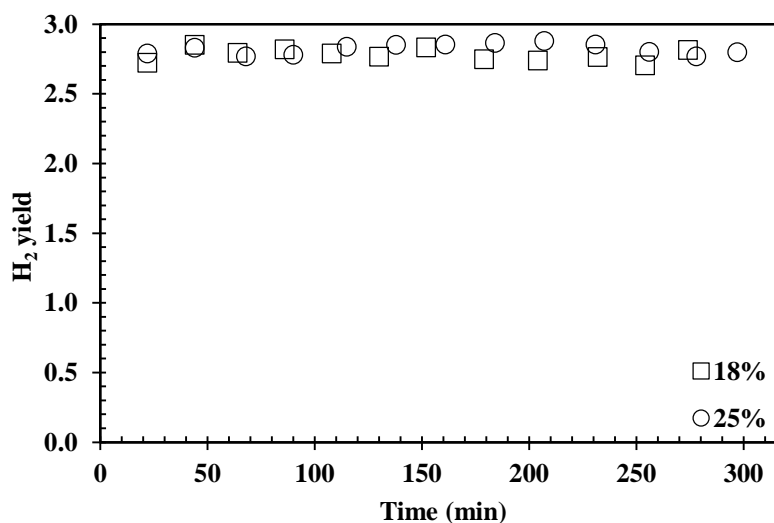


Figure 7.35. Effect of total metal loading amount on hydrogen yield ($P=1\text{ atm}$, $T=250^\circ\text{C}$, $\text{H}_2\text{O}/\text{CH}_3\text{OH}=1$).

Methanol conversion slightly increased from 92.4% to 93.0% as the result of raising the total metal loading amount of the catalyst. In a similar fashion, a minor increase from 92.7% to 94% was observed in hydrogen yield. However, the gas composition was remained unchanged (Table 7.6). The slightly higher activity of 18.75Cu6.25Zn/CMK-3/300 can be attributed to its higher copper content, as well as the higher zinc content which enhanced the copper dispersion and hence the catalyst activity.

Table 7.6. Average hydrogen production results from the catalysts with different total metal loading amount.

Catalyst	Total Metal Loading Amount (%)	Gas Composition			Methanol Conversion, (%)	Hydrogen Yield, (%)
		y _{H₂} , (%)	y _{CO} , (%)	y _{CO₂} , (%)		
13.5Cu4.5Zn/CMK-3/300	18	75.2	0	24.8	92.4	92.7
18.75Cu6.25Zn/CMK-3/300	25	75.9	0	24.1	93.0	94.0

To sum up, the best configuration to design the finest catalyst was decided according to their activity in the MSR reaction. Since there was no CO formation in the experiments with all the tested catalysts, so the only important criterion to select the best catalyst is the activity. Consequently, the catalyst with Cu/Zn ratio of 3, total metal loading of 25%, and calcined at 300°C (18.75Cu6.25Zn/CMK-3/300) was chosen for the rest of this study.

7.2.1.4. EFFECT OF REACTION TEMPERATURE ON METHANOL CONVERSION AND HYDROGEN YIELD

The methanol steam reforming reaction, as an endothermic reaction, intensively depends on the operating temperature. Accordingly, the effect of reaction temperature

was investigated on the hydrogen production from the MSR reaction in a temperature range of 200-300°C. The best catalyst, 18.75Cu6.25Zn/CMK-3/300, was used. Figure 7.36 shows the average product distribution at different temperatures.

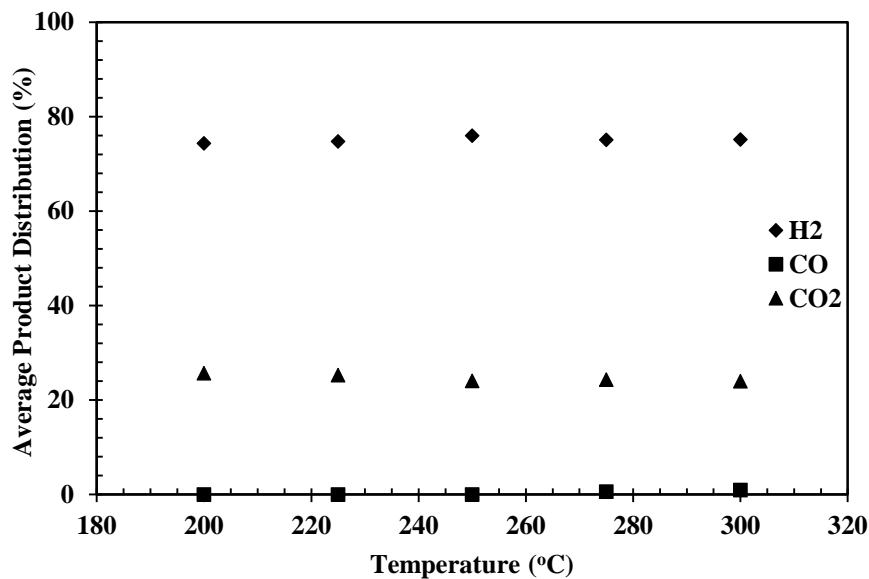


Figure 7.36. Effect of reaction temperature on the average product distribution ($P=1$ atm, $H_2O/CH_3OH=1$, Catalyst: 18.75Cu6.25Zn/CMK-3/300).

As can be seen from Figure 7.36, the hydrogen composition slightly increased from 74.3% to 75.9% with an increase in the temperature from 200°C to 250°C. However, it stabilized at almost 75% at higher temperatures than 250°C. Additionally, CO formation began when the temperature was higher than 250°C and reached to its maximum value at 300°C (0.89%). This was a sign that proved the methanol decomposition reaction (3.2) taking place at high temperatures due to its endothermic nature, in addition to steam reforming of methanol reaction (3.1). Moreover, the water-gas shift reaction also occurs in a reverse direction at high temperatures and led to transformation of CO₂ to CO.

Figure 7.37 presents the average methanol conversion with respect to the reaction temperature. The methanol conversion dramatically went up from 31.5% to 93.0% with an increase in the temperature from 200°C to 250°C. Afterward, it gradually increased to 96.4% at 300°C. There was an overall increasing trend in methanol conversion as temperature rose, which was mainly attributed to the endothermic methanol steam reforming reaction (3.1). Similarly, contribution of the methanol decomposition reaction (3.3) was also significant to improve the methanol conversion at the higher temperatures. The same behavior was also observed in hydrogen yield (Figure 7.38). The maximum achieved hydrogen yield was 2.93 out of 3 (the maximum theoretical hydrogen yield) which is 97.7% of the maximum theoretical value.

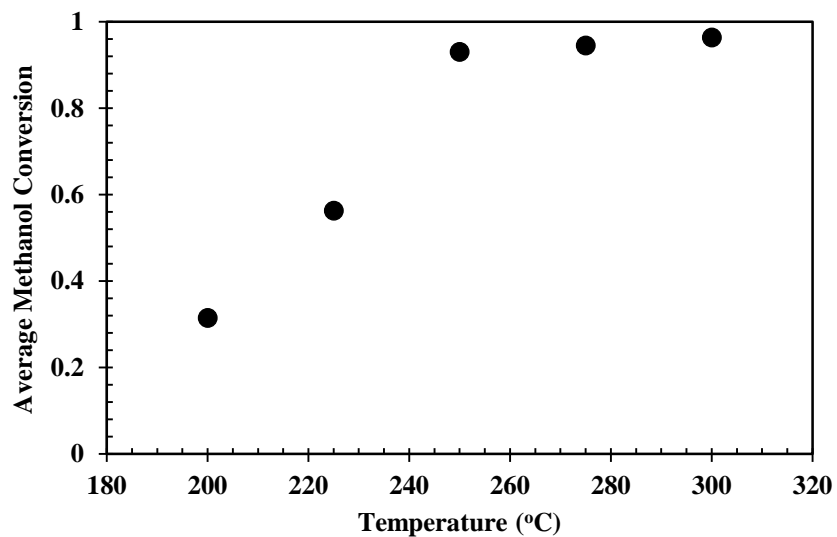


Figure 7.37. Effect of reaction temperature on the average methanol conversion ($P=1\text{ atm}$, $\text{H}_2\text{O}/\text{CH}_3\text{OH}=1$, Catalyst: 18.75Cu6.25Zn/CMK-3/300).

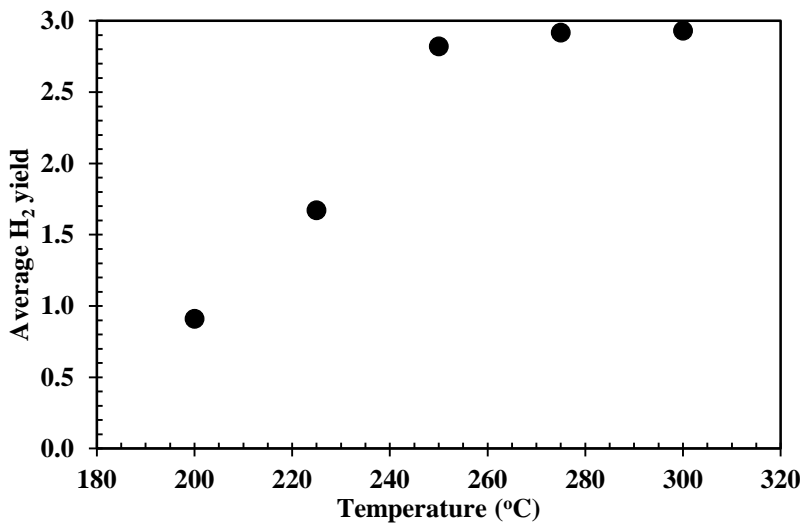


Figure 7.38. Effect of reaction temperature on the average hydrogen yield ($P=1$ atm, $H_2O/CH_3OH=1$, Catalyst: 18.75Cu6.25Zn/CMK-3/300).

It can be said that although the methanol conversion and hydrogen yield are important and decisive parameters, CO formation is also a key factor especially for the purpose of this study. As it was explained before, the acceptable CO concentration for the onboard fuel cell applications is less than 100 ppm [25]. In conclusion, 250 °C seems to be an appropriate and optimum temperature for sustainable and CO-free onboard fuel cell applications with the highest methanol conversion and hydrogen yield.

In the literature, methanol conversion of the MSR reaction with 15%Cu/MCM-41 catalyst at 300 °C was reported as 89% [68]. In another study, an average methanol conversion of 92% and average hydrogen yield of 2.75 was reported with 15% copper-loaded silica aerogel at the operating temperature of 280 °C with a steam to methanol molar ratio of 2.2 [39]. Comparatively, it can be stated that a higher average methanol conversion (93%) and hydrogen yield (2.82) was obtained in this study with 18.75Cu6.25Zn/CMK-3/300 at a lower operating temperature (250 °C).

7.2.2. FOCUSED-MICROWAVE HEATED REACTOR SYSTEM

The best catalyst, 18.75Cu6.25Zn/CMK-3/300, was used in the focused-microwave heated reactor system. The experiments were performed at a temperature range of 250–300 °C. The average product distribution, methanol conversion, and hydrogen yield are shown in Figures 7.39-7.41.

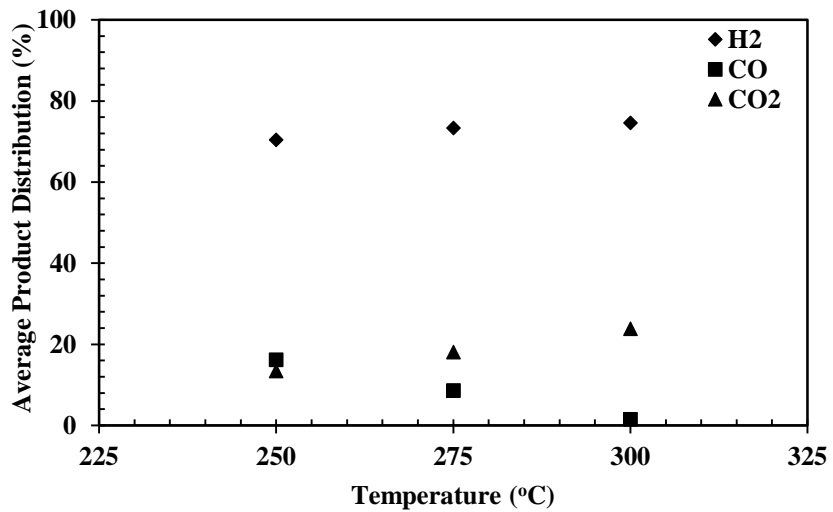


Figure 7.39. Average product distribution at different temperatures obtained from the focused-microwave heated reactor system ($P=1$ atm, $H_2O/CH_3OH=1$, Catalyst: 18.75Cu6.25Zn/CMK-3/300).

The effluent stream of the focused-microwave heated reactor contains CO. The average product distribution shows that CO formation declined as the temperature increased, while CO₂ content increased. The hydrogen was also increased slightly with the reaction temperature which shows that the methanol steam reforming reaction (3.1) was dominant compared to the other side reactions. The average methanol conversion had a minor increase with the reaction temperature; however, hydrogen yield rose considerably as the result of temperature rise.

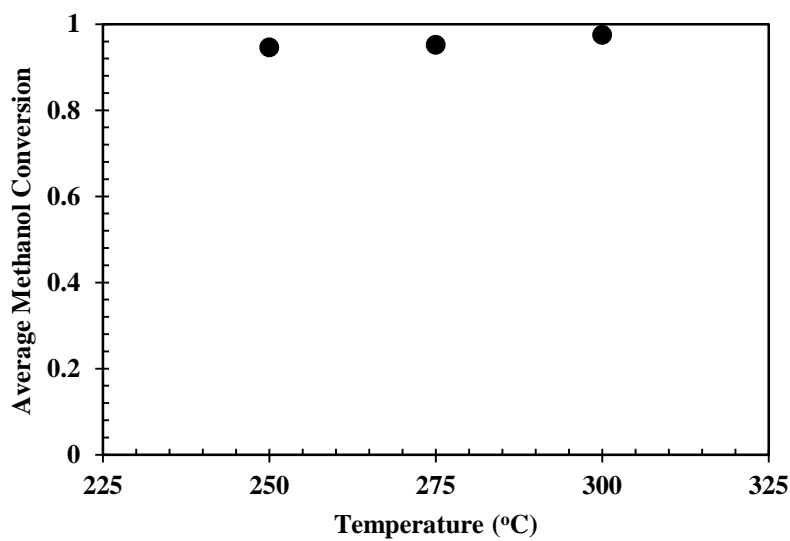


Figure 7.40. Average methanol conversion at different temperatures obtained from the focused-microwave heated reactor system ($P=1$ atm, $H_2O/CH_3OH=1$, Catalyst: 18.75Cu6.25Zn/CMK-3/300).

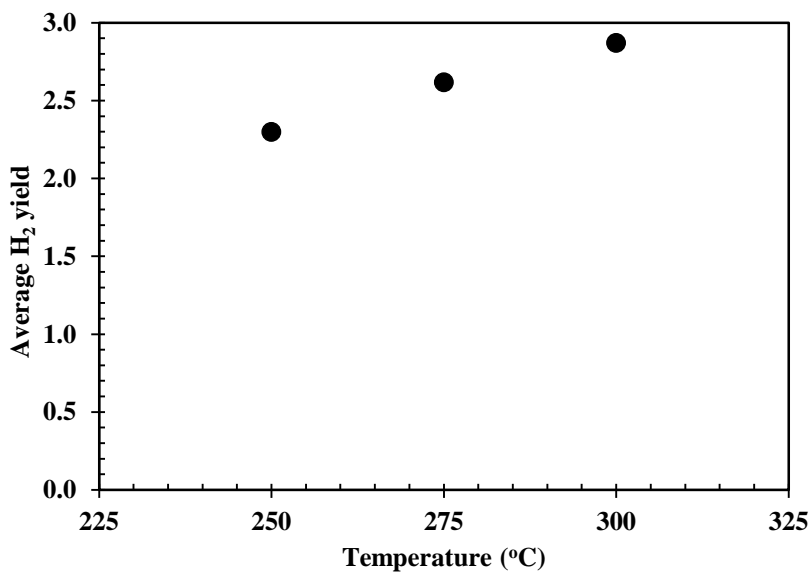


Figure 7.41. Average hydrogen yield at different temperatures obtained from the focused-microwave heated reactor system ($P=1$ atm, $H_2O/CH_3OH=1$, Catalyst: 18.75Cu6.25Zn/CMK-3/300).

Table 7.7 compares the acquired results in both conventionally-heated and focused-microwave heated reactor systems using the best catalyst.

Table 7.7. Average hydrogen production results for both the conventionally-heated and the focused-microwave heated reactor systems at different temperatures ($P=1$ atm, $H_2O/CH_3OH=1$, Catalyst: 18.75Cu6.25Zn/CMK-3/300).

Temperature (°C)	Reactor System	Gas Composition (%)			Methanol Conversion, (%)	Hydrogen Yield, (%)
		y _{H₂}	y _{CO}	y _{CO₂}		
250	CONV.	75.9	0	24.1	93.0	94.0
	MIC.	70.4	16.2	13.4	94.6	76.6
275	CONV.	75.1	0.6	24.3	94.5	97.3
	MIC.	73.3	8.6	18.1	95.2	87.2
300	CONV.	75.1	0.9	24.0	96.4	97.7
	MIC.	74.6	1.5	23.9	97.5	95.6

As can be seen from Table 7.7, slightly higher methanol conversion in the focused-microwave heated reactor system than the conventionally-heated system was achieved at each reaction temperature. However, the hydrogen yield acquired in the conventionally-heated system was higher than that of the focused-microwave reactor system at each experiment. With an increase in temperature, hydrogen yield values in the focused-microwave heated reactor system were getting closer to the hydrogen yield values obtained with the conventionally-heated reactor system.

One of the major differences between the conventionally-heated systems and the focused-microwave heated reactor system is the large temperature gradient taking place in the former. This phenomenon accelerates a chemical reaction, so-called Boudouard reaction ($2CO \leftrightarrow CO_2 + C$), which can be confirmed by the higher amount of CO_2 in the results obtained from conventionally-heated system than CO . However, CO concentration in the focused-microwave system was higher than CO_2 at 250°C which shows the Boudouard reaction occurrence may be less favored at this temperature due to the low temperature gradient at the catalyst bed. Although by increasing the temperature, the temperature gradient became larger as well as the hot

spot formation on the catalyst surface. Therefore, Boudouard reaction became more favorable and the CO₂ concentration surpassed the CO concentration.

Comparatively, the CO formation in the focused-microwave heated reactor system was higher than that of the conventionally-heated system at each temperature. However, in the focused-microwave heated reactor system less amount of CO₂ was produced compared to the conventionally-heated reactor system.

The energy consumption of the focused-microwave heated reactor system to reach and maintain the desired reaction temperature is also reported in Table 7.8 by means of the magnetron average power output during the process.

Table 7.8. *The focused-microwave reactor system energy consumption*

Temperature (°C)	Average power output (W)
250	150
275	160
300	180

Comparing the power outputs of the focused-microwave heated reactor system and that of the conventionally-heated system (~950 W), it is clear that the focused-microwave reactor system was more energy efficient.

CHAPTER 8

CONCLUSIONS

In the scope of the presented study, the methanol steam reforming process was investigated in both conventionally-heated and focused-microwave heated reactor systems. For this purpose, Cu-Zn incorporated mesoporous carbon (CMK-3) catalysts were synthesized and characterized in order to catalyze the mentioned reaction. Concluding observations of this study are listed as follows:

- XRD results showed that CMK-3 was successfully synthesized. All the synthesized CMK-3 materials exhibited Type IV isotherm with H₂ hysteresis.
- CMK-3 preparation method, which is used widely in the literature, was optimized studying the effects of the reaction temperature and the silica removing agent on its textural properties. As a result of this investigation, it was observed the one step reaction temperature at 160 °C leads to a significant improvement in the material textural properties. Furthermore, HF had a better performance in removing silica template from the mesoporous carbon material compared to NaOH. It was observed that among all CMK-3 materials, the best support had the BET surface area of 1120 m²/g, pore volume of 1.19 cm³/g, and average pore size of 3.7 nm.
- Cu-Zn was successfully impregnated on CMK-3 to form loaded mesoporous carbon catalysts. XRD results revealed that metal-loaded materials contained CuO and ZnO solid phases in addition to carbon phase. The synthesized catalysts preserved the CMK-3 ordered structure and isotherm Type IV with H₂ hysteresis. A decrease in the support surface area, pore volume, and microporosity was observed after metals impregnation which was a sign of blocking of the pore with metals.

- The higher calcination temperature of the catalyst caused the copper particles to sinter which was confirmed by a larger crystallite size of 12Cu6Zn/CMK-3/450 than that of 12Cu6Zn/CMK-3/300. With an increase in calcination temperature of the catalyst, the methanol conversion and hydrogen yield were also decreased due to sintering of metal particles.
- Methanol conversion and hydrogen yield of the catalysts strongly depended on Cu/Zn ratio. The catalyst with Cu/Zn=1 showed very low activity having the methanol conversion of 39.3% and hydrogen yield of 43.2%. The increase in Cu/Zn ratio from 2 to 3 resulted in an increase in the methanol conversion and hydrogen yield from 90.5% to 92.4% and 90.8% to 92.7%, respectively.
- An increase in methanol conversion and hydrogen yield of the catalysts was observed due to an increase the total metal loading amount of the catalysts.
- The best catalyst configuration for the MSR catalyst was 18.75Cu6.25Zn/CMK-3/300, with the total metal loading of 25%, Cu/Zn ratio of 3, and calcination temperature of 300 °C. The average hydrogen molar flow rate was 0.000234 mole/min for this catalyst.
- The increase in the reaction temperature leaded to a rise the methanol conversion and hydrogen yield due to the endothermic nature of the process. The maximum methanol conversion and hydrogen yield were achieved at 300 °C with the values of 96.35% and 97.71%, respectively. However, CO formation was observed at the reaction temperatures of 275 °C and 300 °C as 0.6% and 0.9%, respectively.
- The experiments in the focused-microwave heated reactor system were performed over the best catalyst at a temperature range of 250-300 °C. The methanol conversion in the focused-microwave heated system was slightly higher compared to the conventionally-heated system. Furthermore, the hydrogen yield values obtained in the focused-microwave heated reactor system were gradually getting closer to the hydrogen yield values in the conventionally-heated system. The CO formation in the focused-microwave

heated reactor system declined by increasing the reaction temperature and reached to its minimum (1.51%) at 300 °C. Energy efficiency of the focused-microwave heated reactor system was higher compared to that of the conventionally-heated reactor system.

- The effect of other synthesis parameters, such as calcination gas and impregnation of different promoters, on the catalyst properties and activity can be also investigated. Sorption-enhanced methanol steam reforming in focused-microwave heated reactor can be a proper way to produce CO-free hydrogen. Moreover, long-life experiment of MSR is recommended to check the catalyst activity and stability.

REFERENCES

- [1] NASA's Goddard Institute for Space Studies (GISS) NASA's Goddard Institute for Space Studies (GISS), "Global climate change," *NASA*, 2018. [Online]. Available: <https://climate.nasa.gov/vital-signs/global-temperature/>. [Accessed: 21-Apr-2018].
- [2] NOAA National Centers for Environmental Information, "State of the Climate: Global Analysis for Annual 2016," *NOAA*, 2017. [Online]. Available: <https://www.climate.gov/news-features/understanding-climate/climate-change-global-temperature>. [Accessed: 21-Apr-2018].
- [3] Sandra May, "What is climate change?," *NASA*, 2017. [Online]. Available: <https://www.nasa.gov/audience/forstudents/k-4/stories/nasa-knows/what-is-climate-change-k4.html>. [Accessed: 24-Apr-2018].
- [4] Volker Quaschning, "Volker Quaschning: Renewable Energy and Climate Change," https://www.volker-quaschning.de/publis/index_e.php, 2016. [Online]. Available: https://www.volker-quaschning.de/publis/index_e.php.
- [5] J. D. Holladay, J. Hu, D. L. King, and Y. Wang, "An overview of hydrogen production technologies," *Catal. Today*, vol. 139, no. 4, pp. 244–260, 2009.
- [6] OPEC, "OPEC Share of World Crude Oil Reserves," *OPEC annual statistical bulletin*, 2017. [Online]. Available: 2018-04-24.
- [7] J. Hamilton, "Energy & Resources Renewable & Nonrenewable," 2010. [Online]. Available: <https://slideplayer.com/slide/5670450/>. [Accessed: 20-Apr-2018]
- [8] F. Barbir, "*PEM fuel cells: theory and practice*". Academic Press, pp. 1–16, 2013.
- [9] G. A. Olah, A. Goeppert, and G. K. S. Prakash, "Beyond Oil and Gas: The Methanol Economy: Second Edition," *Beyond Oil Gas Methanol Econ. Second Ed.*, Wiley-VCH: New York, pp. 1–334, 2009.
- [10] A. G. Stern, "A new sustainable hydrogen clean energy paradigm," *Int. J.*

Hydrogen Energy, vol. 43, no. 9, pp. 4244–4255, 2018.

- [11] F. Barbir, "PEM fuel cells: theory and practice". Academic Press, pp. 469–508, 2013.
- [12] P. P. Edwards, V. L. Kuznetsov, W. I. F. David, and N. P. Brandon, "Hydrogen and fuel cells: Towards a sustainable energy future," *Energy Policy*, vol. 36, no. 12, pp. 4356–4362, 2008.
- [13] Jefferson Lab, "The elemental hydrogen," *JEFFERSON SCIENCE ASSOCIATES, LLC*, 2018. [Online]. Available: <https://education.jlab.org/itselemental/ele001.html>. [Accessed: 24-Apr-2018].
- [14] P. Table, "Hydrogen," *Royal Society of Chemistry*, 2018. [Online]. Available: <http://www.rsc.org/periodic-table/element/1/hydrogen>. [Accessed: 24-Apr-2018].
- [15] Famous Scientists, "Antoine Lavoisier," *famousscientists.org*. [Online]. Available: <https://www.famousscientists.org/antoine-lavoisier/>. [Accessed: 24-Apr-2018].
- [16] T. P. N. N. Laboratory, "Basic hydrogen properties," *Hydrogen tools*, 2018. [Online]. Available: <https://www.h2tools.org/hyarc/hydrogen-data/basic-hydrogen-properties>. [Accessed: 24-Apr-2018].
- [17] T. Linde, "Hydrogen applications," *The Linde Group*. [Online]. Available: http://www.linde-gas.com/en/processes/process_chemistry_and_refining/hydrogen_applications/index.html. [Accessed: 25-Apr-2018].
- [18] W. L. Jolly, "Hydrogen," *Encyclopedya Britannica, inc.* [Online]. Available: <https://www.britannica.com/science/hydrogen/Production-and-applications-of-hydrogen>. [Accessed: 25-Apr-2018].
- [19] T. Linde, "Hydrogen in refining," *The Linde Group*. [Online]. Available: http://www.linde-gas.com/en/processes/petrochemical-processing-and-refining/hydrogen_applications_refineries/index.html.
- [20] C. Agca, "Hydrogen production from formaldehyde," M.Sc. thesis, Middle East Technical University, 2016.

- [21] R. Chaubey, S. Sahu, O. O. James, and S. Maity, “A review on development of industrial processes and emerging techniques for production of hydrogen from renewable and sustainable sources,” *Renew. Sustain. Energy Rev.*, vol. 23, pp. 443–462, 2013.
- [22] F. Barbir, “*PEM fuel cells: theory and practice*”. Academic Press, pp. 17–32, 2013.
- [23] D. D. Boettner and M. J. Moran, “Proton exchange membrane (PEM) fuel cell-powered vehicle performance using direct-hydrogen fueling and on-board methanol reforming,” *Energy*, vol. 29, no. 12–15 SPEC. ISS., pp. 2317–2330, 2004.
- [24] N. Muratova, “Highly distributed copper nanoparticles on carbon supports for methanol steam reforming”, Ph.D. dissertation, Max-Planck-Institut für Kohlenforschung, 2007.
- [25] D. R. Palo, R. A. Dagle, and J. D. Holladay, “Methanol steam reforming for hydrogen production,” *Chem. Rev.* 107 3992-4021, vol. 107, no. PNNL-SA-53246, pp. 3992–4021, 2007.
- [26] Pubchem, “Methanol,” <https://pubchem.ncbi.nlm.nih.gov>. [Online]. Available: <https://pubchem.ncbi.nlm.nih.gov/compound/methanol#section=Related-Records>.
- [27] M. alcohol MSDS, *Sciencelab*. [Online]. Available: <http://www.scienceLab.com/msds.php?msdsId=9927227>. [Accessed: 30-Apr-2018].
- [28] S. Sá, H. Silva, L. Brandão, J. M. Sousa, and A. Mendes, “Catalysts for methanol steam reforming-A review,” *Appl. Catal. B Environ.*, vol. 99, no. 1–2, pp. 43–57, 2010.
- [29] 6th ed The Columbia Encyclopedia, “Methanol,” *Encyclopedia.com*. [Online]. Available: <https://www.encyclopedia.com/science-and-technology/chemistry/organic-chemistry/methanol>. [Accessed: 30-Apr-2018].
- [30] T. E. of E. Britannica, “Methanol,” *Encyclopedya Britannica, inc.* [Online]. Available: <https://www.britannica.com/science/methanol>. [Accessed: 30-Apr-

2018].

- [31] ReciprocalNet, “Methanol,” *reciprocalnet.org*. [Online]. Available: <http://www.reciprocalnet.org/recipnet/showsamplebasic.jsp?sampleId=27344672>. [Accessed: 30-Apr-2018].
- [32] H. Purnama, “Catalytic Study of Copper based Catalysts for Steam Reforming of Methanol”, Ph.D. dissertation, Max -Planck-Society(MPG), 2003.
- [33] R. L. Borup, M. A. Inbody, T. A. Semelsberger, J. I. Tafoya, and D. R. Guidry, “Fuel composition effects on transportation fuel cell reforming,” *Catal. Today*, vol. 99, no. 3–4, pp. 263–270, Jan. 2005.
- [34] B. A. Peppley, J. C. Amphlett, L. M. Kearns, and R. F. Mann, “Methanol–steam reforming on Cu/ZnO/Al₂O₃. Part 1: the reaction network,” *Appl. Catal. A Gen.*, vol. 179, no. 1–2, pp. 21–29, 1999.
- [35] B. A. Peppley, J. C. Amphlett, L. M. Kearns, and R. F. Mann, “Methanol–steam reforming on Cu/ZnO/Al₂O₃ catalysts. Part 2. A comprehensive kinetic model,” *Appl. Catal. A Gen.*, vol. 179, no. 1–2, pp. 31–49, 1999.
- [36] R. Thattarathody, M. Artoul, R. M. Digilov, and M. Sheintuch, “Pressure, Diffusion, and S/M Ratio Effects in Methanol Steam Reforming Kinetics,” *Ind. Eng. Chem. Res.*, vol. 57, no. 9, pp. 3175–3186, 2018.
- [37] J. P. Breen and J. R. . Ross, “Methanol reforming for fuel-cell applications: development of zirconia-containing Cu–Zn–Al catalysts,” *Catal. Today*, vol. 51, no. 3–4, pp. 521–533, 1999.
- [38] X. Gu and W. Li, “First-Principles Study on the Origin of the Different Selectivities for Methanol Steam Reforming on Cu (111) and Pd (111),” *J. Phys. Chem. c*, vol. 114, no. 111, pp. 21539–21547, 2010.
- [39] Pinar Degirmencioglu, “Methanol Steam Reforming Over Silica Aerogel Supported,” Middle East Technical University, 2018.
- [40] I. Fechete, Y. Wang, and J. C. Védrine, “The past, present and future of heterogeneous catalysis,” *Catal. Today*, vol. 189, no. 1, pp. 2–27, 2012.
- [41] J. Hagen, I. Chorkendorff, and J. W. Niemantsverdriet, "Concepts of Modern Catalysis and Kinetics Catalysis from A to Z Principles and Practice of

Heterogeneous Catalysis Catalytic Membranes and Membrane Reactors Spectroscopy in Catalysis". Wiley-VCH: New York, 2006.

- [42] D. Sanfilippo, "Catalysis: through cultural synergism to the target," *Catal. Today*, vol. 34, no. 3–4, pp. 261–267, 1997.
- [43] I. Chorkendorff and J. W. Niemantsverdriet, "Concepts of Modern Catalysis and Kinetics." Wiley-VCH: New York, 2003.
- [44] I. Chorkendorff and J. W. Niemantsverdriet, "Solid Catalysts," in *Concept of Modern Catalysis and Kinetics*, Weinheim, FRG: Wiley-VCH Verlag GmbH & Co. KGaA, pp. 167–214, 2003.
- [45] H. Marko Hapke, "Homogeneous vs. heterogeneous catalysts," *Leibniz-institut fur katalyse e.V.*, 2015. [Online]. Available: https://www.catalysis.de/fileadmin/user_upload/MAIN-dateien/1_Forschung/FB_Rosenthal/Probevorlesung_Hapke_Hand-out.pdf. [Accessed: 04-May-2018].
- [46] G. Rothenberg, "Heterogeneous Catalysis," in *Catalysis*, Weinheim, Germany: Wiley-VCH Verlag GmbH & Co. KGaA, p. Chapter 4, p 127-187, 2008.
- [47] C. Perego and P. Villa, "Catalyst preparation methods," *Catal. Today*, vol. 34, no. 3–4, pp. 281–305, 1997.
- [48] C. Buzea, I. I. Pacheco, and K. Robbie, "Nanomaterials and nanoparticles: Sources and toxicity," *Biointerphases*, vol. 2, no. 4, pp. MR17-MR71, Dec. 2007.
- [49] S. Chaturvedi, P. N. Dave, and N. K. Shah, "Applications of nano-catalyst in new era," *J. Saudi Chem. Soc.*, vol. 16, no. 3, pp. 307–325, 2012.
- [50] A. Taguchi and F. Schüth, Ordered mesoporous materials in catalysis, *Microporous Mesoporous Mater.*, vol. 77, no. 1. 2005.
- [51] M. E. Davis, "Ordered porous materials for emerging applications," *Nature*, vol. 417, no. 6891, pp. 813–821, 2002.
- [52] U. Ciesla and F. Schüth, "Ordered mesoporous materials," *Microporous Mesoporous Mater.*, vol. 27, no. 2–3, pp. 131–149, Feb. 1999.
- [53] J. Lee, J. Kim, and T. Hyeon, "Recent progress in the synthesis of porous

carbon materials,” *Adv. Mater.*, vol. 18, no. 16, pp. 2073–2094, 2006.

- [54] P. Niebrzydowska *et al.*, “A simplified route to the synthesis of CMK-3 replica based on precipitation polycondensation of furfuryl alcohol in SBA-15 pore system,” *Carbon N. Y.*, vol. 64, pp. 252–261, Nov. 2013.
- [55] H. Huwe and M. Fröba, “Iron (III) oxide nanoparticles within the pore system of mesoporous carbon CMK-1: Intra-pore synthesis and characterization,” *Microporous Mesoporous Mater.*, vol. 60, no. 1–3, pp. 151–158, 2003.
- [56] S. M. Lee, S. C. Lee, W. G. Hong, and H. J. Kim, “N₂ and H₂ adsorption behavior of KOH-activated ordered mesoporous carbon,” *Chem. Phys. Lett.*, vol. 554, pp. 133–136, 2012.
- [57] C. Liang, Z. Li, and S. Dai, “Mesoporous carbon materials: Synthesis and modification,” *Angew. Chemie - Int. Ed.*, vol. 47, no. 20, pp. 3696–3717, 2008.
- [58] Q. Wang *et al.*, “Size control of SBA-15 by tuning the stirring speed for the formation of CMK-3 with distinct adsorption performance,” *Nano Res.*, vol. 9, no. 8, pp. 2294–2302, 2016.
- [59] K. Ghani, N. Kiomarsipour, and H. Jaberi, “Evaluation of optical properties of CMK-1 and CMK-3 mesoporous carbons and introduction them as very interesting black pigments,” *Dye. Pigment.*, vol. 122, pp. 126–133, 2015.
- [60] H. Huwe and M. Fröba, “Synthesis and characterization of transition metal and metal oxide nanoparticles inside mesoporous carbon CMK-3,” *Carbon N. Y.*, vol. 45, no. 2, pp. 304–314, 2007.
- [61] R. Ryoo and S. Hoon Joo, “Nanostructured carbon materials synthesized from mesoporous silica crystals by replication,” in *Studies in Surface Science and Catalysis*, vol. 148, pp. 241–260, 2004.
- [62] S. Jun, S. H. Joo, R. Ryoo, and M. Kruk, “Synthesis of New Nanoporous Carbon with Hexagonally Ordered Mesostructure,” no. 11, pp. 10712–10713, 2000.
- [63] R. Ryoo, S. H. Joo, S. Jun, T. Tsubakiyama, and O. Terasaki, “Ordered mesoporous carbon molecular sieves by templated synthesis: the structural varieties,” in *Phys. Chem. B.*, vol. 103, p. 150, 2001.

- [64] S. H. Joo, S. Jun, and R. Ryoo, “Synthesis of ordered mesoporous carbon molecular sieves CMK-1,” *Microporous Mesoporous Mater.*, vol. 44–45, pp. 153–158, 2001.
- [65] Y. Xia and R. Mokaya, “Synthesis of ordered mesoporous carbon and nitrogen-doped carbon materials with graphitic pore walls via a simple chemical vapor deposition method,” *Adv. Mater.*, vol. 16, no. 17, pp. 1553–1558, 2004.
- [66] S. Inagaki, Y. Yokoo, T. Miki, and Y. Kubota, “Improvement of electric double-layer capacitance of ordered mesoporous carbon CMK-3 by partial graphitization using metal oxide catalysts,” *Microporous Mesoporous Mater.*, vol. 179, pp. 136–143, 2013.
- [67] L. Shi, Y. Xu, L. Xing, X. Li, C. Yang, and S. Lin, “Synthesis and characterization of ordered mesoporous carbons CMK-3 produced by tailoring the mesopores of an AlSBA-15hard template synthesized without acid,” *Carbon N. Y.*, vol. 85, pp. 448–449, 2015.
- [68] V. G. Deshmane, R. Y. Abrokwah, and D. Kuila, “Synthesis of stable Cu-MCM-41 nanocatalysts for H₂ production with high selectivity via steam reforming of methanol,” *Int. J. Hydrogen Energy*, vol. 40, no. 33, pp. 10439–10452, 2015.
- [69] B. Lindström, L. J. Pettersson, and G. Menon, “Activity and characterization of Cu/Zn, Cu/Cr and Cu/Zr on γ -alumina for methanol reforming for fuel cell vehicles,” *Appl. Catal. A Gen.*, vol. 234, no. 1–2, pp. 111–125, 2002.
- [70] N. Takezawa and N. Iwasa, “Steam reforming and dehydrogenation of methanol: Difference in the catalytic functions of copper and group VIII metals,” *Catal. Today*, vol. 36, no. 1, pp. 45–56, 1997.
- [71] R. Thattarathody and M. Sheintuch, “Kinetics and dynamics of methanol steam reforming on CuO/ZnO/alumina catalyst,” *Appl. Catal. A Gen.*, vol. 540, no. April, pp. 47–56, 2017.
- [72] S. Gunduz, “Hydrogen Production From Ethanol Over Mesoporous Alumina Based Catalysts and Microwave Reactor Applications,” Ph.D. dissertation, Middle East Technical University, 2014.

- [73] K. K. Rana and S. Rana, “Microwave Reactors: A Brief Review on Its Fundamental Aspects and Applications,” *OALib*, vol. 01, no. 06, pp. 1–20, 2014.
- [74] H. Will, P. Scholz, and B. Ondruschka, “Microwave-assisted heterogeneous gas-phase catalysis,” *Chem. Eng. Technol.*, vol. 27, no. 2, pp. 113–122, 2004.
- [75] J. A. Menéndez *et al.*, “Microwave heating processes involving carbon materials,” *Fuel Process. Technol.*, vol. 91, no. 1, pp. 1–8, 2010.
- [76] National Research Council., Microwave processing of materials., National Academy Press:Washington, D.C. 1994.
- [77] C. O. Kappe and D. Dallinger, “Controlled microwave heating in modern organic synthesis: Highlights from the 2004-2008 literature,” *Mol. Divers.*, vol. 13, no. 2, pp. 71–193, 2009.
- [78] X. Zhang and D. O. Hayward, “Applications of microwave dielectric heating in environment-related heterogeneous gas-phase catalytic systems,” *Inorganica Chim. Acta*, vol. 359, no. 11, pp. 3421–3433, Aug. 2006.
- [79] J. H. Ng, S. K. Leong, S. S. Lam, F. N. Ani, and C. T. Chong, “Microwave-assisted and carbonaceous catalytic pyrolysis of crude glycerol from biodiesel waste for energy production,” *Energy Convers. Manag.*, vol. 143, pp. 399–409, 2017.
- [80] L. Dai *et al.*, “Production of hydrocarbon-rich bio-oil from soapstock via fast microwave-assisted catalytic pyrolysis,” *J. Anal. Appl. Pyrolysis*, vol. 125, pp. 356–362, 2017.
- [81] W. H. Chen, J. G. Jheng, and A. B. Yu, “Hydrogen generation from a catalytic water gas shift reaction under microwave irradiation,” *Int. J. Hydrogen Energy*, vol. 33, no. 18, pp. 4789–4797, 2008.
- [82] D. Varisli, C. Korkusuz, and T. Dogu, “Microwave-assisted ammonia decomposition reaction over iron incorporated mesoporous carbon catalysts,” *Appl. Catal. B Environ.*, vol. 201, pp. 370–380, 2017.
- [83] S. Gündüz and T. Dogu, “Hydrogen by steam reforming of ethanol over Co-Mg incorporated novel mesoporous alumina catalysts in tubular and microwave

- reactors,” *Appl. Catal. B Environ.*, vol. 168–169, pp. 497–508, 2015.
- [84] W. H. Chen and B. J. Lin, “Effect of microwave double absorption on hydrogen generation from methanol steam reforming,” *Int. J. Hydrogen Energy*, vol. 35, no. 5, pp. 1987–1997, 2010.
- [85] W. L. Perry, A. K. Datye, A. K. Prinja, L. F. Brown, and J. D. Katz, “Microwave heating of endothermic catalytic reactions: Reforming of methanol,” *AICHE J.*, vol. 48, no. 4, pp. 820–831, 2002.
- [86] T. Durka, G. D. Stefanidis, T. Van Gerven, and A. I. Stankiewicz, “Microwave-activated methanol steam reforming for hydrogen production,” *Int. J. Hydrogen Energy*, vol. 36, no. 20, pp. 12843–12852, 2011.
- [87] D. Zhao, “Triblock Copolymer Syntheses of Mesoporous Silica with Periodic 50A to 300A ;Angstrom Pores,” *Science (80-.).*, vol. 279, no. 5350, pp. 548–552, 1998.
- [88] P. H. Matter, D. J. Braden, and U. S. Ozkan, “Steam reforming of methanol to H₂ over nonreduced Zr-containing CuO / ZnO catalysts,” vol. 223, pp. 340–351, 2004.
- [89] L. Hao, J. Wang, L. Shen, J. Zhu, B. Ding, and X. Zhang, “Synthesis and electrochemical performances of mixed-valence vanadium oxide/ordered mesoporous carbon composites for supercapacitors,” *RSC Adv.*, vol. 6, no. 30, pp. 25056–25061, 2016.
- [90] Z. Obali, N. A. Sezgi, and T. Doğu, “The synthesis and characterization of aluminum loaded SBA-type materials as catalyst for polypropylene degradation reaction,” *Chem. Eng. J.*, vol. 176–177, pp. 202–210, 2011.

APPENDICES

A. CATALYST LOADING CALCULATIONS

In order to synthesis the catalysts, copper nitrate trihydrate ($\text{Cu}(\text{NO}_3)_2 \cdot 3\text{H}_2\text{O}$) and zinc nitrate tetrahydrate ($\text{Zn}(\text{NO}_3)_2 \cdot 4\text{H}_2\text{O}$) salts were used as the metal precursors. Considering the following molecular weights: 241.6 g/mol for $\text{Cu}(\text{NO}_3)_2 \cdot 3\text{H}_2\text{O}$, 261.4 g/mol for $\text{Zn}(\text{NO}_3)_2 \cdot 4\text{H}_2\text{O}$, 63.55 g/mol for Cu, and 65.38 g/mol for Zn, a general equation can be written to calculate the required amount of each precursor according to the catalyst configuration, as below:

Precursor required amount (g)=

$$\frac{(\text{Metal \%})(\text{Total metal loading wt. \%})(m_{CMK-3} \text{ g})(MW_{Precursor} \text{ g/mol})}{MW_{Metal} \text{ g/mol}}$$

For example, the aim was incorporation of 18 wt. % total loading with Cu/Zn ratio of 2 onto 0.3 g CMK-3. According to the abovementioned equation, 0.134 g $\text{Cu}(\text{NO}_3)_2 \cdot 3\text{H}_2\text{O}$ and 0.074 g $\text{Zn}(\text{NO}_3)_2 \cdot 4\text{H}_2\text{O}$ were required.

B. XRD DATA AND CRYSTALLITE SIZE CALCULATION

PDF cards of the used chemical species are given in Tables B.1-3.

Table B.1. *PDF card for C.*

Formula: C			
PDF Card No: 411487			
Radiation: CuK α_1			
Wavelength: 1.54060 Å			
2θ, °	d-spacing (Å)	Intensity, %	h k l
26.68	3.376	100.0	0 0 2
42.22	2.139	2.0	1 0 0
44.39	2.039	6.0	1 0 1
50.45	1.807	1.0	1 0 2
54.54	1.681	4.0	0 0 4
59.69	1.548	1.0	1 0 3
77.24	1.234	3.0	1 1 0
83.18	1.160	3.0	1 1 2
86.82	1.121	1.0	0 0 6
93.59	1.057	1.0	2 0 1

Table B.2. PDF card for CuO.

Formula: CuO PDF Card No: 10800076 Radiation: CuK α_1 Wavelength: 1.54060 Å			
2 θ , °	d-spacing (Å)	Intensity, %	h k l
32.48	2.754	5.5	1 1 0
35.39	2.535	25.8	0 0 2
35.54	2.524	100.0	-1 1 1
38.64	2.328	44.2	1 1 1
38.97	2.309	16.4	2 0 0
46.25	1.961	1.4	-1 1 2
48.85	1.863	19.4	-2 0 2
51.23	1.782	0.9	1 1 2
53.36	1.716	6.9	0 2 0
56.59	1.625	0.6	0 2 1
58.16	1.585	9.6	2 0 2
61.52	1.506	8.1	-1 1 3
65.66	1.421	9.6	0 2 2
66.34	1.408	6	-3 1 1
66.51	1.405	3.4	3 1 0
67.73	1.382	8.5	1 1 3
68.02	1.377	8.9	2 2 0
68.85	1.363	0.3	-2 2 1
71.84	1.313	0.2	-3 1 2
72.34	1.305	6.3	3 1 1
72.81	1.298	0.3	2 2 1
74.86	1.267	3.3	0 0 4
75.23	1.262	3.6	-2 2 2
79.56	1.204	0.1	0 2 3
80.26	1.195	1.1	-2 0 4
82.54	1.168	3.7	-3 1 3
82.86	1.164	3.2	2 2 2
83.34	1.159	0.2	3 1 2
83.69	1.155	2.1	4 0 0
86.81	1.121	0.8	-4 0 2
87.74	1.112	0.1	1 1 4
89.57	1.093	1.4	-1 3 1
91.44	1.076	3	1 1 3
95.27	1.043	0.6	2 0 4
96.59	1.032	0.1	-1 3 2
98.17	1.019	1.3	0 2 4
99.44	1.010	1.3	3 1 3
100.37	1.003	0.1	1 3 2
101.85	0.992	0.5	4 0 2
103.26	0.983	1.7	-1 1 5

Table B.2 (cont'd) *PDF card for CuO.*

2θ, °	d-spacing (Å)	Intensity, %	h k l
103.53	0.981	2	-2 2 4
105.91	0.965	0.1	-4 2 1
107.05	0.958	1	4 2 0
109.23	0.945	1.8	-1 3 3
110.33	0.938	1.5	-4 2 2
111.59	0.931	0.8	-4 0 4
113.11	0.923	0.9	1 1 5
113.89	0.919	1.7	-3 3 1
115.30	0.912	0.7	1 3 3
117.14	0.903	1.3	-5 1 1
119.68	0.891	1.3	2 2 4
120.19	0.889	1.3	3 3 1
120.75	0.886	1	-5 1 2
122.42	0.879	0.1	3 1 4
123.89	0.873	0.1	0 2 5
127.48	0.859	1.1	4 2 2
127.78	0.858	0.5	0 4 0
128.10	0.857	0.7	-2 2 5
128.26	0.856	0.9	5 1 1
131.49	0.845	1	-5 1 3
132.57	0.841	0.6	-3 3 3
133.57	0.838	0.6	3 3 2
136.14	0.83	0.1	-1 1 6
140.45	0.819	0.7	-4 2 4
142.87	0.813	1	0 4 2
146.63	0.804	1	2 4 0
148.07	0.801	0.1	-2 4 1

Table B.3. *PDF card for ZnO*

Formula: ZnO			
PDF Card No: 10751526			
Radiation: CuK α_1			
Wavelength: 1.54060 Å			
2θ, °	d-spacing (Å)	Intensity, %	h k l
32.07	2.789	56.2	1 0 0
34.47	2.600	40.4	0 0 2
36.53	2.458	100.0	1 0 1
47.79	1.902	20.0	1 0 2
57.17	1.610	28.3	1 1 0
63.10	1.472	25.7	1 0 3
67.07	1.394	3.6	2 0 0
68.49	1.369	19.0	1 1 2
69.77	1.347	9.6	2 0 1
72.67	1.300	1.5	0 0 4
77.64	1.229	2.8	2 0 2
81.65	1.178	1.5	1 0 4
90.31	1.086	5.8	2 0 3
93.91	1.054	1.8	2 1 0
96.44	1.033	5.5	2 1 1
99.21	1.011	2.9	1 1 4
104.11	0.977	2	2 1 2
104.46	0.974	4.6	1 0 5
108.21	0.951	0.6	2 0 4
111.93	0.93	2.2	3 0 0
117.59	0.901	5.6	2 1 3
123.29	0.875	2.7	3 0 2
125.44	0.867	0.4	0 0 6
135.04	0.834	2.2	2 0 5
137.09	0.828	0.6	1 0 6
140.39	0.819	0.7	2 1 4
146.22	0.805	1.5	2 2 0

Table B.4. PDF card for Na_2CO_3 .

Formula: Na_2CO_3 PDF Card No: 01-077-2082 Radiation: CuK α_1 Wavelength: 1.54060 Å			
2 θ , °	d-spacing (Å)	Intensity, %	h k l
14.94	5.924	0.1	0 0 1
19.75	4.492	2.9	1 1 0
20.33	4.365	0.2	2 0 0
22.79	3.900	2.9	-2 0 1
23.59	3.768	5.6	-1 1 1
26.06	3.417	17.2	1 1 1
27.65	3.224	21.9	2 0 1
30.15	2.962	81.7	0 0 2
33.01	2.711	18.1	-2 0 2
34.20	2.619	47.6	0 2 0
34.51	2.597	51.2	-1 1 2
35.25	2.544	100.0	3 1 0
35.91	2.499	3.8	-3 1 1
37.51	2.396	5.5	0 2 1
38.01	2.365	86.3	1 1 2
39.98	2.253	45.5	2 0 2
40.11	2.246	29.6	2 2 0
41.13	2.193	30.7	-4 0 1
41.49	2.174	50.4	-2 2 1
42.65	2.118	2.7	-3 1 2
44.53	2.033	25.0	2 2 1
45.92	1.975	0.3	0 0 3
46.23	1.963	1.0	0 2 2
46.54	1.950	28.3	-4 0 2
47.08	1.928	6.9	4 0 1
48.27	1.884	56.2	-2 2 2
48.40	1.879	33.5	-1 1 3
51.16	1.784	3.5	3 1 2
53.46	1.712	9.5	1 3 0
53.60	1.708	26.3	-3 1 3
54.70	1.677	14.3	4 2 0
55.21	1.662	1.2	-1 3 1
55.42	1.656	4.7	5 1 0
56.30	1.633	12.5	-4 0 3
56.46	1.628	8.4	1 3 1
57.09	1.612	6.9	4 0 2
58.50	1.577	11.0	0 2 3
59.01	1.564	12.3	-4 2 2
59.48	1.553	0.9	4 2 1
60.76	1.523	1.6	5 1 1

Calculation of crystallite sizes of metal using XRD pattern was done by Scherrer equation. In Scherrer equation:

$$t_{Crystal} = \frac{c\lambda}{B\cos(\theta)}$$

$t_{particle}$ is the crystallite size (nm). c represents the crystal shape factor (=0.89). λ defines wavelength of the radiation, while B is determined by the width of the peak at its half height in radian. Finally, θ is the Bragg angle in radian.

In this example, λ was 0.10546 nm. For the 12Cu6Zn/CMK-3/300 catalyst, B value related to CuO peak was calculated as 0.22° for the 2θ value of 35.48° which was the highest characteristic peak of CuO. CuO particle size can be determined as follows:

$$t_{Crystal} = \frac{(0.89)(0.15406)}{\left(\frac{0.22\pi}{180}\right)\cos\left(\frac{35.48\pi}{2 \times 180}\right)} = 37.49\text{nm}$$

C. EDX RESULTS OF THE CARBON MATERIALS

The EDX results of the synthesized CMK-3 samples are given in Figure C.1.

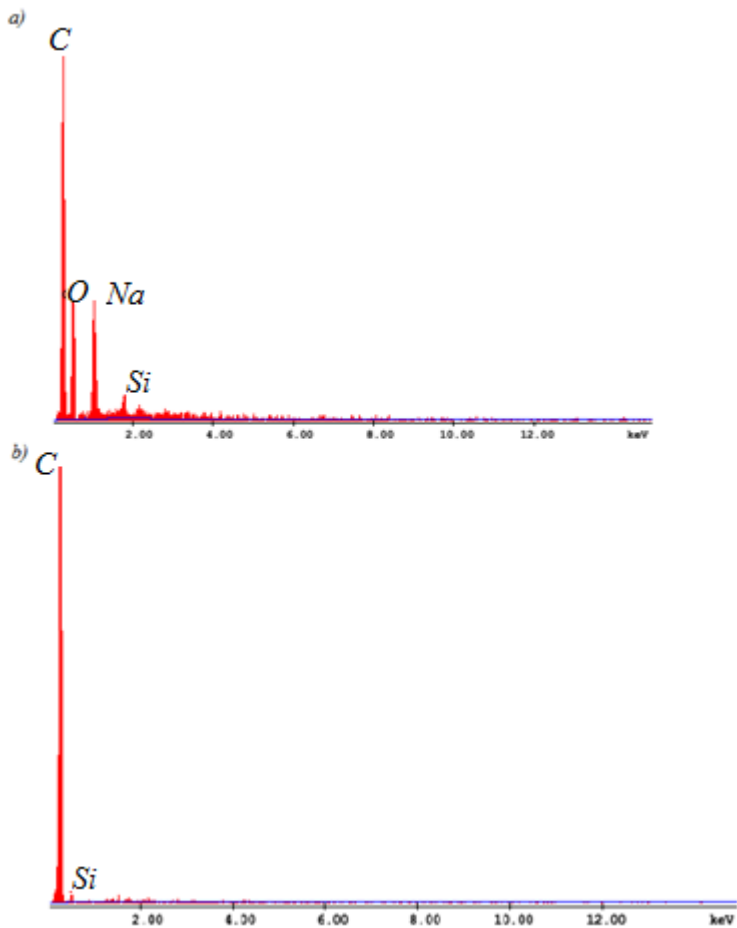


Figure C.1. EDX results of a)CMK-3/2-NaOH, b)CMK-3/2-HF.

D. GC CALIBRATION FACTORS

Outcome of each online GC analysis was in the form of area under the intensity-retention time graph which should be transformed into moles of the gas or liquid. For this purpose, a calibration factor is needed for each component based on the analyzed sample physical state. Table D.1 indicates the calibration factors and retention times of the compounds used in this study.

Table D.1. *Calibration factors and retention times of the components.*

Compound	Product Stream	Retention time (min)	Calibration β factor
H_2	<i>Gas</i>	0.964	0.0998
CO	<i>Gas</i>	1.152	1.536
CO_2	<i>Gas</i>	4.18	1
H_2O	<i>Liquid</i>	8.413	1
CH_3OH	<i>Liquid</i>	10.045	0.88

E. CALCULATION OF THE MOLE FRACTION OF EACH MSR PRODUCT, METHANOL CONVERSION, AND HYDROGEN YIELD

The mole fraction of each component can be determined by eqn. E.1.

$$y_i = \frac{N_i}{N_{total}} \times 100 = \frac{A_i \beta_i}{A_{H2} \beta_{H2} + A_{CO} \beta_{CO} + A_{CO2} \beta_{CO2}} \times 100 \quad \text{E.1}$$

where N shows the number of moles, A represents the area under the corresponding peak and β is the GC calibration factor (given in Table D.1). Density values (ρ_i) and molar flow rate of species in the product gas stream (F_i) can be calculated using eqn. E.2 and E.3, respectively:

$$\rho_i = \frac{P \times MW_i}{R} \quad \text{E.2}$$

$$F_i = Q_i \times \frac{\rho_i}{MW_i} = (Q_{product} - Q_{Ar}) \times y_i \times \frac{\rho_i}{MW_i} \quad \text{E.3}$$

where T is the room temperature (298 K), P is the operating pressure (1 bar), and R is the universal gas constant (82.1 atm/mol.K). $Q_{product}$ and Q_{Ar} are the volumetric flow rates of the product stream and the carrier gas (0.5 ml/s), respectively.

The molar flow rate of liquid methanol can be determined by eqn. E.4.

$$F_{CH3OH,L} = \frac{x_{CH3OH,L} \times m_{liquid}}{(x_{CH3OH} \times MW_{CH3OH,L} + x_{H2O} \times MW_{H2O})} \quad \text{E.4}$$

where x is the mole fraction in the liquid product. Methanol conversion can be obtained using eqn. E.5:

$$X_{CH3OH} = \frac{F_{CH3OH,0} - F_{CH3OH,L}}{F_{CH3OH,0}} \quad \text{E.5}$$

where x_i is the mole fraction in liquid product. $F_{CH3OH,0}$ is the initial molar flow rate of methanol/water mixture (mol/s). It can be calculated by eqn. E.6.

$$F_{CH_3OH,0} = F_{CO} + F_{CO_2} + F_{CH_3OH,L} \quad E.6$$

Finally, hydrogen yield is achieved by eqn. E.7:

$$Y_{H_2} = \frac{F_{H_2}}{F_{CH_3OH,0}} \quad E.7$$